TECHNISCHE UNIVERSITÄT MÜNCHEN

Max-Planck-Institut für Biochemie

Proteomic and phosphoproteomic analysis of lysophosphatidic acid-induced G protein-coupled receptor signalling

Nina Carolin Mäusbacher

Vollständiger Abdruck der von der Fakultät für Chemie der Technischen Universität München zur Erlangung des akademischen Grades eines

Doktors der Naturwissenschaften

genehmigten Dissertation.

Vorsitzender: Univ.-Prof. Dr. J. Buchner

Prüfer der Dissertation:

1. Priv.-Doz. Dr. H. Daub
2. Univ.-Prof. Dr. St. Sieber

Die Dissertation wurde am 30.08.2010 bei der Technischen Universität München eingereicht und durch die Fakultät für Chemie am 10.11.2010 angenommen.

For my parents

Introductory remark

This thesis was prepared at the Max-Planck-Institute of Biochemistry under the supervision of PD Dr. Henrik Daub. Due to the time-consuming measurements of the global phosphoproteomic time-course study of LPA-induced SCC-9 cells, equal parts of experimental work in this project were done by Thiemo Schreiber and me.
Parts of this study have been published in international journals.

Table of contents

Summary 1

English version 1

Deutsche Version 3

1. Introduction 5

1.1 Cell signalling 5

1.2 Role of protein phosphorylation in cell signalling 6

1.3 Lysophosphatidic acid 7

1.4 G protein-coupled receptors and signalling pathways 8

1.5 MMPs and ADAMs of the metalloproteinase metzincin family 10

1.6 ADAM17 and its implication in EGFR transactivation 11

1.7 Implication of LPA, GPCRs and ADAM17 in cancer 14

1.8 Mass spectrometry 15

1.8.1 Mass spectrometry-based proteomics 15

1.8.2 Quantitative proteomics 17

1.8.3 Phosphoproteomics 19

1.9 Aim of this PhD thesis 22

2. Materials and Methods 23

2.1 Materials 23

2.1.1 Cell line 23

2.1.2 Antibodies 23

2.1.3 siRNA-oligonucleotides 23
2.1.4 Media and additives 24
2.1.5 Commonly used buffers 24
2.1.6 Chemicals, reagents and other material 25
2.1.7 Kits 27
2.1.8 Instruments 27
2.1.9 Software and online tools 27
2.2 Methods 29
2.2.1 Cell culture techniques 29
2.2.1.1 Cell culture and LPA stimulation 29
2.2.1.2 Cell lysis 29
2.2.2 Affinity chromatographies 30
2.2.2.1 Lectin-affinity pull-down 30
2.2.2.2 ADAM17-Immunoprecipitation 30
2.2.2.3 EGFR-Immunoprecipitation 31
2.2.3 Molecular biological methods 31
2.2.3.1 siRNA transfection 31
2.2.3.2 Migration and proliferation assay 32
2.2.4 Protein analytical methods 32
2.2.4.1 Sodium dodecyl sulfate-polyacrylamide gel electrophoresis (SDS-PAGE) 32
2.2.4.2 Western blot analysis 33

2.2.4.3 Colloidal blue staining of polyacrylamid gels 33
2.2.4.4 Protein precipitation 34
2.2.5 Mass spectrometry sample preparation 34
2.2.5.1 In-gel digest 34
2.2.5.2 In-solution digest 35
2.2.5.3 Phosphopeptide enrichment with TiO_2 beads 36
2.2.5.4 Phosphopeptide enrichment with IMAC beads 36
2.2.5.5 Strong cation exchange chromatography 37
2.2.5.6 Desalting of samples 37
2.2.6 Mass Spectrometric Analysis 38
2.2.7 Data processing 38
2.2.8 Bioinformatic analysis 40
2.2.8.1 Time-dependent clustering: SOTA 40
2.2.8.2 Time-dependent clustering: fuzzy c-means clustering 40
2.2.8.3 DAVID 40
2.2.8.4 Motif-X 41
2.2.8.5 String networks 41
2.2.8.6 Hierarchical clustering 42
3. Results 43
3.1 Establishment of a quantitative MS workflow to identify LPA-dependent interaction partners of ADAM17 43

3.1.1 Co-immunoprecipitations with ADAM17 343 antibody 43

3.1.2 Lectin pull-down for protein identification 47

3.1.3 Two consecutive ADAM17 immunoprecipitations 49

3.2 Glycoprotein capture and quantitative phosphoproteomics indicate coordinated regulation of cell surface proteins upon lysophosphatidic acid stimulation 54

3.2.1 Experimental strategy for quantitative glycoproteome analysis 54

3.2.2 Quantitative analysis of LPA-induced regulation 58

3.2.3 Bioinformatics analysis of LPA-induced phosphoregulation 64

3.2.4 Time-dependent phosphorylation profiles of lectin-enriched proteins upon LPA stimulation 68

3.2.4.1 LPA-triggered phosphoregulation of the EGFR and ADAM17 70

3.2.4.2 Phosphoregulation of GPCRs, ion co-transporters and exchangers 72

3.2.4.3 Regulation of cell adhesion proteins 73

3.2.4.4 LPA-dependent regulation of Wnk1 and its role in cell migration 74

3.3 Time-resolved phosphorylation site analysis in the entire SCC-9 cell proteome upon LPA treatment 80

3.3.1 Experimental design for LPA-induced time-resolved phosphorylation analysis 80

3.3.2 Interaction network of LPA-regulated phosphoproteins 83

3.3.3 Hierarchical clustering of time-dependent phosphorylation profiles 85

3.3.4 Clustering of time-dependent phosphorylation profiles and analysis of resulting phosphoprotein networks 89

4. Discussion 97

4.1 LPA-induced transactivation process in SCC-9 cells 97

4.1.1 ADAM17 interaction partners 97

4.1.2 Time-dependent phosphorylation profiles of ADAM17 and the EGFR 101

4.2 Discussion of the glycoproteome study 103

4.2.1 Lectin pull-down strategy and changes in protein abundance upon LPA treatment in the enriched subfraction 103

4.2.2 LPA-dependent regulation of the phosphoproteins implicated in a variety of functions including cell migration 104

4.2.3 Regulation mechanisms of LPA-induced phosphosites 108

4.3 Comparison of the glycoproteome and the time-course study 110

4.4 Outlook 113

5. References 115

6. Publications 127

7. Acknowledgement 128

Summary

English version

The lipid mediator lysophosphatidic acid (LPA) is a serum component that regulates various cellular functions via specific G protein-coupled receptors (GPCRs). LPA-induced signal transduction controls proliferation, migration and survival in a wide range of non-transformed as well as cancer cells. The underlying signalling mechanisms are still incompletely understood, including the metalloproteinase ADAM17-mediated transactivation of the epidermal growth factor receptor (EGFR) and EGFR-independent LPA signalling events. Therefore, the aims of this study were the development of approaches to shed light on the EGFR transactivation process and especially LPA-regulated ADAM17 interaction partners as well as the time-resolved analysis of phosphorylation changes upon LPA stimulation as a general approach towards cellular LPA signalling. Both analyses were performed in SCC-9 squamous carcinoma cells that were selected due to their pronounced EGFR transactivation and general signalling responses upon LPA. For unbiased and comprehensive protein analysis highly sensitive and accurate SILAC-based quantitative mass spectrometry (MS) was used throughout this study. To identify yet unknown proteins involved in the transactivation process quantitative MS was combined with ADAM17 downregulation, lectin affinity purification or subsequent depletion of ADAM17 by consecutive immunoprecipitation. LPA-evoked phosphoregulation was first explored with a focus on cell surface proteins, for which glycoproteome enrichment by immobilized lectins was combined with SILAC-based quantitative phosphoproteomics. Interestingly, upon 1.5 and 5 min of LPA stimulation phosphoregulation could be detected on various GPCRs, receptor tyrosine kinases, ion transporters as well as cell adhesion molecules that operate at the plasma membrane to modulate cell-cell and cell-matrix interactions in LPA-promoted cell migration. Moreover, the serine/threonine kinase Wnk1, which was found to be rapidly phosphorylated in its activation loop upon LPA treatment, could be identified as a previously unknown factor in LPA-induced cell migration.

Analysis of the lectin-enriched subfraction was finally expanded to global time-resolved phosphorylation analysis covering the initial 90 min upon LPA stimulation. Time course analysis revealed rapid phosphoregulation on cell adhesion and G protein signalling molecules as well as more slowly induced phosphorylation events on transcription factors and proteins involved in splicing, translation and chromatin architecture.

Notably, the transfer of functional information about sites already characterised in contexts other than GPCR signalling to previously unknown, LPA-regulated phosphorylations offered insights into highly coordinated and multi-factorial regulation of various cell processes. Thus, the accumulated cellular biochemistry data contributes to the understanding of fundamental processes in LPA signalling and provides a vastly extended knowledge basis for further functional studies on physiological and disease-related aspects of LPA-induced signal transduction processes.

Deutsche Version

Das Phospholipid Lysophosphatidsäure (LPA) ist ein Bestandteil des Serums, der über spezifische G-Protein-gekoppelte Rezeptoren unterschiedliche zelluläre Funktionen reguliert. Proliferations-, Migrations- und Überlebensprozesse werden sowohl in gesunden Zellen als auch vielen Krebszellen durch LPA-induzierte Signalweiterleitung kontrolliert. Die zugrunde liegenden Mechanismen der Signalübertragung, einschließlich der von ADAM17 vermittelten Transaktivierung des Epidermalen Wachstumsfaktor Rezeptors (EGFR) und der von diesem Rezeptor unabhängigen LPA-induzierten Signalwege sind bisher nicht vollständig aufgeklärt. Ziel dieser Studie war deshalb sowohl die Entwicklung eines experimentellen Ansatzes zur genaueren Untersuchung des EGFR Transaktivierungsprozesses und insbesondere LPA-regulierter ADAM17 Interaktionspartner, als auch die zeitliche Analyse der durch LPA vermittelten Phosphorylierungsänderungen als genereller Ansatz zur Untersuchung LPA-abhängiger Signalwege. Beide Analysen wurden in humanen SCC-9 Plattenepithelkarzinomzellen der Kopf-Hals-Region durchgeführt, die sich auf Grund ihrer ausgeprägten Transaktivierung des EGFRs und ihres allgemeinen Verhaltens nach LPA-Stimulation besonders für die Untersuchung dieser Fragestellungen eigneten. Um eine eindeutige und vollständige Analyse der Proteine zu gewährleisten, wurde im Rahmen dieser Studie die äußerst sensitive und genaue Methode der auf SILAC basierenden quantitativen Massenspektrometrie (MS) angewendet. Zur Identifikation noch unbekannter am Transaktivierungsprozess beteiligter Proteine wurde die MS-Analyse mit der siRNA-induzierten Expressionshemmung von ADAM17, der Lektinaffinitätsaufreinigung oder der stufenweisen Depletion von ADAM17 durch aufeinanderfolgende Immunopräzipitationsreaktionen, kombiniert. Die durch LPA bedingte Phosphoregulation wurde zuerst für Zelloberflächenproteine untersucht, wofür die Anreicherung von Glykoproteinen mit Hilfe immobilisierter Lektine mit der SILAC-basierten Phosphoproteomik kombiniert wurde. Interessanterweise wurde Phosphoregulation nach LPA-Stimulation von 1,5 und 5 min an unterschiedlichen G-Protein-gekoppelten Rezeptoren, Rezeptortyrosinkinasen, Ionentransportern und Adhäsionsmolekülen, die während der LPA-gesteuerten Zellmigration an der Plasmamembran als Modulatoren der Zell-Zell und Zell-Matrix Interaktionen fungieren, festgestellt. Des weiteren konnte die Serine/Threoninkinase Wnk1, die in ihrer Aktivierungsregion nach LPA-Behandlung sehr schnell phosphoryliert wurde, als ein bisher unbekannter Faktor der LPA-induzierten Zellmigration identifiziert werden.

Die Analyse von Lektin-aufgereinigten Subfraktionen wurde schließlich auf eine globale, zeitaufgelöste Phosphorylierungsanalyse ausgeweitet, welche die initialen 90 min nach LPA Stimulation abdeckte. Die Analyse der Zeitreihen zeigte eine schnelle Phosphoregulation von Zelladhäsionsproteinen und G-Protein-Signaltranduktionsmolekülen sowie langsamer induzierte Phosphorylierungsereignisse an Transkriptionsfaktoren und Proteinen, welche beim Spleißen, der Translation und der Regulation der Chromatinarchitektur beteiligt sind. Die Übertragung funktioneller Informationen über Phosphorylierungsstellen, welche in einem anderen biologischen Zusammenhang als der Signalübermittlung mittels G-Protein-gekoppelter Rezeptoren charakterisiert waren, auf bisher unbekannte LPA-regulierte Phosphorylierungsereignisse, ermöglichte Einblicke in eine offenbar hoch koordinierte und multifaktorielle Regulation unterschiedlicher zellulärer Prozesse. Somit tragen die Ergebnisse dieser Arbeit zum Verständnis fundamentaler Prozesse in der LPA-vermittelten Signalübertragung bei und bieten eine erweiterte Basis für zukünftige funktionelle Studien zu physiologischen und krankheitsrelevanten Aspekten LPA-induzierter Signalübertragungsprozesse.

1. Introduction

1.1 Cell signalling

Cell signalling contributes to the regulation of nearly all biological processes and is critically involved in cell fate decisions. The accuracy of cell signalling events ensures the sensing of environmental cues and their translation into appropriate biological responses. Generally, such signals follow a path that consists of several steps. Ligand binding to a receptor relays an incoming signal to the cytoplasmic compartment, which is followed by intracellular signal propagation through signalling cascades and finally terminates in the activation of downstream effectors that can be as distinct as the transcription machinery in the nucleus or adhesion molecules on the cell surface. To induce a distinct biological outcome, intracellular or extracellular signals do not act through isolated linear pathways but rather through interconnected signalling networks, also referred to as signalling crosstalk (Dumont, Pecasse *et al.*, 2001; Barrera, Morales *et al.*, 2005). In addition, cellular signalling is specified by spatial organization as well as temporal dynamics. Hence, one ligand or stimulus can activate different pathways depended on the cellular context or, *vice versa,* different stimuli can target and converge on the same effector proteins (Kholodenko, Hancock *et al.*, 2010). The outcome of a signal also depends on its intensity, which has to be distinguishable from background noise. All these parameters allow to generate unique signal transduction responses depending on the specific cellular setting.

Pathways that are triggered by external stimuli start at the plasma membrane. Due to its separating function between the interior of a mammalian cell and the extracellular environment, the plasma membrane is the first cellular compartment exposed to external stimuli and therefore serves as major platform for signal integration and transduction. To respond to external signals, cells possess various types of plasma membrane-spanning receptors, such as receptor tyrosine kinases or G protein-coupled receptors that communicate to the intracellular signalling machinery in a ligand-regulated manner. Furthermore, the plasma membrane represents a scaffold to bring signalling molecules together and facilitate their interactions. The architecture of the plasma membrane with its sub-compartments of different protein composition, such as lipid rafts, can dictate signalling network properties. Regarding kinase cascades triggered upon external stimuli the first protein kinase is typically activated on the plasma membrane and subsequent signal propagation is then executed by activating distinct downstream kinases.

In general, signal propagation through kinase cascades modifies protein functionality on three different levels: post-translational modification (PTM) of proteins, protein-protein interactions and protein expression changes. The interplay of all three aspects defines the organization and outcome of signalling processes, with the latter two typically depending on initial signal-induced PTMs. Phosphorylation on distinct amino acids can generate new binding sites and thus enable protein associations. For example, phosphorylated tyrosines in a specific sequence context on receptor tyrosine kinases serve as docking sites for SH2-domain containing interaction partners (Schlessinger, 2000; Schlessinger and Lemmon, 2003). Cellular protein levels can be regulated via ubiquitinylation that in most cases triggers proteasomal degradation, as exemplified by the well-characterised, phosphorylation-triggerd ubiquitinylation and subsequent degradation of the inhibitor IκB of transcription factor NFκB (Skaug, Jiang *et al.*, 2009). Besides phosphorylation and ubiquitylation, other forms of PTMs such as acetylation, methylation and glycosylation are involved in signalling. Generally, protein alterations on the PTM level do not only facilitate protein associations and influence protein abundance but can also result in protein activation as well as protein localization changes.

These processes also represent overall regulatory mechanisms of cell signalling. Whereas regulation via protein abundances is rather slow, alterations of PTMs can occur very rapidly and are in most cases reversible. Furthermore, positive or negative feedback loops dynamically act on pathways to ensure an optimal signalling output.

1.2 Role of protein phosphorylation in cell signalling

The most prominent PTM in cell signalling is phosphorylation, with an estimated 30% of all human proteins being phosphorylated at any given time. The phosphoproteome is estimated to consist of more than 100,000 distinct phosphorylation sites and probably most of them are involved in a variety of signalling pathways (Choudhary and Mann, 2010). Phosphorylation modifications mostly occur on the amino acid serine followed by threonine, whereas phosphorylation events on tyrosine residues are rare by comparison. Accordingly, on average 86%, 12% and 2% of site-specific phosphorylations are found on serine, threonine and tyrosine residues, respectively. The addition or removal of a phosphate group can result in a conformational change of the respective protein and thus impact its activation state. Whether phosphorylation events trigger activation or inhibition of proteins does not follow defined

rules and therefore has to be elucidated individually, although in the majority of cases functionally relevant phosphorylations play a role in protein activation, such as e.g. phosphorylation-dependent activation of kinases. Protein kinases and phosphatases act antagonistically and hence ensure the reversibility of the phosphomodifications, which is a hallmark of cell signalling. In addition, each kinase and phosphatase is characterised by its individual substrate specificity which is primarily defined by the residue to be modified plus its surrounding amino acid sequence. Regulation of proteins also includes concerted multisite phosphorylations that may be performed by different kinases in a sequential manner as well as coordinated reciprocal modification events on the same protein. In protein phosphorylation research the focus is predominantly on sites regulated upon a specific stimulus, as these are likely to be of importance in the biological processes induced upon cell treatment. Although the large number of phosphorylation events carried out by kinases raise the question to which extent these modifications are functionally relevant, the huge number of about 500 protein kinase genes that constitute about 2% of the human genome emphasize the major importance of protein kinases and their cellular functions in biological processes (Manning, Whyte *et al.*, 2002; Lienhard, 2008).

1.3 Lysophosphatidic acid

Lysophosphatidic acid (LPA) is a small, naturally occurring phospholipid that acts as an extracellular signalling molecule and induces pleiotropic biological responses. The phospholipid derivate is ubiquitously found in cellular membranes at rather low concentrations compared to major phospholipid species. However, higher LPA concentrations in the sub-micromolecular range are measured in blood plasma. LPA levels are regulated by two major pathways. One originates from membrane phospholipids such as phosphatidylcholine, phosphatidylethanolamine and phosphatidylserine, which are sequentially processed either by phospholipase D and phospholipase A_2 or, alternatively, by phospholipase A_2 and lysophospholipase D (Figure 1). Previously, autotaxin was found to possess lysophospholipase D acitivity that removes the choline group from lysophosphatidylcholine (Tokumura, Majima *et al.*, 2002; Umezu-Goto, Kishi *et al.*, 2002), which was further shown to be the major source of plasma LPA (Tanaka, Okudaira *et al.*, 2006; van Meeteren, Ruurs *et al.*, 2006).

The bioactive lipid triggers various biological processes including cell proliferation, survival, cytoskeletal reorganization and migration (Radeff-Huang, Seasholtz *et al.*, 2004). The activation of the corresponding pathways that result in such diverse biological responses can be mediated by at least five known high affinity LPA receptors, namely LPA_1 to LPA_5 and the three recently published putative LPA receptors GPR87, P2Y5 and P2Y10 (Choi, Herr *et al.*, 2010). The heterogeneity of the receptor subtypes as well as their individual expression patterns in different tissues further contribute to an enhanced complexity and diversity of LPA-induced cell signalling. However, all LPA receptors share the same underlying signalling mechanism based on heterotrimeric G protein activation, which classifies them as G protein-coupled receptors.

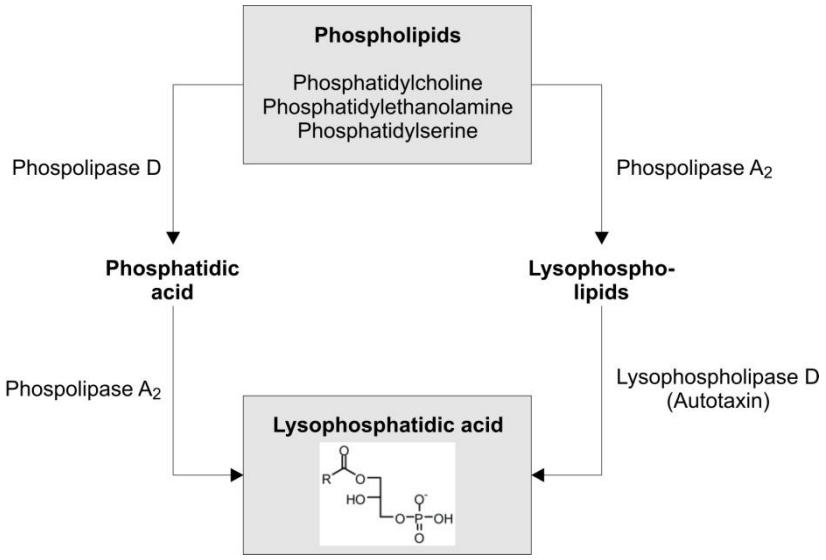

Figure 1: Two major metabolic pathways of LPA production. Membrane phospholipids are either subsequently processed by phospholipase D and phospholipase A_2, or phospholipase A_2 and autotaxin, which exhibits lysophospholipase D activity. (Illustration modified from Choi, Herr et al. 2010)

1.4 G protein-coupled receptors and signalling pathways

With approximately 1000 members, G protein-coupled receptors (GPCRs) constitute the largest superfamily of cell surface receptors in mammalians. This class of integral plasma membrane receptors possesses seven transmembrane helices with distinct relative orientations to each other. The second extracellular loop connecting two of the helices covers

the ligand binding site that is partly situated in the transmembrane domain (Kristiansen, 2004). A plethora of different factors are known to bind to or act on GPCRs, including peptide ligands, proteases, nucleotides as well as bioactive lipid molecules such as LPA. In response to extracellular ligand binding, GPCRs mediate intracellular activation of heterotrimeric G proteins, which is a hallmark of this class of receptors. Upon ligand binding the cognate receptors undergo a conformational change resulting in the activation of receptor-specific subsets of heterotrimeric G-proteins by guanine nucleotide exchange on the intracellular side (Oldham and Hamm, 2008). Hereupon, the catalyzed GTP binding to the α-subunit of the heterotrimeric G proteins causes its dissociation from the βγ-subunit. According to their different α–subunits heterotrimeric G proteins are divided into the four families G_i, G_s, G_q and $G_{12/13}$ which induce different pathways through their distinct α–subunits.

$G_{\alpha s}$ induces cAMP-dependent signalling by directly activating adenylate cyclase that triggers the production of cAMP from ATP. Enhanced levels of the second messenger cAMP activate protein kinase A which then phosphorylates various downstream targets. In contrast to $G_{\alpha s,}$ the $G_{\alpha i}$-subunit mainly decreases the production of cAMP by inhibiting adenylate cyclase. The phospholipase C pathway is regulated by $G_{\alpha q}$ which activates phospholipase C to cleave phosphatidylinositol 4,5-bisphosphate (PIP_2) into inositol 1,4,5-trisphosphate (IP_3) and diacyl glycerol (DAG). IP_3 mainly acts on Ca^{2+}-channels at the endplasmic reticulum resulting in Ca^{2+}-release into the cytosol, while DAG together with the elevated Ca^{2+}-levels stimulates the activation of various protein kinase C isoforms. The fourth group of G_α-subunits, $G_{\alpha 12/13}$, is involved in Rho family GTPase signalling. Through the activation of guanine exchange factors that induce Rho and downstream effectors such as ROCK and LIM kinases, both $G_{\alpha 12}$ and $G_{\alpha 13}$ are implicated in actin cytoskeleton remodeling and consequently in cell migration (Wang, Tan *et al.*, 2006).

Upon dissociation of the G_α-subunit the $G_{\beta\gamma}$ subunits remain as a complex that itself mediates second messenger generation or ion channel activation. The reconstitution of the heterotrimeric complex follows GTP hydrolysis in the the α-subunit, which can be triggered by either effector binding or GTPase-activating proteins from the regulators of the G protein signalling family. The desensitisation of the cognate receptors can further be directly triggered by β-arrestins, which prevent heterotrimeric G proteins from binding, and hence contribute to a tight regulation of these signalling events. Furthermore, different forms of

GPCR oligomerisation add another level of complexity to these signalling processes that are implicated in various physiological roles.

1.5 MMPs and ADAMs of the metalloproteinase metzincin family

Matrix metalloproteinases (MMPs) and disintegrin metalloproteinases (ADAMs) both belong to the superfamily of metzincins that are part of the enzyme class of zinc-metalloproteinases (Figure 2A) (Murphy, 2008). In general, metalloproteinases are responsible for the proteolytic processing of growth factors, receptor activation by internal cleavage or degradation of the extracellular matrix. They are essential for proliferation, differentiation, remodelling of the extracellular matrix (ECM) and cell migration. The activity of these enzymes depends on the presence of a metal ion coordinated by three histidine imidazoles in the active site of the enzyme. Consequently, in zinc metalloproteinases this essential ion is Zn^{2+} which is required for proteolytic hydrolysis of peptide bonds. Accordingly, the common characteristics of metzincin superfamily members is the zinc-binding motif HEXXHXXGXXH containing the three zinc-coordinating histidine residues and additionally a conserved methionine-turn in the active-site helix downstream of that motif (Stocker and Bode, 1995).

The family of matrix metalloproteinases, one subgroup of metzincins, consists of 28 endopeptidases that can cleave collagen, elastin, gelatins and casein among other ECM components. The categorisation of these enzymes is partly based on their substrates as well as on their differing structures, and members are accordingly referred to as collagenases, gelatinases, stromelysins, matrilysins and membrane-bound MMPs. Furthermore, MMPs also possess cleavage activity against non-ECM proteins such as cytokines, chemokines and growth factors (Page-McCaw, Ewald *et al.*, 2007). Most MMPs are expressed in a latent proform that requires cleavage of its prodomain for full proteolytic activity. The observation that this class of proteins is able to activate its own proforms suggests a self-enhancing mechanism of MMP activation. To prevent an uncontrolled degradation of the ECM, regulatory mechanisms counteract this process e.g. by transcriptional regulation of MMP expression or inactivation via α-macroglobulins and tissue inhibitors (TIMPs). The so far known TIMPs 1-4 (Crocker, Pagenstecher *et al.*, 2004) are the major endogenous regulators not only of MMPs but also of ADAMs.

The ADAM family consists of 21 members that are characterised by a disintegrin and metalloproteinase domain. Thus, ADAMs possess both a cell adhesion region that enables the interaction with integrin receptors as well as a catalytic region. Due to the lack of the conserved zinc-binding catalytic sequence in the metalloproteinase domain of some ADAMs only 13 family members exhibit full proteolytic activity. Apart from the soluble splice variants of ADAM12 (Gilpin, Loechel *et al.*, 1998) and ADAM33 (Powell, Wicks *et al.*, 2004), all members of the ADAM family are type I transmembrane proteins with their N-termini facing the extracellular side. Like MMPs, ADAMs are expressed as proforms and achieve shedding activity upon removal of the auto-inhibitory prodomain. Concerning the common structural organization of ADAMs, the prodomain is followed by the metalloproteinase domain, the disintegrin-like domain, a cystein-rich region, EGF-like repeats, a transmembrane domain and a cytoplasmic tail (Figure 2B). As enzymes that cleave cell surface proteins, also referred to as ectodomain sheddases, ADAMs are implicated in the proteolytic processing of cytokines, growth factors, cell surface receptors and cell adhesion molecules.

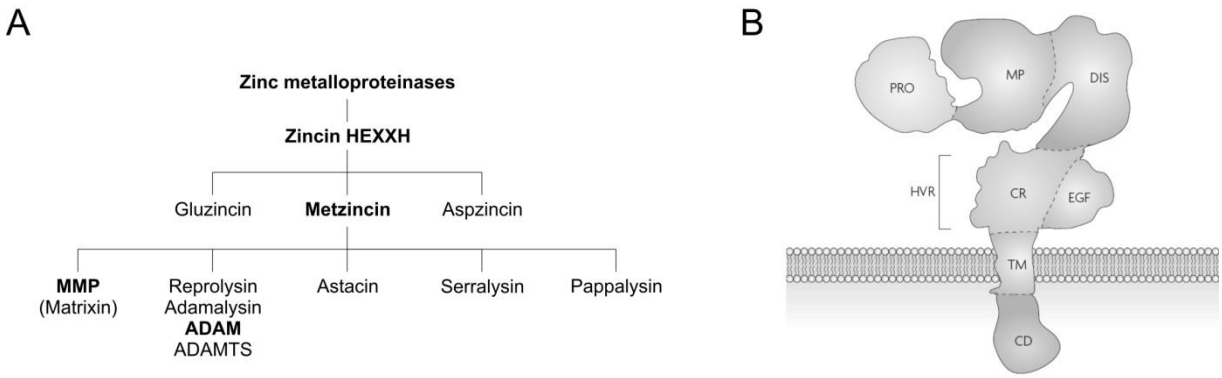

Figure 2: Hierarchy of zinc metalloproteinases (A) and structural organisation of ADAMs (B). CD, cytoplasmic domain; CR, cystein-rich region; DIS, disintegrin-like domain; EGF, EGF-like repeats; MP, metalloproteinase domain; PRO, prodomain; TM, transmembrane domain. (Illustration modified from Murphy, 2008)

1.6 ADAM17 and its implication in EGFR transactivation

The best-characterised member of the ADAM family is ADAM17, also named TACE (tumour necrosis factor-α convertase) due to its initial characterisation as a cleaving enzyme of the membrane-bound, inactive precursor of the inflammatory cytokine tumor necrosis

factor (TNF)-α (Black, Rauch *et al.*, 1997; Moss, Jin *et al.*, 1997). The sheddase activity of ADAM17 is directed against a broad range of cell surface molecules, including e.g. MUC1 (Thathiah, Blobel *et al.*, 2003), Notch1 receptor (Brou, Logeat *et al.*, 2000), cellular prion protein (Vincent, Paitel *et al.*, 2001), erbB4/HER4 (Rio, Buxbaum *et al.*, 2000), TGFα (Peschon, Slack *et al.*, 1998) and other EGF-like ligands (Sunnarborg, Hinkle *et al.*, 2002). The shedding activity of ADAM17 is known to be triggered by phosphorylation. Activation upon phosphorylation on Thr-735 was first described by Diaz-Rodriguez *et al*, who identified extracellular signal-regulated kinase as modifying enzyme (Diaz-Rodriguez, Montero *et al.*, 2002). Recently, in the context of EGFR-dependent cell proliferation, ADAM17 activation was shown to be mediated by phosphorylation on Ser-819 and/or Thr-735, and the latter site was described to be modified by p38 MAP kinase (Xu and Derynck, 2010). Furthermore, dephosphorylation of Ser(P)-791 was linked with the active form of the metalloproteinase (Xu and Derynck, 2010).

The importance of ADAM17 and other metalloproteinases was widely recognized upon their identification as cleaving enzymes of all EGFR ligands in cell culture. ADAM17 was identified as major convertase of epiregulin, transforming growth factor α, amphiregulin, and heparin-binding EGF-like growth factor (HB-EGF) (Sunnarborg, Hinkle *et al.*, 2002; Hinkle, Sunnarborg *et al.*, 2004; Sahin, Weskamp *et al.*, 2004; Blobel, 2005). The essential role of ADAM17 for the transactivation of the EGFR *in vivo* was demonstrated by the analysis of ADAM17 knockout mice that exhibited severe lethal defects similar to those of EGFR knockout mice (Peschon, Slack *et al.*, 1998). Notably, in earlier work, EGFR transactivation had been discovered as an essential element in GPCR-induced mitogenesis of rat fibroblasts (Daub, Weiss *et al.*, 1996). Upon treatment of cells with the G protein-coupled receptor agonists LPA, endothelin-1 and thrombin, EGFR and its relative receptor tyrosine-protein kinase erbB-2 (HER2) were found to be rapidly phosphorylated on tyrosines indicative of cellular receptor tyrosine kinase activation. Later on, Prenzel *et al.* provided the first evidence for a model of EGFR transactivation relying on GPCR-induced and metalloproteinase-mediated cleavage of proEGF-like growth factor ligands (Prenzel, Zwick *et al.*, 1999). The underlying "triple-membrane-passing-signal" mechanism involves different EGFR ligands, depending on the cell type and the stimulus (Figure 3A). For example, LPA or thrombin stimulation of SCC-9 cells results in the release of the EGFR ligands amphiregulin or HB-EGF , respectively, which are both shedded by ADAM17 in a GPCR ligand-specific manner (Hart, 2004). EGFR tyrosine phosphorylation can be observed upon GPCR ligand

stimulation, and the transactivation process is blocked upon downregulation of ADAM17 levels (Figure 3B and C). The function of this pathway is essential for the development of epithelial cells, including EGFR-mediated survival, proliferation as well as migration. Therefore dysregulation of pathway elements can cause severe pathogenic processes.

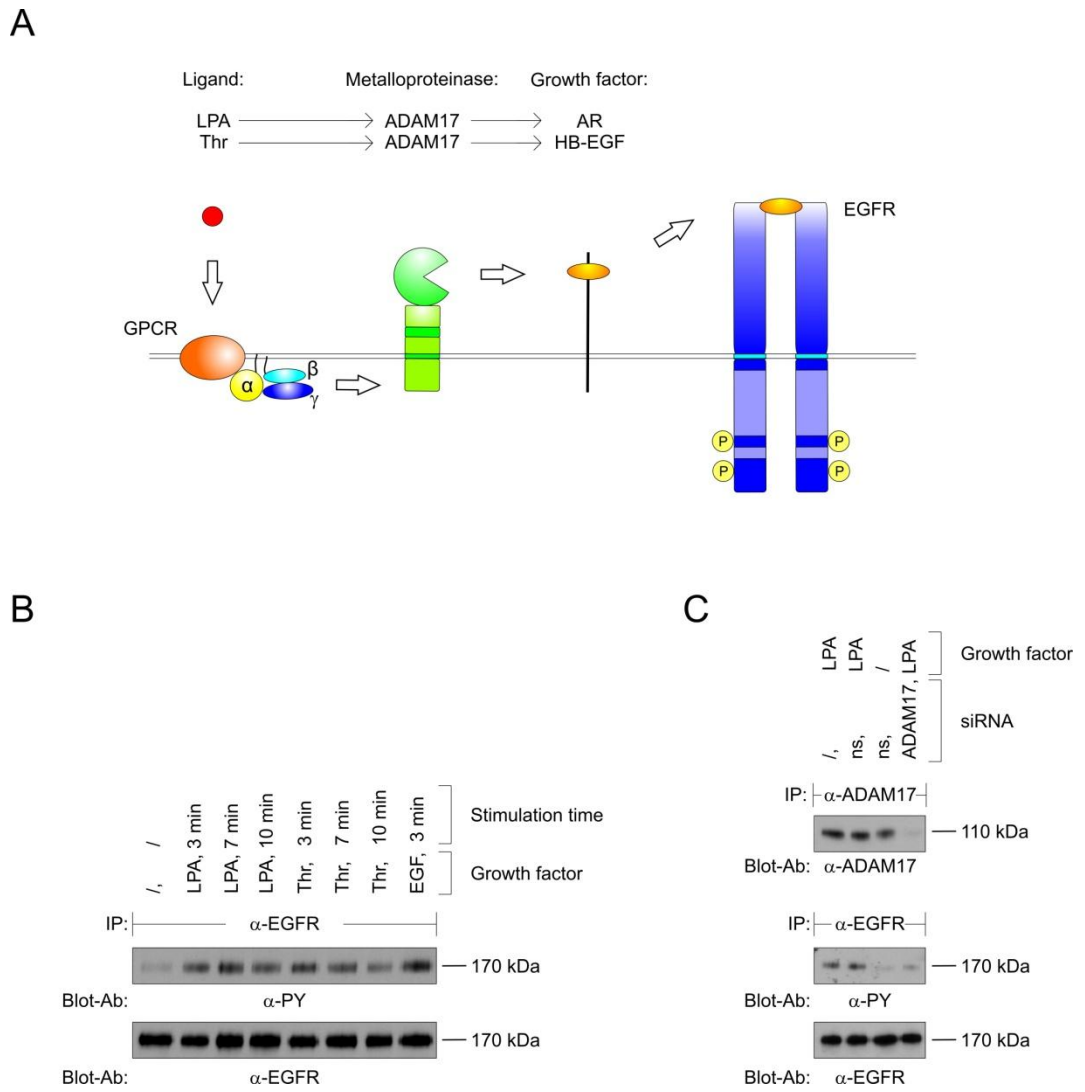

Figure 3: EGFR transactivation in SCC-9 cells upon LPA and thrombin (Thr) stimulation. A, Schematic illustration of the 'triple-membrane-passing-signal' mechanism underlying the EGFR transactivation via GPCR-induced and metalloproteinase-mediated cleavage of proEGF-like growth factor ligands. As indicated, LPA or Thr stimulation of SCC-9 cells result in the ADAM17-mediated cleavage of amphiregulin or HB-EGF, respectively. B, Immunoblot analysis of EGFR tyrosine phosphorylation upon stimulation with LPA, Thr and EGF. In contrast to unstimulated cells, phosphorylation increased upon stimulation with the GPCR ligands LPA and Thr and the direct EGFR ligand EGF. C, Immunoblot analysis of EGFR tyrosine phosphorylation upon stimulation with LPA in ADAM17 downregulated cells.

Whereas phosphorylation of EGFR was induced in the presence of ADAM17, it was drastically reduced in absence of cellular ADAM17 expression. Immunoblot analysis further indicated that EGFR phosphorylation was unaffected by transfection with non-silencing siRNA. AR, amphiregulin; ns, non-silencing siRNA; Thr, thrombin. (Reproduction of published data in SCC-9 cells from Gschwind, Prenzel *et al.*, 2002; Gschwind, Hart *et al.*, 2003)

1.7 Implication of LPA, GPCRs and ADAM17 in cancer

LPA, GPCRs and metalloproteinases function at different stages to trigger processes such as proliferation, migration and survival, which can, in case of imbalanced signalling, turn into uncontrolled growth, invasion and even metastasis. All these incidents are intrinsically related to the onset and progession of human cancer.

For example, elevated LPA levels lead to increased LPA-mediated cell migration and invasion (Mills and Moolenaar, 2003). The pathobiological effect of LPA is caused by the dysregulation of the LPA-synthesizing enzyme autotaxin, which is often overexpressed by cancer cells (Nam, Clair *et al.*, 2000; Kishi, Okudaira *et al.*, 2006; Masuda, Nakamura *et al.*, 2008). This effect is consolidated by elevated secretion of the autotaxin substrate phosphatidylcholin by a variety of different cancer cell lines (Umezu-Goto, Kishi *et al.*, 2002). LPA-dependent hyperproliferation can furthermore be caused by the overexpression of distinct LPA receptors that increase LPA-induced signalling. Out of the three best-characterised receptors LPA1, 2 and 3 the latter two exhibit unusually high expression levels in cancer cells and are therefore of great importance in this context (Mills and Moolenaar, 2003).

Moreover, in various other G protein-coupled receptors numerous mutations were reported that confer constitutive receptor activity and potentially contribute to cancer development. For example, the *mas* oncogene, which encodes a GPCR, was connected to cellular transformation already more than two decades ago (Young, Waitches *et al.*, 1986). Additionally, activating mutations of the thyroid-stimulating hormone and luteinizing hormone receptors have been found in adenomas. Interestingly, these mutations increased receptor activity due to a reduction of receptor ligand specificity (Parma, Duprez *et al.*, 1993; Shenker, Laue *et al.*, 1993). Even some viruses such as the Kaposi's sarcoma-associated herpesvirus encode active forms of GPCRs which have been shown to induce cancer in animal models (Montaner, Sodhi *et al.*, 2003). Besides the importance of GPCRs some of their associated G_{α}-subunits are also involved in cellular transformation and oncogenes such

as *gsp* and *gip2* arise through activating mutations in the $G_{\alpha s}$, $G_{\alpha i2}$ subunits (Landis, Masters *et al.*, 1989; Lyons, Landis *et al.*, 1990).

Furthermore, severe diseases are caused by dysregulation of the metalloproteinase ADAM17 that sheds a large variety of substrates and is therefore involved in a broad spectrum of biological processes. ADAM17 has been implicated in cancer due to its often up-regulated cellular activity in cancer cells that results in increased processing of EGFR ligands and aberrant EGFR signalling. For example, unusually high EGFR signalling and ADAM17 expression levels have been detected in most non-small cell lung cancer (NSCLC) patients. In NCSLC it could be shown that elevated ADAM17 levels correlate not only with EGFR but also HER3 activation, which points to ADAM17 as a therapeutic target at least as valuable as the EGFR (Zhou, Peyton *et al.*, 2006). ADAM17 overexpression has further been found in breast cancer cells, where high expression levels relied on transcriptional as well as post-transcriptional mechanisms and were strongly associated with tumor progression and metastasis (Borrell-Pages, Rojo *et al.*, 2003; McGowan, Ryan *et al.*, 2007). Moreover, several other types of cancer exhibit elevated levels of the metalloproteinase, including human colorectal tumors (Merchant, Voskresensky *et al.*, 2008), pancreatic ductal carcinoma (Ringel, Jesnowski *et al.*, 2006), prostate cancer (Karan, Lin *et al.*, 2003), ovarian cancer (Tanaka, Miyamoto *et al.*, 2005) and oral squamous cell carcinoma (Takamune, Ikebe *et al.*, 2007). The strong correlation of elevated LPA levels, constitutively active GPCRs, ADAM17 overactivity and increased EGFR signalling with cancer induction and progression emphasizes the importance to fully understand the LPA-induced and metalloproteinase-mediated EGFR transactivation process. To learn more about the underlying signalling mechanisms and regulation processes, highly sensitive analysis techniques are required.

1.8 Mass spectrometry

1.8.1 Mass spectrometry-based proteomics

Mass spectrometry (MS)-based techniques applied in biological studies aim to identify and analyse the proteome of a cell, tissue or body fluid. Herein, the proteome is defined as the collection of all proteins and their modifications present in a given state. Analysis techniques covering such complex issues in a comprehensive manner were so far mainly restricted to gene expression analysis based on high throughput microarrays. In comparison, the field of cellular biochemistry was dominated by classical antibody-based techniques such as western

blot analysis as well as protein-array and ELISA technologies, which require a certain *a priori* knowledge about the proteins to be examined and are furthermore mostly restricted to a certain number of proteins to be analysed. In contrast, large-scale and global proteomic studies of cellular biochemistry are enabled by the application of mass spectrometry, which allows the unbiased identification and characterisation of hundreds to thousands of cellular proteins within one study.

Such MS-based approaches encompass several steps, including 1) extraction, fractionation and/or enrichment of protein and/or proteolytically derived peptide mixtures, 2) peptide separation and ionisation, 3) measurement and collection of mass spectra and 4) analysis of the obtained data.

After extraction from biological material, proteins have to be fractionated and digested in a first step. Therefore, protein mixtures are either separated by one-dimensional polyacrylamide gel electrophoresis (1D PAGE) followed by 'in-gel' digestion (Shevchenko, Tomas *et al.*, 2006) or alternatively protein mixtures are digested in solution (Link, Eng *et al.*, 1999; Washburn, Wolters *et al.*, 2001). Depending on the complexity of the sample the latter approach often necessitates additional separation steps, which are e.g. based on ion exchange chromatography on the peptide level. Prior to analysis, purified peptides have to be ionised and transferred into the gas-phase, which is mainly achieved either by matrix-assisted laser desorption/ionisation (MALDI) or electrospray ionisation. While in the first method peptides are embedded in a matrix and ionisation is triggered by pulsed laser beams, the second method relies on peptide separation on a nanoscale reversed phase chromatography column and subsequent ionisation of the eluting peptides by electrospray ionisation. Peptide ions are then directly transferred into the vacuum of the mass spectrometer. Peptide analysis is based on the measurement of peptide mass, intensity (for quantitative information) and fragmentation products. While the mass and intensity of peptides are measured in the MS mode of the MS instrument, peptide fragments are detected in the MS/MS mode upon prior fragmentation of the peptide ions. Fragmentation is for example triggered by collision with an inert gas at low pressure, called collision-induced dissociation (CID), or resonant excitation by an electric field. Further fragmentation techniques are higher energy collision dissociation (HCD) (Olsen, Macek *et al.*, 2007; Olsen, Schwartz *et al.*, 2009), electron capture dissociation (ECD) (Zubarev, Horn *et al.*, 2000) and electron transfer dissociation (ETD) (Syka, Marto *et al.*, 2004). MS and MS/MS modes can be carried out in the same mass analyser or, such as for hybrid mass spectrometers, in different mass analysers of the same instrument, with the resulting spectra acquired in both modes essential for peptide

identification. For MS applications in proteomics, mainly two configurations of mass spectrometers are used as implemented in quadrupole time-of-flight (TOF) instruments and hybrid linear ion trap-orbitrap instruments. These two instrument types differ in the way mass spectra are obtained. In TOF instruments, peptide ions are separated by their time-shifted arrival at the detector. In contrast, orbitrap mass analysers measure the frequency of peptide ions oscillating in the trap and mass spectra are obtained by Fourier transformation (Domon and Aebersold, 2006; Choudhary and Mann, 2010). Finally, for data analysis, the peptide mass and list of fragment masses of each peptide are searched against a protein sequence database, which allows the identification of peptides and proteins they are originating from. Beyond this qualitative aspect of protein identification, MS analysis is further applicable to quantitative comparisons.

1.8.2 Quantitative proteomics

Quantitative proteomics serves to directly compare protein levels in two or more different biological states. Due to its ability to accurately quantify up to several thousands of distinct proteins, quantitative MS is far more powerful than classical protein analysis techniques. Differential quantitative MS analysis requires the introduction of distinguishable isotopes into the proteomes of the cell populations or tissues to be compared. The applied labelling techniques are either based on the incorporation of isotopic labels through normal protein biosynthesis, named metabolic labelling (Ong and Mann, 2005), or the covalent addition of chemical groups as performed in a variety of chemical isotope labelling strategies (Leitner and Lindner, 2006). Whereas the first technique depends on living cells for metabolic incorporation, the second group of techniques can be applied to lysates derived from cell populations as well as from extracted tissues.

One example of metabolic labelling is stable isotope labelling by amino acids in cell culture (SILAC), which most commonly uses arginine and lysine labelled with stable, non-radioactive ^{2}H, ^{13}C and/or ^{15}N isotopes (Figure 4A). Due to the use of three different combinations of isotopic variants, which are Arg0/Lys0, Arg6/Lys4 and Arg10/Lys8, a maximum of three different conditions can be comparatively evaluated in an individual SILAC experiment. Further multiplexing is possible by merging quantitative datasets from, for example, two triple labelling experiments that have one shared condition as a common reference. Upon full incorporation of the labelled amino acids, the digestion of proteins with

trypsin that cleaves after arginine and lysine residues, results in peptides containing labelled arginine or lysine at their carboxy-termini. Light and heavy states of the same peptide can then be distinguished in the MS mode due to the defined mass offsets of the introduced amino acids (Figure 4A). The corresponding intensities of labelled peptides directly provide a quantitative measure of peptide abundance in both states. The successful use of the SILAC technique is not restricted to cell culture and has already been demonstrated in mouse models (Kruger, Moser *et al.*, 2008) and human tumour tissues (Geiger, Cox *et al.*, 2010). A great advantage of SILAC is the early mixing of differentially labelled samples which avoids quantitative errors introduced during further fractionation and preparation steps (Ong, Blagoev *et al.*, 2002; Mann, 2006). In contrast, chemical labelling strategies typically introduce isotopic labels at a very late stage of sample processing and therefore require separate processing steps of samples prior to the labelling step.

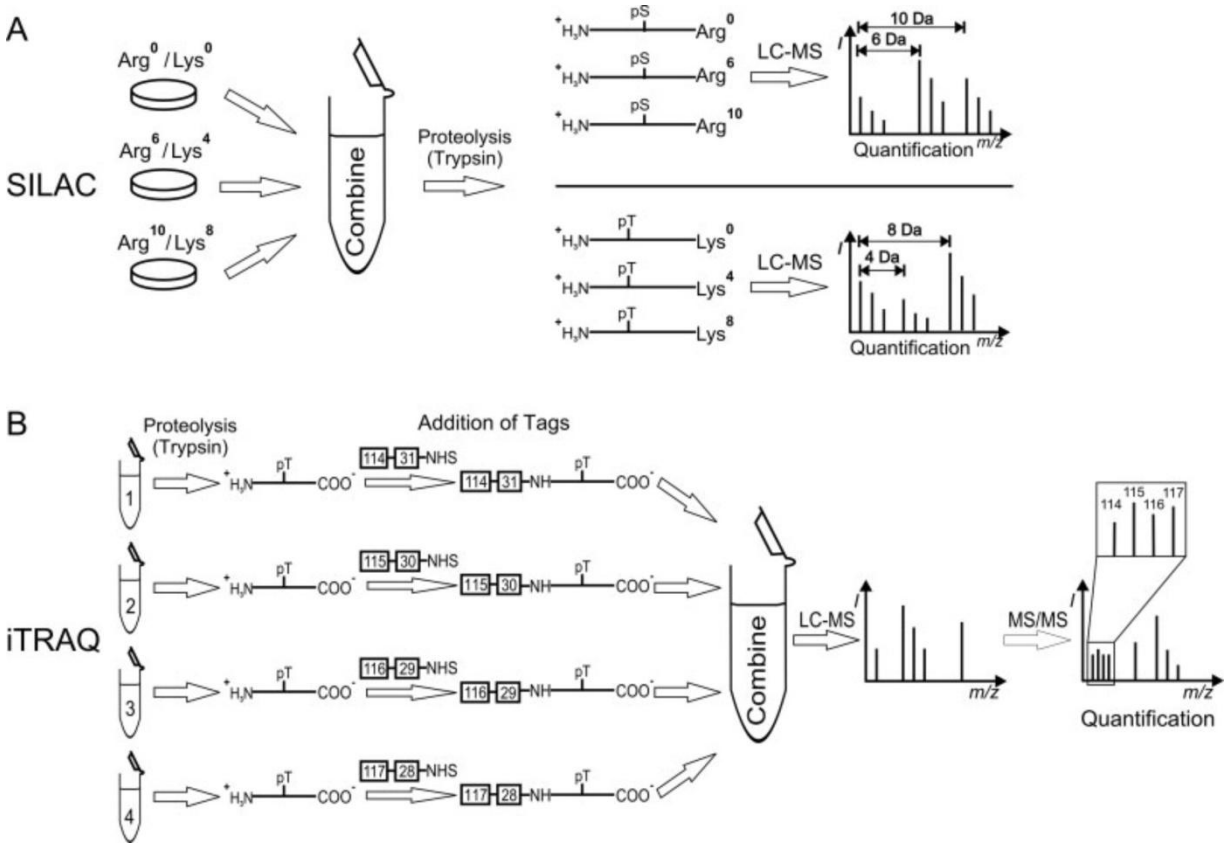

Figure 4: Two popular labelling strategies, SILAC and iTRAQ, in quantitative proteomics. A, Schematic illustration of SILAC-based quantitation. Metabolic labelling with isotope-containing forms of arginine and lysine enable the direct comparison of up to three different states in an individual experiment. Lysates of the differentially labelled cell populations can be combined directly after cell lysis and upon subsequent tryptic digestion and measurement, defined mass shifts of the labelled peptide triplets in MS

scans allow for quantitative evaluation. B, Schematic workflow for the labelling process with iTRAQ reagents. Up to four different samples are chemically labelled with four isobaric tags and are combined at the end of sample preparation. Due to isobaric tags differentially labelled peptides are not distinguishable in MS scans but become quantitatively comparable upon peptide fragmentation in MS/MS scans due to the release of differentially labelled reporter groups. (Illustration from Schreiber, Mäusbacher *et al.*, 2008)

The currently most popular chemical labelling strategy is based on an isobaric tag for relative and absolute quantification (iTRAQ) (Figure 4B). Typically, four different isobaric tags are coupled to the N-terminus of peptides and the ε-amino group of lysine residues via N-hydroxysuccimide (NHS) chemistry. The tags possess identical masses but differ in the reporter and balancer groups they consist of. Due to the fact that the groups of every tag add up to a constant mass the differentially labelled peptides are not distinguishable in MS survey scans, however the differential labelling is apparent in MS/MS scans upon peptide fragmentation. Due to the use of four different reporter ion masses in the range of 114.1 to 117.1 Da this technique enabled the quantitative comparison of four states (Ross, Huang *et al.*, 2004), which was recently further increased by the introduction of eight different reporter ion masses (Pierce, Unwin *et al.*, 2008).

Besides the mentioned techniques, several other labelling strategies, for example with isotope-coded affinity tags (ICAT), tandem mass tags (TMT), metal coded tags (MeCAT), further N-terminal labelling strategies and even label-free quantitative analysis have been applied. However, SILAC and iTRAQ are the most common strategies for metabolic and chemical labelling, respectively, and have also been applied for quantitative analysis of PTMs such as phosphorylations.

1.8.3 Phosphoproteomics

Phosphorylation is the most common reversible posttranslational modification and especially interesting due to its fundamental role in all signalling events. The field of MS-based PTM analysis currently focuses on phosphoproteomic studies (Gruhler, Olsen *et al.*, 2005; Olsen, Blagoev *et al.*, 2006; Christensen, Kelstrup *et al*, 2010.; Olsen, Vermeulen *et al.*, 2010) although modifications such as acetylation, methylation, glycosylation and ubiquitylation are also amenable to investigation. The so far largest MS-based phosphoproteome study identified 20,443 phosphosites in the human HeLa cell line (Olsen, Vermeulen *et al.*, 2010),

whereas the other modifications mentioned above are detected with a by comparsion much lower number of sites, namely 3,600 acetylated, 141 O-GlcNAc-glycosylated, 110 ubiquitylated and 59 methylated sites corresponding to the largest MS studies in the respective fields (Peng, Schwartz *et al.*, 2003; Ong, Mittler *et al.*, 2004; Choudhary, Kumar *et al.*, 2009; Wang, Udeshi *et al.*, 2010). This is due to the frequency of these distinct modifications as well as their stability during sample preparation and MS analysis. In comparison to the time-consuming characterisation of phosphorylation events by classical methods, which was done by *in vitro* or *in vivo* labelling with radioactive ^{32}P-phosphate, phosphopeptide mapping and peptide sequencing by Edman degradation, often combined with mutational analysis to localise and verify the modified residue(s) (van der Geer and Hunter, 1994; Johnson and Hunter, 2005), MS is a fast and highly specific method to detect phosphorylation events and PTMs in general (Jensen, 2006; Witze, Old *et al.*, 2007). Furthermore, MS analysis enables the detection of yet unknown phosphorylation sites, whereas *a priori* knowledge about phosphosite localisation is required to generate and perform analyses with phosphoepitope-specific antibodies. The detection of phosphorylation events in MS analysis relies on the distinct mass the phosphate group adds to a peptide, which results in a mass shift in the MS scan compared to the unmodified peptide species. The subsequent MS/MS scan then often detects sequence-informative fragment ions that allow localising the modification to a single amino acid. Due to the fact that most phosphorylations occur in a substoichiometric manner and hence phosphorylated as well as unphosphorylated peptide forms are present in the same sample, database searches are more complex as they have to match acquired spectra against many more possible peptide forms. Algorithms including modified peptide identification, the calculation of modification site probabilities as well as quantitative evaluation of the detected phosphorylations are implemented in software suites such as MaxQuant (Cox and Mann, 2008; www.maxquant.org). Although MS analysis on state-of-the-art instruments in combination with sophisticated identification and quantitation algorithms is highly sensitive and accurate, modified peptides constitute only a minority of all peptides and thus need to be enriched for proteome-wide modification analysis (Zhao and Jensen, 2009). Phosphorylated peptides are most commonly enriched by metal affinity complexation of their phosphogroups, which can be achieved with immobilised metal ions such as Fe^{3+} and Ga^{3+} or metal oxides such as TiO_2 and ZrO_2 (Macek, Mann *et al.*, 2009). Such enrichment techniques enhance the detection of phosphopeptides in MS analysis, while their identification in combination with quantitative analysis enables the extraction of a subset of regulated sites. Such phosphosites, which are e.g. regulated due to altering growth

conditions or external stimulation with growth factors, are typically the most interesting as they are likely to be functionally important in the biological process of interest.

1.9 Aim of this PhD thesis

The LPA-induced transactivation of the EGFR has been discovered in the late 1990s and further studies uncovered its great impact on a variety of different pathways and several biological processes. Moreover, both elevated LPA levels and aberrant EGFR signalling have been implicated in the onset and progression of human cancers. Consequently, proteins involved in early LPA signalling are valuable targets for drug development. However, the underlying mechanisms of LPA-triggered EGFR transactivation and LPA signalling in general are still incompletely understood.

Therefore, the aims of this thesis were to contribute to the analysis of the LPA-induced and ADAM17-mediated EGFR transactivation and, additionally, to chart the numerous effects LPA-induced signalling evokes on the level of cellular protein phosphorylation. Experimentally, both scientific issues should be addressed in an unbiased way by SILAC-based quantitative proteomic and phosphoproteomic studies. Furthermore, the first part focuses on the establishment of an approach to detect yet unknown ADAM17-binding proteins possibly involved in the transactivation process, while the second part concentrates on temporal LPA-induced phosphorylation changes in the cell surface sub-proteome as well as the entire proteome of a cancer cell line. Thereby, this study aims to shed light on signalling and phosphoregulation underlying already described biological effects of LPA as well as to find and evaluate new regulatory mechanisms.

2. Materials and Methods

2.1 Materials

2.1.1 Cell line

For all described experiments the squamous cell carcinoma cell line SCC-9 was used, which was originally obtained from the American Type Culture Collection.

2.1.2 Antibodies

Name	Species	Application	Dilution	Purchased from
Primary antibodies				
α-Wnk1	rabbit	Western blot	1:1000	Cell Signalling Technology
α-EGFR	rabbit	Western blot	1:1000	Cell Signalling Technology
α-EGFR Tyr(P)-1173	rabbit	Western blot	1:1000	Cell Signalling Technology
α-tubulin	mouse	Western blot	1:10000	Sigma
α-Tyr(P) 4G10	mouse	Western blot	1:5000	homemade
α-ADAM17	rabbit	Western blot	1:1000	Chemicon
α-EGFR	mouse	IP	1 µg/mg cell lysate	homemade
α-ADAM17 (343)	mouse	IP	30 µg/mg cell lysate	homemade
Secondary antibodies				
α-mouse	goat	Western blot	1:10000	Sigma
α-rabbit	goat	Western blot	1:14000	Dianova

2.1.3 siRNA-oligonucleotides

GL2	sense: 5’ CGUACGCGGAAUACUUCGAtt 3’ antisense: 5’ UCGAAGUAUUCCGCGUACGtt 3’	Dharmacon
ADAM17 (1)	sense: 5’ AGUUUGCUUGGCACACCUUtt 3’ antisense: 5’ AAGGUGUGCCAAGCAAACUtt 3’	Dharmacon
ADAM17 (2)	sense: 5’ AGUAAGGCCCAGGAGUGUUtt 3’ antisense: 5’ AACACUCCUGGGCCUUACUtt 3’	Dharmacon

ADAM17 (3)	sense: 5’ AGCCCUGUACAGUAGGAUUtt 3’	
	antisense: 5’ AAUCCUACUGUACAGGGCUtt 3’	Dharmacon

Silencer select negative control siRNA #1	Ambion
Wnk1 s35233	Ambion
Wnk1 s35234	Ambion

2.1.4 Media and additives

DMEM	Gibco, Eggenstein
DMEM without arginine and lysine	Gibco, Eggenstein
Ham’s F12	Gibco, Eggenstein
Ham’s F12 without arginine and lysine	Gibco, Eggenstein
FBS	Gibco, Eggenstein
FBS (dialysed)	SAFC Biosciences, Hamburg
L-Glutamin	Gibco, Eggenstein
Sodiumpyruvat	Gibco, Eggenstein
Hydrocortisol	Sigma, Taufkirchen
Penicillin/Streptomycin, 100x	PAA, Germany
L-arginine (Arg0)	Gibco, USA
L-Arginine: HCl, U-$^{13}C_6$ $^{14}N_4$	Cambridge Isotope Laboratories, USA
L-Arginine: HCl, U-$^{13}C_6{}^{15}N_4$	Cambridge Isotope Laboratories, USA
L-Lysin (Lys0)	Gibco, USA
L-Lysine: 2 HCl, $^{2}H_4$	Cambridge Isotope Laboratories, USA
L-Lysine: 2 HCl, U-$^{13}C_6{}^{15}N_2$	Cambridge Isotope Laboratories, USA

2.1.5 Commonly used buffers

Laemmli buffer (3x)	100 mM Tris/HCl pH 6.8
	3.0 % SDS
	45.0 % Glycerol
	0.01 % Bromphenol blue
	7.5 % ß-Mercaptoethanol

NET	50.0 mM Tris/HCl pH 7.4 5.0 mM EDTA 0.05 % Triton X-100 150.0 mM NaCl
PBS	137.0 mM NaCl 27.0 mM KCl 80.9 mM Na_2HPO_4 1.5 mM KH_2PO_4 pH 7.4
SD-Transblot	50.0 mM Tris/HCl pH 7.5 40.0 mM Glycine 20.0 % Methanol 0.004 % SDS
"Strip" buffer	62.5 mM Tris/HCl pH 6.8 2.0 % SDS 100.0 mM β-Mercaptoethanol

2.1.6 Chemicals, reagents and other material

Phosphatase Inhibitor Cocktail 1 + 2	Sigma, Taufkirchen
Phenylmethanesulfonyl fluoride (PMSF)	Sigma, Taufkirchen
Sodiumorthovanadat	Sigma, Taufkirchen
Sodiumfluoride p.a.	Merck, Darmstadt
Calyculin A	Alexis Biochemicals
Aprotinin	Alexis Biochemicals
Leupeptin	Alexis Biochemicals
Acetonitrile for HPLC	Sigma, Taufkirchen
Ammoniumbicarbonate	Sigma, Taufkirchen
Ammonium hydroxide	Merck, Darmstadt

Antioxidance	Invitrogen, Eggenstein
2,5-Dihydroxybenzoic acid	Fluka, Taufkirchen
DTT	Sigma, Taufkirchen
Iodoacetamide	Sigma, Taufkirchen
N-octosylglucoside	Roche, Mannheim
Lys-C	WAKO, Neuss
Trypsin (seq. grade modified)	Promega, USA
Urea	Merck, Darmstadt
Thio urea	Invitrogen, Eggenstein
K_2HPO_4	Roth, Karlsruhe
KH_2PO_4	Roth, Karlsruhe
Gelatine	Sigma, Taufkirchen
NaCl	Sigma, Taufkirchen
KCl	Sigma, Taufkirchen
$MgCl_2$	Sigma, Taufkirchen
$MnCl_2$	Sigma, Taufkirchen
$CaCl_2$	Sigma, Taufkirchen
EDTA	Merck, Darmstadt
EGTA	Sigma, Taufkirchen
Nonidet P-40	Sigma, Taufkirchen
HEPES	Roth, Karlsruhe
Ponceau S	Sigma, Taufkirchen
SDS (Sodium dodecyl sulfate)	Roth, Karlsruhe
Batimastat	British Biotech, UK
Acrylamide/bisacrylamide 37.5:1	Serva, Heidelberg
Ammoniumperoxodisulfate (APS)	Bio-Rad, München
N,N,N',N'-tetramethylethylenediamine (TEMED)	Serva, Heidelberg
LPA	Sigma, Taufkirchen
Lipofectamine 2000	Invitrogen, Eggenstein
Sepharose CL-4B	Amersham Pharmacia, Freiburg
Protein A-Sepharose	Amersham Pharmacia, Freiburg
Protein G-Sepharose	Amersham Pharmacia, Freiburg
Wheat germ agglutinin (WGA)	Sigma, Taufkirchen

Lentil	Sigma, Taufkirchen
Concanavalin A	Sigma, Taufkirchen

2.1.7 Kits

BCA assay	Pierce, Sankt Augustin
Bradford assay	Biorad, München
ECL Kit	PerkinElmer, Köln
Colloidal staining kit	Invitrogen, Eggenstein

2.1.8 Instruments

LTQ-Orbitrap MS 2.2	Thermo, Dreieich
Proxeon Easy-nLC VI 2.0	Proxeon, Denmark
Vacuum Concentrator 5301	Eppendorf, Hamburg
Thermomixer comfort	Eppendorf, Hamburg
ÄKTA Explorer	GE Healthcare
Polysulfoethyl A 250*9.4mm 5µm 200Å	PolyLC
Ressource S 1 ml	GE Healthcare
XCell SureLock^{TM} Mini Cell	Invitrogen, Eggenstein
Incubator HeraCell 150	Thermo, Dreieich
Z1 cell and particle counter	Beckman Coulter, USA
Axiovert 135	Carl Zeiss, Göttingen
Observer A1	Carl Zeiss, Göttingen
Digital camera Visitron System	Visitron Systems, Puchheim
Centrifuge 5415 R	Eppendorf, Hamburg

2.1.9 Software and online tools

XCalibur 2.0	Thermo, Dreieich
Unicorn 5.1	Thermo, Dreieich
MaxQuant Suite	MPI of Biochemistry dept. Mann
Sigmaplot 10	Systat Software, Erkrath
Excel 2007	Microsoft, Unterschleißheim

R 2.8	www.r-project.org
DAVID	www.david.abcc.ncifcrf.gov
MeV 4.1 / 4.2	www.tm4.org/mev/
Motif-x	www.motif-x.med.harvard.edu
Phosphosite	www.phosphosite.org
String	www.string.embl.de

2.2 Methods

2.2.1 Cell culture techniques

2.2.1.1 Cell culture and LPA stimulation

SCC-9 cells were cultured in a 1:1 mixture of F12 Ham (Invitrogen) and Dulbecco's modified Eagle's medium (DMEM, Invitrogen) supplemented with L-glutamine (2 mM, PAA Laboratories), sodium pyruvate (1 mM, Invitrogen), hydrogencortisone (0.4 mg/l, Sigma), 1% penicillin/streptomycin (PAA Laboratories) and 10 % fetal bovine serum (FBS, Invitrogen). Cell culture conditions were 37 °C and 7% CO_2 in a humidified atmosphere. For SILAC experiments cells were cultured in medium containing either unlabelled L-arginine (Arg0) at 42 mg/l and L-lysine (Lys0) at 71 mg/l or equimolar amounts of the isotopic variants L-[U-$^{13}C_6$,$^{14}N_4$]arginine and L-[$^{2}H_4$]lysine (Arg6, Lys4), or L-[U-$^{13}C_6$,$^{15}N_4$]arginine and L-[U-$^{13}C_6$,$^{15}N_2$]lysine (Arg10, Lys8) (Cambridge Isotope Laboratories or Sigma) for at least six cell doublings. For LPA stimulation, cells were seeded in 10-cm dishes (Falcon) in case of SILAC-based experiments and prior to treatment with 10 µM LPA (Sigma) serum-starved for 48 h with a further exchange of media without FBS 16 h before lysis.

2.2.1.2 Cell lysis

The stimulation of cells was stopped by removing media containing LPA and directly lysing the cells on ice. For the projects based on the lectin-enriched subproteome and ADAM17 immunoprecipitates ice-cold lysis buffer consisting of 50 mM Tris pH 7.5, 150 mM NaCl, 1% Nonidet P-40, 0.1% sodium deoxycholate, 1 mM EDTA, 10 µg/ml aprotinin, 10 µg/ml leupeptin, 1 mM phenylmethylsulfonylfluorid (PMSF), 10 mM sodium fluoride, 2.5 mM sodium orthovanadate, 50 ng/ml calyculin A, 5 µM batimastat, 1:100 phosphatase inhibitor cocktails 1 and 2 (Sigma), was used. After at least 15 min incubation on ice lysates of each labelled cell population were collected separately and pre-cleared by centrifugation at 4900 g and 4 °C for 15 min and subsequent filtration through a 0.45-µm mixed cellulose ester filter membrane (Millipore). Protein concentrations were determined by BCA-assay (Pierce). Cells for the LPA time-course project were lysed with urea-containing lysis buffer (8 M Urea, 75 mM NaCl, 50 mM Tris pH 8.2, 1 mM EDTA, 1 mM EGTA, 10 µg/ml Aprotinin, 10 µg/ml Leupeptin, 1 mM PMSF, 10 mM NaF, 2.5 mM Na_3VO_4, 50 ng/ml Calyculin A, 1% phosphatase inhibitor cocktail 1 and 2 (Sigma)) and removed from the plates by scrapping.

Lysates were sonicated three times for one minute on ice, pre-cleared as described above and protein concentrations determined by Bradford assay (Biorad). Lysates of the unstimulated, 3 min, 10 min LPA treated cells (part A) and 10 min, 30 min and 90 min LPA treated cells (part B) were then pooled at equal protein amounts, respectively.

2.2.2 Affinity chromatographies

2.2.2.1 Lectin-affinity pull-down

Equal protein amounts of the differentially SILAC-encoded lysates were adjusted to the same volume and then subjected to pre-clearing with CL4B Sepharose beads (Sigma) for 2.5 h at 4 °C on a rotating wheel. Pre-cleared lysates were used for affinity purification with lectin beads. Therefore, concanavalin A, wheat-germ agglutinin (WGA) and lentil agarose beads (all obtained from Sigma) were mixed at a ratio of 1:1:2 and then washed with lysis buffer and metal ion-containing buffer (1M NaCl, 5 mM $MgCl_2$, 5 mM $MnCl_2$, 5 mM $CaCl_2$). For each labelled lysate six affinity pull-downs were carried out in 1.5 ml Eppendorf tubes, with each containing 4 mg (4.7 mg) of lysate incubated with 100 µl mixed lectin beads in the first (second) biological replicate experiment on a rotating wheel at 4 °C overnight. Afterwards, lectin beads were washed once with lysis buffer and twice with detergent-free buffer. Bound proteins were eluted with 0.3x LDS-buffer (Invitrogen), 50 mM DTT in H_2O dest. for 10 min at 70 °C. Subsequently, all elution fractions from all incubations with the different SILAC lysates were combined.

2.2.2.2 ADAM17-Immunoprecipitation

SILAC-labelled lysates derived from seven 10-cm dishes per labelled cell population were subjected to two consecutive ADAM17 immunoprecipitations. According to the experimental setup two IPs were carried out simultaneously for the low and high label and four IPs were performed for the middle label. For each IP 78.7 µg of ADAM17 343-antibody were added to 40 µl of Sepharose G beads and 400 µl of lysis-buffer and incubated on a rotating wheel at 4 °C for 2 h. After pre-coupling of the antibody beads were washed once with lysis buffer and then incubated with 1 mg of lysate for 3 h at 4 °C on a rotating wheel. During this incubation step pre-coupling of antibodies to the beads was performed as described for the second round of IPs. After the first round of IPs, lysates were transferred to the freshly prepared beads for a

second incubation again for 3 h at 4 °C on a rotating wheel. Whenever first and second round of incubations were finished beads were washed once with lysis-buffer (50 mM Tris pH 7.5, 150 mM NaCl, 1% Nonidet P-40, 0.1% sodium deoxycholate, 1 mM EDTA) and twice with wash-buffer, which equaled the lysis buffer but did not contain any detergents. Bound proteins were eluted with 50 µl LDS-buffer per reaction and in-gel digested while further processing.

2.2.2.3 EGFR-Immunoprecipitation

For immunoprecipitation of EGFR, 1.5 µg of anti-EGFR antibody was added together with 30 µl of protein A-Sepharose (GE Healthcare) to ~300 µg lysate and incubated over night at 4 °C on a rotating wheel. Precipitates were washed three times with HNTG buffer (20 mM HEPES, pH 7.5, 150 mM NaCl, 0.1% Triton X-100, 10% glycerol, 10 mM tetra-sodium-pyrophosphate), and precipitated proteins were eluted with 1.5x SDS sample buffer (2x stock: 65 mM Tris/HCl pH 6.8, 3% SDS, 30% glycerol, 0.01% bromphenol blue, 5% 2-mercaptoethanol).

2.2.3 Molecular biological methods

2.2.3.1 siRNA transfection

SCC-9 cells were seeded in 10-cm plates with a confluency of 70-80% and the next day transfected with two different siRNAs directed against Wnk1 (Ambion, s35233, s35234) and silencer select negative control siRNA #1 (Ambion), respectively. For downregulation of ADAM17 cells were transfected with a 1:1:1 mixture of three different siRNAs directed against ADAM17 (Dharmacon) and GL-2 siRNA (Dharmacon) for non-silencing control. GL-2 siRNA is directed against non-human luciferase mRNA. The transfection was carried out with the transfection reagent Lipofectamine™ 2000 (Invitrogen) and performed as recommended by the manufacturer. Briefly, 600 pmol siRNA in a volume of 30 µl and 30 µl of transfection reagent were separately incubated with 720 µl of OptiMEM (Invitrogen) for 5 min at 25 °C, then combined and incubated for a further 30 min incubation step at 25 °C. Afterwards, the transfection solution was added to the cells to a final volume of 6 ml OptiMEM (Invitrogen). Cells were washed with PBS after 4 h and medium was replaced by normal F12 Ham/DMEM medium for SCC-9 cell culture.

2.2.3.2 Migration and proliferation assay

24 h after transfection in 10-cm dishes cells were trypsinated and seeded into 12-wells with a confluency of 100% for the scratch assay and with a confluency of 25% for the proliferation assay. On the following day cells were starved with medium lacking FBS for another 24 h. Scratches were done with 200 µl pipette tips and afterwards cells were washed four times with PBS to remove loose or dead cells. Cells were then incubated either with starvation medium with or without 10 µM LPA. Pictures were taken immediately after scratching and 22 h later. The distances between the boundaries of the scratches were measured with Adobe Photoshop CS, version 8.0.1. To check for proliferation in parallel to the scratch assay, transfected cells in replicate dishes were counted at the time of the scratch or treated with LPA for 22 h as performed in the scratch assay and then counted. At the same time the knock-down efficiency for Wnk1 was monitored by immunoblot analysis.

2.2.4 Protein analytical methods

2.2.4.1 Sodium dodecyl sulfate-polyacrylamide gel electrophoresis (SDS-PAGE)

Proteins were separated in 7.5% sodium dodecyl sulfate-polyacrylamide gels. The 7.5% resolving gel (lower gel) was overlaid with a 4% stacking gel (upper gel). Samples were loaded together with a homemade protein standard consisting of the following proteins (purchased from Sigma) with their respective molecular weights: myosin (205 kDa), beta-galactosidase (116.25 kDa), phosphorylase b (97.4 kDa), BSA (66.2 kDa), ovalbumin (42.7 kDa), carboanhydrase (29 kDa), trypsin-inhibitor (21.5) and lysozym (14.4 kDa). Electrophoresis was performed in 1x tris-glycin-SDS buffer under a constant power of 24 mA until the loading dye reached the bottom of the resolving gel.

Lysates derived from SILAC labelled cells were reduced to a suitable amount in a vacuum concentrator and then separated by electrophoresis on a 10% NuPAGE Novex Bis-Tris gel (Invitrogen). Electrophoresis was carried out at 200 V in 1x NuPAGE MOPS SDS running buffer (Invitrogen) supplemented with 0.1% NuPAGE antioxidant (Invitrogen). Proteins of the lectin-enriched subproteome were separated using the whole range of the gel, whereas ADAM17 immunoprecipitates were only separated over half the gel-length.

2.2.4.2 Western blot analysis

Proteins separated on polyacrylamid gels were transferred to a PVDF membrane by the semi-dry blotting method. Six sheets of whatman paper, a nitrocellulose membrane and the gel were equilibrated in SD-transblot solution. Three sheets of whatman paper were overlaid with the membrane, the gel and another three sheets of whatman paper so that the membrane is facing the anode and the gel facing the cathode. The transfer was performed with transblot-SD solution for 2.5 h under a constant current of 0.8 mA/cm^2. After transfer Ponceau S (2 g/l in 2% TCA) staining enabled control of protein transfer and labelling of protein standard bands. The destaining of the membrane and blocking of unspecific protein binding sites was performed by a 1 h incubation with 0.25% gelatine in 1x NET. For immunodetection first antibodies were diluted in 0.25% gelatine in 1x NET and incubated with the membrane under constant horizontal shaking over night at 4°C. Unbound antibodies were removed by washing the membrane four times for 15 min with NET-gelatine solution. Peroxidase-coupled species specific second antibody was diluted in the same solution to an appropriate degree and incubated with the membrane for 1 h at 25 °C. Afterwards, the membrane was washed four times with NET-gelatine solution for 15 min. The detection of specific protein bands was performed with the ECL-kit (Amersham) according to the manufacturer's instructions. The membrane was exposed to X-ray films (Amersham Hyperfilm MP) for different time periods. For further use of the membrane bound antibodies were removed by incubation of the membrane in stripping solution (62.5 mM Tris/HCl pH 6.8, 100 mM β-mercaptoethanol, 2% SDS) at 52 °C for 40 min in a water bath.

2.2.4.3 Colloidal blue staining of polyacrylamid gels

Protein bands in the NuPAGE Novex bis-tris gels were stained with the colloidal blue staining kit (Invitrogen) according to the manufacturer's instructions with the exception that only 50 ml of solutions were utilised for each incubation step. The gel was incubated in fixing solution (50% methanol, 10% acetic acid) for 10 min at RT under constant shaking, then transferred to the staining solution without stainer B for another 10 min incubation step. After addition of stainer B final concentrations in the staining solutions were 20% methanol, 20% stainer A and 5% stainer B. The gel was stained for 3 h at RT and the staining process stopped by exchanging the solution to deionized water. The background of the gel was destained by incubating the gel in deionized water at 4 °C over night.

2.2.4.4 Protein precipitation

Proteins from 20% of the eluate derived by lectin pull-down were chloroform-methanol precipitated according to the Wessel-Fluegge protocol (Wessel and Flugge, 1984) in order to remove detergents. Precipitations were carried out in 1.5 ml Eppendorf tubes and a volume of 150 µl protein solution per tube. All steps were performed at RT. 600 µl methanol was added to the protein solution, briefly vortexed and centrifugated for 10 sec at 20,000 g in a table centrifuge. 225 µl chloroform was added to the sample, followed by another mixing and centrifugation step as described before. After the addition of 450 µl H_2O dest and vigorous mixing samples were sonicated in a water bath and the phases separated during centrifugation for 2 min at 20,000 g. The upper phase was carefully removed and the interphase and lower phase mixed with 450 µl methanol. After 20 min of centrifugation at 20,000 g the remaining organic solvent was completely removed from the precipitated pellet. The protein sample was then subjected to trypsin digestion in solution.

2.2.5 Mass spectrometry sample preparation

2.2.5.1 In-gel digest

According to the molecular weight of colloidal blue stained protein bands in the NuPAGE Novex Bis-Tris gels the lanes were cut into an appropriate number of slices. Afterwards each slice was separately cut into pieces of 1x1 mm and transferred to 1 ml 50% EtOH/25 mM ABC-buffer in 2 ml Eppendorf tubes for destaining. Destaining was performed stepwise, each step including the exchange of solution and incubation on an Eppendorf shaker at RT, 1,000 rpm for 20 min. Gel pieces were then dehydrated in 1 ml 100% ethanol and 10 min incubation steps at RT and 1,000 rpm were repeated in fresh ethanol until gel pieces turned white in colour and possessed a rigid texture. Gel pieces were dried in a vacuum concentrator for 15 min and rehydrated in 10 mM DTT, 50 mM ABC-buffer so that all gel pieces were covered with solution. Samples were incubated at 56 °C, 1000 rpm for 60 min to assure optimal conditions for the reduction of disulfide bonds by DTT. After completely removing the DTT-containing solution the gel pieces were covered with 55 mM IAA in 50 mM ABC-buffer for alkylation at 25 °C, 1000 rpm for 45 min. Due to the light sensitivity of IAA samples were kept in the dark for this incubation step. To wash the gel pieces the IAA-containing solution was completely removed and gel pieces were incubated in 1 ml 50 mM ABC-buffer for 20 min, 1000 rpm at 25 °C. Gel pieces were then dehydrated in 100% ethanol

as described above and again washed in 50 mM ABC-buffer. To prepare the gel pieces for the tryptic digest dehydration was performed in 100% ethanol followed by drying of gel pieces in the vacuum concentrator as already described. Trypsin was added to 50 mM ABC-buffer so that the amount of trysin corresponded to 1/50 of the protein amount and gel pieces were rehydrated in an appropriate amount of the solution. A small amount of 50 mM ABC-buffer was added to cover the gel pieces. The digest was performed at 37 °C, 1000 rpm over night and the following day stopped by acidifying the samples with 2 µl 100% TFA each. Liquids were transferred to fresh Eppendorf tubes and peptides subsequently extracted from the gel matrix by the following incubation steps. The first two extraction steps were carried out with 300 µl 30% ACN, 3% TFA for 10 min at 25 °C, 1000 rpm, followed by incubation in 300 µl 100% ACN. The last step was repeated until all peptides were extracted and the gel pieces turned white in colour and possessed a rigid texture. The acidified trypsin solution of each sample was combined with all supernatants of subsequent extraction steps of the same sample and reduced to 20% of the original volume in a vacuum concentrator. Samples were devided and either subjected to phosphopeptide enrichment or directly loaded on home-made C_{18} stage tips. For immobilization on C_{18} stage tips C_{18} material in 200 µl pipette tips was activated with 50 µl methanol, washed twice with 200 µl 0.5% acetic acid, 0.1% TFA and a 1:1 mixture of the sample with 1% TFA, 5% ACN was subjected to the stage tip. Stage tips were then washed with 200 µl 0.5% acetic acid, 0.1% TFA and stored at 4°C until MS analysis.

2.2.5.2 In-solution digest

Precipitated proteins were resolved in urea buffer (7 M urea, 2 M thiourea, 50 mM Hepes, pH 7.5, 1% n-octyl glucoside). Protein samples derived from the cell lysis with urea-containing lysis buffer were adjusted to 6 M urea and 1.5 M thiourea. All incubation steps were carried out at 25 °C on an Eppendorf shaker at 450 rpm or on a rotating wheel for samples exceeding a volume of 2 ml. Proteins were reduced in a final concentration of 1 mM DTT for 45 min and then alkylated in 5.5 mM IAA for 30 min avoiding light exposure of the samples. Proteins were sequentially digested with Lys-C (Wako) and modified trypsin (sequencing grade, Promega) at an enzyme/substrate ratio of 1/150. Therefore, samples were incubated with Lys-C for 4 h and prior to incubation with trypsin over night diluted 1:4 with H_2O dest. Trypsin activity was stopped by adding TFA to a final concentration of 0.5%. Peptide mixtures could directly be used for phosphopeptide enrichment.

2.2.5.3 Phosphopeptide enrichment with TiO_2 beads

For samples derived from the in-gel digest one incubation step with 5 mg TiO_2 beads (GL Sciences) per sample was performed. Therefore, TiO_2 beads were washed once with 100 µl elution buffer (NH_3 water in 20% ACN, pH 10.5) and equilibrated twice with 200 µl washing buffer (50% ACN, 0.1% TFA). Beads were then loaded with dihydroxybenzoic acid (DHB) by incubation with 100 µl loading buffer (5 g/l DHB in 15% ACN). Samples were adjusted to 5 g/l DHB and incubated with 5 mg TiO_2 beads for 45 min at 25 °C on a rotating wheel. Beads were then washed four times with 1.5 ml washing buffer and bound phosphopeptides were eluted twice with 60 µl elution buffer for 10 min at 25 °C. Eluates were cleared by filtration through C_8 StageTips. To release peptides that might have been retained by C_8 StageTips, filters were further washed with 30 µl 80% ACN, 0.5% acetic acid and the resulting flow-through was combined with the filtered sample. ACN was removed by vacuum concentration, samples were then mixed with an equal volume of 5% ACN, 0.1% TFA and analysed by LC/MS.

For samples derived from the in-solution digest phosphopeptide enrichment was performed by three consecutive incubations with 2.5 mg TiO_2 beads with the previous supernatant fractions contacted with fresh beads in each round of incubation. Preparation of beads and elution of phosphopeptides were carried out as described for phosphopeptide enrichment of in-gel digested samples.

2.2.5.4 Phosphopeptide enrichment with IMAC beads

Phosphopeptides of desalted and lyophilized SCX fractions were enriched by ion metal affinity chromatography. Therefore, 5 µl phos-Select Iron Affinity Gel (Sigma) per sample were equilibrated by washing four times with IMAC binding buffer (40% ACN , 25 mM formic acid) and afterwards diluted 1:4 in the same buffer. Each sample fraction was resolved in 200 µl of binding buffer, adjusted to a pH of ~2.5 if necessary and then incubated with 20 µl of diluted beads for one hour. The incubation reactions were performed in 250 µl tubes under constant shaking (1400 rpm) at 25 °C. Beads were then transferred to C_{18} StageTips. Therefore, C_{18} StageTips had been activated with 50 µl methanol, washed once with 70 µl elution buffer (50% ACN, 0.5% acetic acid) and twice with 70 µl washing buffer (1% formic acid) before. Beads loaded on the StageTips were washed twice with 70 µl binding buffer and once with the same amount of 1% formic acid. The transfer of phosphopeptides from the

IMAC beads onto the C_{18} material was performed by three rounds of incubation with 70 µl of 500 mM K_2HPO_4, pH 7. Remaining salts were removed from StageTips by washing twice with 70 µl 1% formic acid. Prior to analysis with mass spectrometry bound peptides were eluted from the C_{18} material with 30 µl 50% ACN, 0.5% acetic acid. The organic phase was removed in a vacuum concentrator and samples were then adjusted to 2% ACN, 0.2% TFA.

2.2.5.5 Strong cation exchange chromatography

Samples were resolved in 500 µl 30% ACN, 7 mM KH_2PO_4, pH 2.65 and after resolution pH was adjusted to 2.65 with formic acid if necessary. The peptide mixture was loaded on a 250 x 9.4 mm PolySULFOETHYL A column, 200 Å pore size and 5 mm particle size (PolyLC) operated with an Äkta Explorer system (GE Healthcare) at 3 ml/min. Peptides were fractionated over a gradient ranging from 0% to 30% elution buffer (30% ACN, 350 mM KCl, 7 mM KH_2PO_4, pH of 2.65). According to the detected UV absorption (215 nm) fractions were pooled to 14 distinct samples and organic solvent removed by lyophilisation for further processing.

2.2.5.6 Desalting of samples

Samples of the LPA time-course were desalted before and after SCX chromatography with C_{18} SepPac columns (Waters). For desalting of total cell lysate after trypsin digestion as well as of large SCX fractions 500 mg cartridges, otherwise 100 mg cartridges, were used. 100 mg/ 500 mg cartridges were washed with 2 ml/ 9 ml 100% ACN in a first step and 1 ml/ 3 ml 50% ACN, 0.5% HAc in a second step. Equilibration of columns was then performed by subjecting 2 ml/ 9 ml 0.1% TFA. Samples were adjusted to 0.5% TFA, according to a pH of ~2.65 and loaded onto the columns. After peptides had bound, C_{18} material was washed by subsequently loading 2 ml/ 9 ml 0.1% TFA and 1 ml/ 2 ml 0.5% HAc. Peptides were eluted twice with 500 µl/ 1.4 ml 50% ACN, 0,5% HAc and resulting fractions were frozen in liquid N_2 and lyophilised with a Lyovac GT2 (Leybold-Heraeus) machine over night.

2.2.6 Mass Spectrometric Analysis

Peptide samples were analysed by online C_{18} reversed phase nanoscale liquid chromatography (LC)-MS. Using an Agilent 1100 nanoflow system (Agilent Technologies) or Proxeon EASY nLC VI system (Proxeon), samples were injected onto a 15-cm reverse phase, fused silica capillary column (75 µm inner diameter, packed in-house with 3-µm ReproSil-AQ Pur C_{18} beads, Dr. Maisch GmbH). The nano-HPLC system was connected to an LTQ-Orbitrap mass spectrometer (Thermo Fisher Scientific) via a nanoelectrospray ion source (Proxeon Biosystems). Loaded peptides were separated in 140 min runs with a gradient from 5 to 40% ACN in 0.5% acetic acid. The Xcalibur software 2.0 was used in the positive ion mode for data-dependent acquisition on the LTQ-Orbitrap as described (Daub, Olsen *et al.*, 2008). The instrument was re-calibrated in real time by co-injection of an internal standard from ambient air into the C-trap ("lock mass option") (Olsen, de Godoy *et al.*, 2005). Full scan MS spectra were recorded in the orbitrap mass analyser with resolution R=60,000 at m/z=400 after accumulation to a target value of 1,000,000 charges in the linear ion trap. In parallel, the most intense multiple charged ions per cycle were isolated and fragmented in the LTQ part of the instrument. These were up to five and ten of the most intense multiple charged ions for samples of the lectin enriched SCC-9 subproteome and samples of the time-course project, respectively. Multi-stage activation was enabled to activate phosphopeptide-derived neutral loss species at 97.97, 48.99, or 32.66 m/z below the precursor ion for 30 ms during fragmentation (pseudo-MS^3) (Schroeder, Shabanowitz *et al.*, 2004). All raw files acquired in these studies were uploaded to the Tranche file-sharing database (ProteomeCommons.org).

2.2.7 Data processing

MS data were processed and analysed with the MaxQuant software suite version 1.0.11.1 for the lectin enriched subproteome and the version 1.0.13.12 for the LPA time-course project, which both perform peak list generation, SILAC-based quantification, estimation of false discovery rates (FDRs), peptide to protein group assembly as well as data filtration as described (Cox and Mann, 2008). The Mascot search engine (version 2.2.0, Matrix Science) was used to search MS data against the human International Protein Index (IPI) database (version 3.37) containing 69,141 entries to which 175 frequently observed contaminants and reversed versions of all sequences had been added. Carbamidomethyl cysteine was set as fixed modification, whereas oxidized methionine, N-pyroglutamate, N-pyrocysteine, N-

terminal acetylation of proteins and phosphorylation of serine, threonine and tyrosine were selected as variable modifications. For all SILAC triplets detected by MaxQuant pre-search Arg6, Arg10, Lys4 and Lys8 were searched as additional fixed modifications, while all spectra for which the SILAC state of the precursor ion could not be determined were searched with Arg6, Arg10, Lys4 and Lys8 as variable modifications. The initial mass tolerances of the precursor and fragment ions were set to 7 ppm and 0.5 Da, respectively. Enzyme specificity was set to trypsin, accepting cleavage N-terminal to proline and further allowing for cleavage between aspartate and proline. The minimum accepted peptide length was six amino acids and up to three missed cleavages and three isotopically labelled amino acids were allowed per peptide. Identifications were filtered for a peptide and protein FDR of 1% and for posterior error probability (PEP) of individual peptide assignments of less than 0.1. Protein quantification was based on integrated peak area of unique peptides assigned to identified protein groups and required at least two measured SILAC ratios for unphosphorylated peptides. Lists generated from the MaxQuant software were finally differentially processed depending on the project.

For the dataset of the lectin-enriched subproteome, quantified peptides were filtered for a maximum mass error of 5 ppm and a Mascot score higher than 7. For phosphopeptide quantification the median ratio of all peptides harbouring the same sequence and number of phosphosites was calculated. From all identified phosphosites only those were used for further bioinformatic analysis that were assigned to a specific amino acid position with a localization probability of at least 0.75 (class I phosphosites). Annotated MS/MS spectra for all class I phosphosites were uploaded to the Tranche file-sharing system (ProteomeCommons.org). The thresholds for significantly regulated phosphopeptides and -sites were defined by Gaussian regression analysis of the frequency distribution of ratio over ratios of quantified peptides for the 1.5 and 5 min time points of LPA stimulation using Sigmaplot (version 10.0, Systat Software, Inc.). Phosphopeptides and -sites were considered as regulated in case of ratios greater than 2.5 σ in both experiments, corresponding to $p < 0.006$.

The phosphoproteome analysis of the LPA time-course project was exclusively based on phosphorylation sites with a localization probability of at least 0.75 (class I). For identified class I sites, annotated phosphopeptide spectra have been up-loaded to the Tranche file-sharing system (ProteomeCommons.org). In case of singly and multiply phosphorylated peptides harbouring the same site, ratios were calculated for singly phosphorylated species only. Furthermore, for quantification mean ratios and coefficients of variation for sites that were quantified for each timepoint in at least two of the three biological replicates were

calculated. Both experimental parts were combined by their common 10 min stimulation condition. Phosphorylation events were defined regulated in case of a mean change of at least two-fold with respect to the control and a coefficient of variation smaller than 0.3 at any timepoint.

2.2.8 Bioinformatic analysis

2.2.8.1 Time-dependent clustering: SOTA

Time-dependent phosphorylation profiles of reproducibly regulated phosphosites were clustered with the self-organizing tree algorithm (SOTA) of the MeV software (version 4.1) (Saeed, Sharov *et al.*, 2003). Therefore, the average ratios of regulated phosphosites of the two biological replicate experiments were calculated. The list of regulated phosphosites was loaded containing the ratios of the 1.5 and 5 min LPA time points as well as a ratio set to 1 for time point 0 min in unstimulated cells. Clustering was done using Euclidean distance as matrix with a maximal number of four cycles and otherwise default settings were used. Prior to clustering, the MeV software performed $\log_2$ transformation and normalisation of all values.

2.2.8.2 Time-dependent clustering: fuzzy c-means clustering

Clustering of phosphorylation profiles from LPA time-course analysis was performed with the open-source statistical language R, applying the package for fuzzy c-means clustering. Accordingly, all values were $\log_{10}$ transformed and normalised to a mean of zero and a standard deviation of 1, including the ratios for unstimulated cells which were set to 1. Subsequently fuzzy-c means clustering was performed as initially described by Olsen *et al* (Olsen, Blagoev *et al.*, 2006). Iteratively a total number of eight clusters and a fuzzification of 2 were determined to be the optimal input parameters.

2.2.8.3 DAVID

Analyses for overrepresented Gene Ontology (GO) annotation terms were performed with the functional annotation tool DAVID (Dennis, Sherman *et al.*, 2003; Huang da, Sherman *et al.*, 2009). IPI identifiers were converted to Ensemble accession numbers prior to submitting the

resulting gene lists for foreground and background data to DAVID. For analysis of the lectin enriched subproteome, specifically proteins with phosphopeptides reproducibly regulated upon LPA treatment were compared to all quantified phosphoproteins for the identification of significantly overrepresented GO biological process terms, as defined by a maximal DAVID EASE score of 0.05 for categories represented by at least two proteins.

2.2.8.4 Motif-X

The Motif-X algorithm (www.motif-x.med.harvard.edu) was applied to extract phosphorylation site motifs of LPA-induced class I phosphorylation sites. From the lectin enriched subproteome dataset all reproducibly upregulated serine and threonine sites were analysed. Serine and threonine amino acids at the central position of the 13 amino acid long sequences were exchanged to X and uploaded (foreground dataset). The background dataset contained all remaining phosphorylated serines and threonines with confident site assignments, and was processed as described for the foreground dataset. The minimum number of motif occurences was set to 5, with a $p < 10^{-4}$ required to be rated as significant. Based on the proportions of serine and threonine sequences denoted to one motif, the central character X was replaced accordingly afterwards.

2.2.8.5 String networks

To generate protein interaction networks of lectin enriched phosphoproteins all quantified proteins harbouring phosphopeptides were uploaded to the STRING protein-protein interaction database, version 8.2 (Jensen, Kuhn *et al.*, 2009). The interaction network was generated on the basis of experimental and database knowledge with highly confident interactions ($p > 0.7$) and visualized with Cytoscape, version 2.7.0.

For the LPA time-course project all proteins that harbour confidently identified LPA-regulated phosphorylation sites were uploaded to the database and the same parameters as described above were applied. Proteins of the network belonging to specific categories of molecular functions and biological processes according to the Gene Ontology annotation were highlighted. Time-dependent networks were created of all phosphoproteins annotated to the eight specific clusters generated by fuzzy c-means clustering, and the interaction confidence was required to be higher than 0.4.

2.2.8.6 Hierarchical clustering

For LPA-regulated phosphorylation sites detected in the LPA time-course project hierarchical clustering was performed with the open-source software MeV (version 4.2). Therefore, confidently assigned phosphosites derived from singly modified phosphopeptides were uploaded and heatmaps were generated for selected Gene Ontology categories.

3. Results

3.1 Establishment of a quantitative MS workflow to identify LPA-dependent interaction partners of ADAM17

Key proteins of the LPA-mediated transactivation process, including the metalloproteinase ADAM17, the membrane-bound ligand amphiregulin and the EGFR, have been identified in the squamous cell carcinoma cell line SCC-9 (Gschwind, Hart *et al.*, 2003). Therefore, SCC-9 cells were chosen for the establishment of a new approach to identify yet unknown proteins in this process. The approach should comply with the following requirements: 1) potential interacting proteins should bind to ADAM17 under physiological conditions, 2) LPA-induced interactions can be identified, 3) stimulation-independent binding partners can also be found, and 4) results are of qualitative and quantitative nature. To address these aspects we applied a SILAC-based proteomic approach to quantitatively compare endogenous ADAM17 expression *versus* ADAM17 knock-down and unstimulated cells *versus* LPA-treated cells, with the goal to identify specific differential binding of ADAM17 interaction partners in these comparisons. In the following sections, four experimental setups are introduced that were designed in the course of the developing process. All experiments were performed in two biological replicates, while labelling schemes were modified regarding cell treatment conditions between each first and second experiment in order to ensure reproducible results and monitor possible variations due to the different labels.

3.1.1 Co-immunoprecipitations with ADAM17 343 antibody

In a first setup SCC-9 cell populations were metabolically labelled with either normal arginine and lysine (Arg0/Lys0) or combinations of heavier isotopic variants of the two amino acids (Arg6/Lys4 and Arg10/Lys8) until full incorporation into SCC-9 cell proteomes was achieved. In the first experiment we transfected Arg6/Lys4- and Arg10/Lys8-labelled cells with non-silencing siRNA and Arg0/Lys0-encoded SCC-9 cells with siRNA directed against ADAM17 (Figure 5A). Subsequently, the differentially transfected cell populations were serum-starved for 48 h to reduce intracellular signalling to a basal level prior to short-term LPA incubations. Arg0/Lys0- and Arg10/Lys8-labelled cells were stimulated with 10 µM LPA for 3 min, whereas Arg6/Lys4-labelled cells were left untreated. The different cell populations were then lysed and the resulting total cell lysates were utilised for separate

co-immunoprecipitations with the ADAM17 343 antibody. This home-made antibody is supposed to interact with the functional active form of ADAM17 (Hart, 2004) and, as it recognises ADAM17 in the extracellular part, should allow to enrich for intracellular binding partners of ADAM17. The elution fractions from the three parallel immunoprecipitations were pooled and then resolved by gel electrophoresis. The gel was cut into five slices and subsequently trypsin digestion was performed in gel slices and the resulting peptide mixtures were measured by high-resolution LC-MS on a linear ion trap/orbitrap hybrid mass spectrometer (LTQ-Orbitrap). The acquired spectra were collectively analysed with the algorithms implemented in the MaxQuant software suite using MASCOT for database searching (Cox and Mann, 2008). MaxQuant performed peptide identifications and peptide to protein assembly in conjunction with false discovery rate determinations and SILAC-based quantification of identified proteins and peptides.

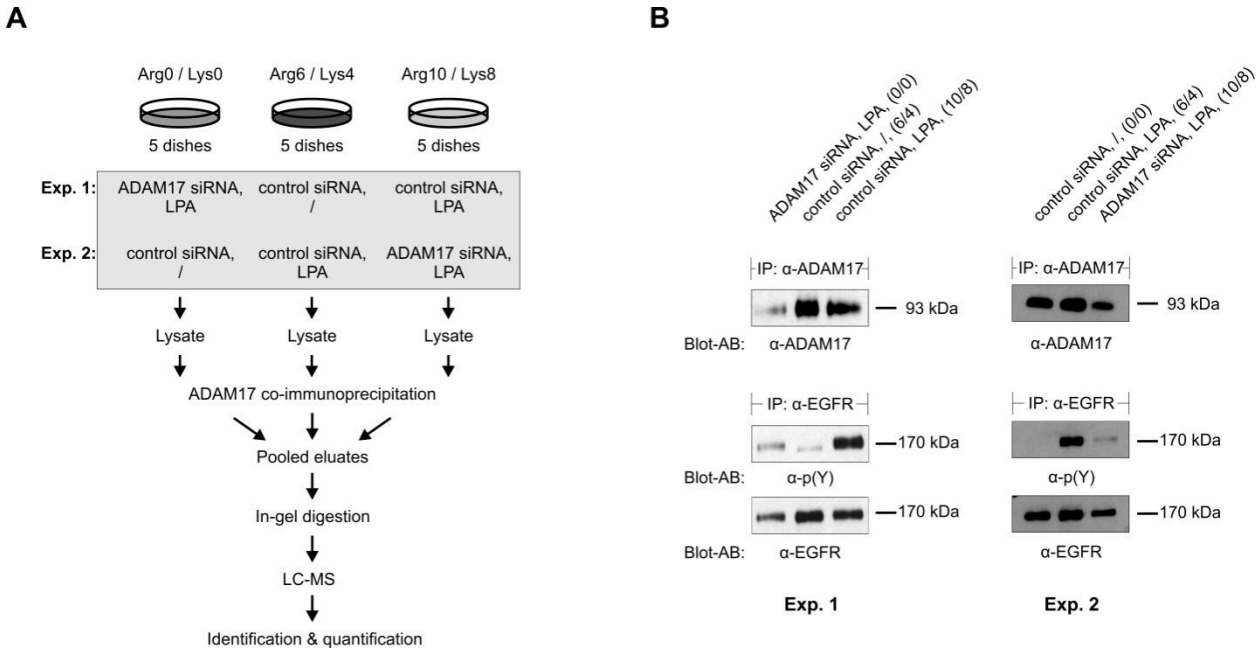

Figure 5: First quantitative proteomics approach to identify ADAM17 interaction partners upon LPA stimulation. A, Experimental workflow showing SILAC labelling, siRNA transfection and stimulation schemes in biological replicate experiments and subsequent processes including ADAM17 co-immunoprecipitation. B, Immunoblot analysis of differentially labelled cell lysates for biological replicate experiments. EGFR and the active form of ADAM17 were immunoprecipitated and analysed by immunoblotting with anti-phosphotyrosine as well as EGFR-specific antibodies and ADAM17 antibody, respectively.

Furthermore, to verify that SILAC conditions did not compromise LPA-stimulated signalling, EGFR was immunopreciptated from the differentially treated SCC-9 total cell lysates followed by immunoblotting with Tyr(P)-specific antibody. As seen in Figure 5B, LPA treatment evoked rapid EGFR phosphorylation on tyrosine residues, demonstrating efficient EGFR transactivation in SILAC cell culture. Due to the reduction of ADAM17 levels in cells transfected with siRNAs directed against the metalloproteinase, the transactivation process upon LPA treatment was disrupted and hence EGFR phosphorylation in this cell population was strongly impaired. In accordance with ADAM17 levels detected by immunoblotting of 343 precipitates (Figure 5B), measured protein abundance of ADAM17 based on the quantification of all ADAM17 peptides, was found more than two-fold reduced in the cell population treated with ADAM17 siRNA in comparison to control-transfected cells (Table 1). Potential ADAM17 interaction partners are expected to exhibit similar ratios as ADAM17. Only four proteins, ATP-dependent RNA helicases DDX1 and DDX5, laminin subunit beta-3 and ataxin-2-like protein were detected with a similar low abundance as ADAM17 in the respective cell population. Notably, among those proteins, ataxin-2-like protein was the only one found in higher amount upon LPA treatment with a ratio of 1.87 in comparison to untreated cells. To validate these potential interaction partners the experiment was repeated and the labels of the differently treated cell populations were changed compared to the first experiment (Figure 5A). Additionally, the number of gel slices and corresponding LC-MS runs was raised from 5 to 10. By raising the number of slices it was likely that low and high abundant proteins are more often located in separate slices and thus peptides originating from low abundance proteins can be detected as they are not superseeded by those from highly abundant analytes. Immunoblot analysis of this experiment was performed as described above (Figure 5B). Analysis of MS data revealed a different set of ten proteins with similar abundance profiles as ADAM17 in the respective cell populations. Laminin subunit beta-3 was detected as potential interaction partner in both experiments, although in the second experiment it was not regulated to the same extent as ADAM17 (Table 1). The results of both experiments differed considerably which could be due to the experimental setup. Unlike the expected background of a high number of unspecific binding partners that are characterised by their constant protein abundances in the differently treated cell populations, a large proportion of quantified proteins showed altering ratios dependent on cell treatment. These observations could result from technical variability in the workflow consisting of separately performed immunoprecipitations for each of the three cell populations. Therefore, the experimental setup was changed in this respect and accordingly equal protein amounts of

the three cell populations were combined after cell lysis and the protein pool subjected to immunoprecipitation reactions (Figure 6). Notably, this procedure bears the risk that proteins deriving from one cell population might bind to ADAM17 molecules of a differentially labelled cell population during the incubation.

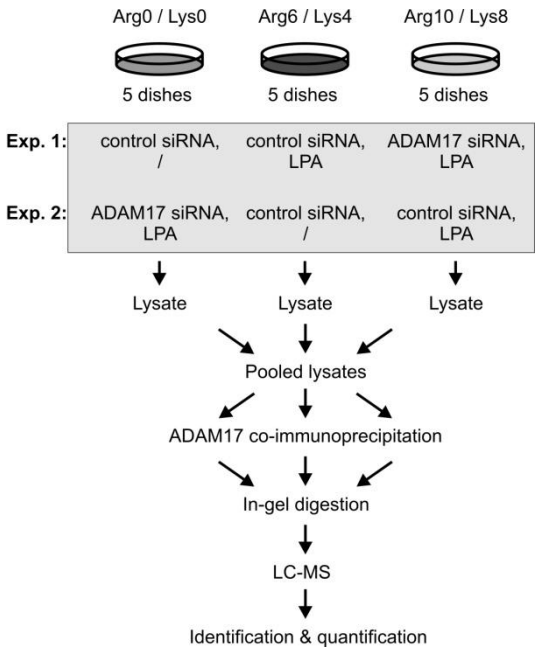

Figure 6: Second quantitative proteomics approach to identify ADAM17 interaction partners upon LPA stimulation. Experimental workflow showing SILAC labelling, siRNA transfection and stimulation schemes in biological replicate experiments and subsequent experimental steps including ADAM17 co-immunoprecipitation.

In both experiments a reduced abundance of ADAM17 was detected in cell populations transfected with siRNA directed against ADAM17, which were the cells labelled with high isotopes and low isotopes of arginine and lysine in experiments 1 and 2, respectively (Table 1). Among a total number of 312 quantified proteins four proteins (heterogeneous nuclear ribonucleoprotein A3, protein SET, 2'-5'-oligoadenylate synthetase 2, histone H1.3) exhibited similar abundance profiles as ADAM17 in experiment 1 and two proteins (heterogeneous nuclear ribonucleoprotein A3, nucleolysin TIA-1 isoform p40) in experiment 2. Three proteins were detected in one of the two experiments, and heterogeneous nuclear ribonucleoprotein A3 was the only protein that was reproducibly found with similar ratios like ADAM17 (Table 1). In comparison to the first setup the altered experimental design in

the second setup showed no improvements regarding the background and, furthermore, the potential candidate laminin subunit beta-3 found by the first approach could not be confirmed but a new candidate, heterogeneous nuclear ribonucleoprotein A3, was found reproducibly regulated. However, the lack of evidence for laminin in the second approach does not disprove a potential role as specific ADAM17 interactors, as there might have been exchange of laminin species from the different SILAC lysates due to their pooling before immunopreciptation in the second approach. Nevertheless, a further strategy was applied in which glycosylated proteins were enriched instead of the more specific immunoprecipitation of ADAM17 molecules, as described in the following section.

3.1.2 Lectin pull-down for protein identification

The pull-down with lectins enriches for glycosylated proteins such as plasma membrane proteins as most of the proteins located at the cell surface or integral to the plasma membrane harbour glycosylation groups. Therefore, the combination of the three lectin resins, lentil, concanavalin A and WGA with different affinities towards sugar modifications (Selby, Larsen *et al.*, 2008), enables a high coverage of the cell surface glycoproteome. Among these proteins ADAM17 binds to all three resins as shown in initial test experiments and the enriched subproteome constitutes a large and stable background against which changes in protein abundance can be detected. Therefore, a strategy was devised to identify changes in protein abundance at the plasma membrane that co-occur with downregulation of ADAM17 or are triggered by short-term stimulation with LPA. Detection of such protein changes might reveal protein candidates that are involved in the transactivation process in SCC-9 cells, which then could be further tested for direct interaction with ADAM17. Two biological replicate experiments were performed with cells labelled according to the scheme in Figure 7A and treated as described for the previous two experimental setups. After lysis equal amounts of protein were subjected to separate *in vitro* associations with lectins and then combined and processed as already described. The measurement of lectin-enriched sample comprised 11 LC-MS runs per biological replicate derived from 11 gel slices. Immunoblot analysis confirmed expected tyrosine phosphorylation events on the EGFR and sufficient downregulation of ADAM17 upon siRNA treatment of cells (Figure 7B).

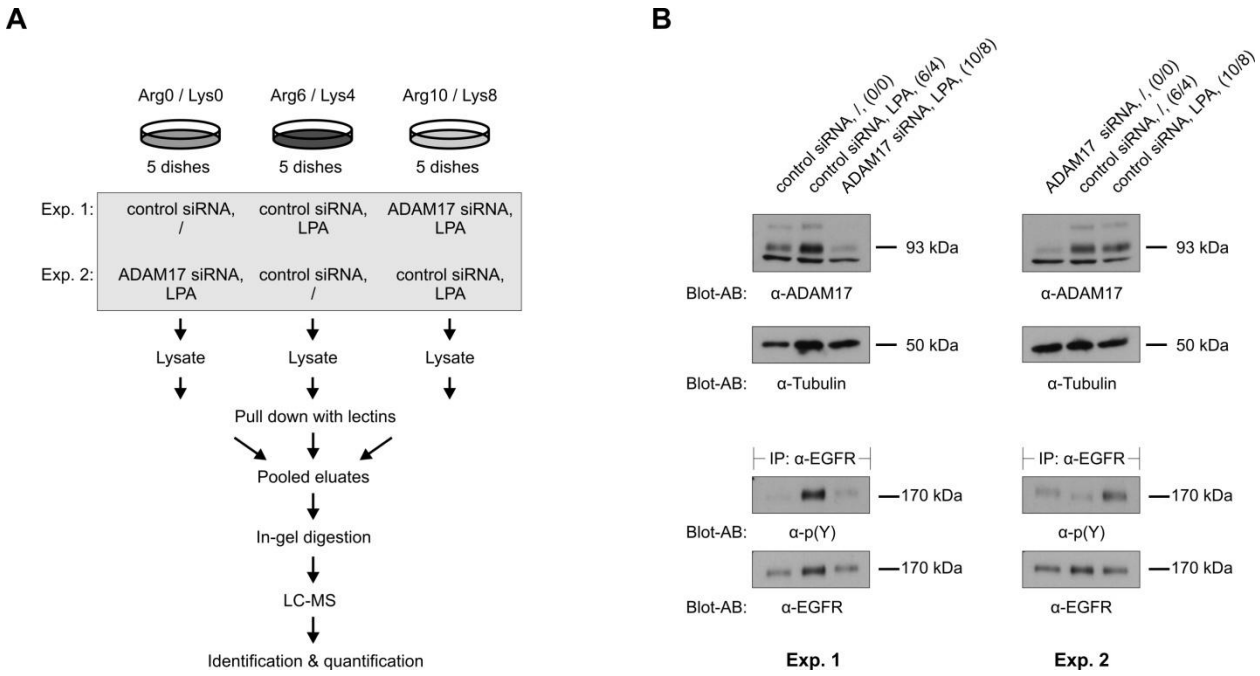

Figure 7: Third quantitative proteomics approach to identify ADAM17 interaction partners upon LPA stimulation. A, Experimental workflow showing SILAC labelling, siRNA transfection and stimulation schemes in biological replicate experiments and subsequent sample steps including a pull-down with lectins. B, Immunoblot analysis of differentially labelled cell lysates for biological replicate experiments. EGFR was immunoprecipitated and analysed by immunoblotting with anti-phosphotyrosine and EGFR-specific antibodies, while ADAM17 was detected in total cell lysate.

More than 1,300 proteins were quantified in experiment 1 and 2 with ADAM17 found reproducibly downregulated 3- to 4-fold in cell populations transfected with ADAM17 siRNA (Table 1). In the cell populations exhibiting low ADAM17 for an additional 45 proteins of experiment 1 and 2 an at least 2-fold reduction was detected in comparison to the corresponding protein levels in control cells. Among them nine proteins (junctional adhesion molecule A, plasminogen activator inhibitor 1, heterogeneous nuclear ribonucleoprotein H2, cell division control protein 2 homolog, desmoglein-2, putative uncharacterised protein FLJ20035, 2'-5'-oligoadenylate synthetase 2 and thrombospondin-1) were found reproducibly regulated in both biological replicates. For none of these proteins an increase could be observed upon LPA stimulation in cells with endogenous ADAM17 expression levels indicating that these proteins do not change their localization due to the stimulus. Furthermore, these proteins did not overlap with those found in the two experimental studies described above.

In addition to quantitatively compare the three differentially labelled lectin eluates among each other, it was further deemed interesting to compare the results with the situation in total cell lysate. In samples with reduced ADAM17 levels specific interaction partners of ADAM17 are expected in reduced amounts after lectin pull-down, but should be found in unchanged protein levels in total cell lysate. To look into this further, total cell extract of experiment 1 was processed according to the same MS sample preparation strategy as used for lectin-enriched fractions. Unexpectedly, subsequent data analysis revealed 27 out of more than 2,000 proteins which exhibited a similar expression pattern as ADAM17 in all three cell populations. The reduced abundances of these proteins in cells in which ADAM17 levels were downregulated via siRNA transfection might either originate from their diminished expression in the functional context of cellular ADAM17 depletion, or, alternatively, result from sequence-specific off-target effects of the transfected ADAM17 siRNAs.

Among those proteins six (junctional adhesion molecule A, heterogeneous nuclear ribonucleoprotein H2, cell division control protein 2 homolog, desmoglein-2, putative uncharacterised protein FLJ20035 and 2'-5'-oligoadenylate synthetase 2) matched the preliminary nine candidates that were reproducibly found regulated in the lectin-enriched subproteome. Consequently these proteins were excluded from the list of potential ADAM17 interaction partners. The two remaining proteins plasminogen activator inhibitor 1 and thrombospondin-1 as well as ADAM17 could not be identified in the total cell extract. Interestingly, laminin subunit beta-3 and heterogeneous nuclear ribonucleoprotein A3 that were reproducibly found regulated in the first and second experimental setup based on their co-immunoprecipitation with ADAM17, could be quantified in total cell lysate in constant protein abundance independent of the different cell treatments.

3.1.3 Two consecutive ADAM17 immunoprecipitations

Due to the high sensitivity of mass spectrometric analysis several off-target effects of siRNAs directed against ADAM17 seemed plausible. Thus, the downregulation of ADAM17 via siRNA seemed a rather unappropriate method for large-scale experiments in which data is raised with highly sensitive and accurate measuring systems. Another possibility to exclusively reduce a specific protein without perturbing endogenous expression levels during cell culture involves step-wise *in vitro* associations of cell lysates in which the protein-of-interest is bound to a high extent in the first incubation and consequently to a much lower

extent in the second incubation of the supernatant fraction. Hereby the comparison of eluates of the first and second incubation provides a quantitative measure to identify specific binders and their interactors.

This strategy was further implemented in the approach to identify ADAM17 interaction partners. Therefore, a triple labelling SILAC experiment was carried out in which cells labelled with light and heavy isotopic variants of arginine and lysine were stimulated with LPA for 3 min, whereas cells labelled with medium isotopic forms of these amino acids were seeded with the double amount of cells and left untreated (Figure 8A). With cell lysates originating from this label two single immunoprecipitations with the 343 antibody directed against the extracellular domain of ADAM17 were performed. Two consecutive ADAM17 immunoprecipitations were carried out separately for lysates derived from light and heavy labelled cells, where supernatants from the first associations were subsequently subjected to a second round of association with the same antibody. To quantitatively compare protein abundances in the precipitates of unstimulated cells with those of stimulated cells from the first and second incubation step, the precipitates were combined with each precipitate possessing a different isotopic label (Figure 8A). One eluate of medium labelled cells was combined with the eluates of the first incubation of light labelled cell extract and of the second round of heavy labelled cell lysate in experiment 1 (and *vice versa* in experiment 2). Hence this approach enables the comparisons of two experiments regarding reproducibly LPA-regulated ADAM17 interaction partners.

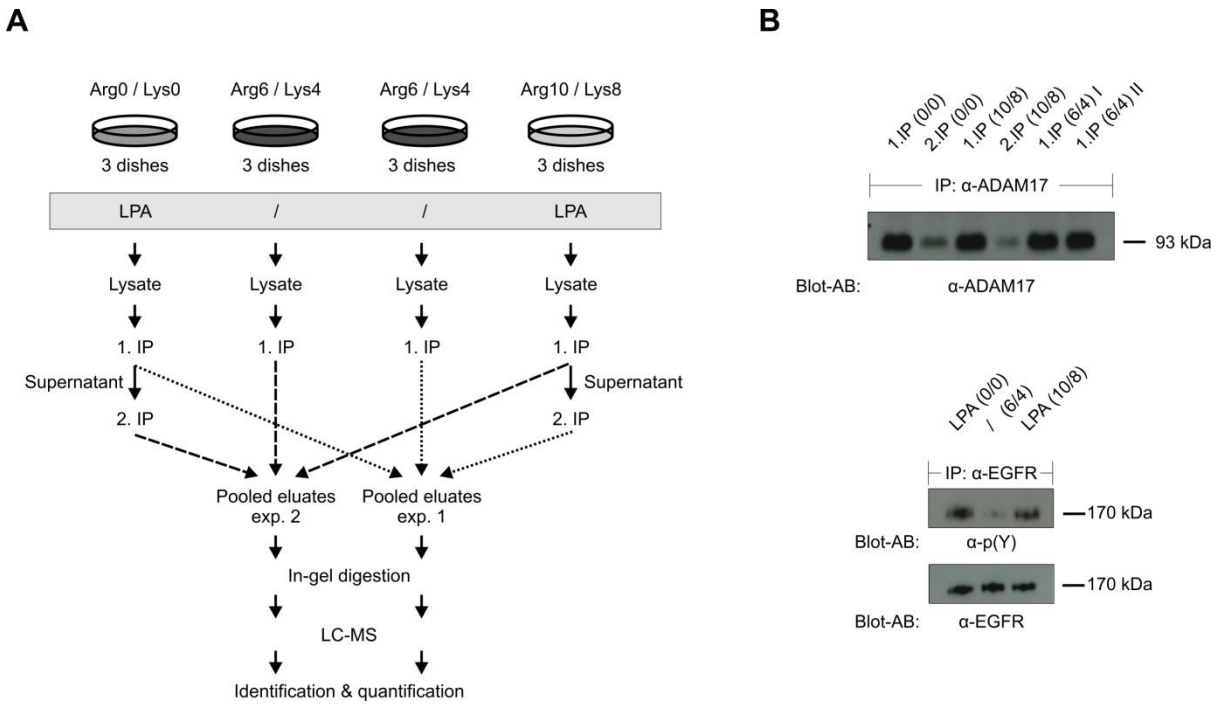

Figure 8: Fourth quantitative proteomics approach to identify ADAM17 interaction partners upon LPA stimulation. A, Experimental workflow showing SILAC labelling, stimulation schemes and subsequent processes including one and two subsequent ADAM17 immunoprecipitations for cells labelled with Arg6/Lys4 and Arg0/Lys0, Arg10/Lys8, respectively. B, Immunoblot analysis of differentially labelled cell lysates. EGFR and the active form of ADAM17 were immunoprecipitated and analysed by immunoblotting with anti-phosphotyrosine as well as EGFR-specific antibodies and ADAM17 antibody, respectively.

Immunoblot analysis of EGFR and ADAM17 precipitates showed EGFR phosphorylation on tyrosine residues upon LPA treatment and a high depletion of ADAM17 in the eluate derived from the second incubation compared to the one derived from the first incubation, respectively (Figure 8B). Likewise, MS data demonstrated small ratios (< 0.2) for the metalloproteinase in precipitates of the first *versus* the second immunoprecipitation for both experiments (Table 1). In experiment 1 eight candidates were detected with corresponding ratios smaller than 0.5 (isoform 1 of granulins precursor, 52 kDa Ro protein, anti-colorectal carcinoma heavy chain, peptidyl-prolyl cis-trans isomerase, histone H2B type 1-N, protein SET, acidic leucine-rich nuclear phosphoprotein 32 family member B, putative uncharacterised protein IGL@), of which six were not quantified in experiment 2. However, although only two candidates were detected in experiment 2, those matched the remaining

candidates from experiment 1. Isoform 1 of granulins precursor and 52 kDa Ro protein were found with reproducibly low ratios in eluates of the first association versus the second association, similar to ADAM17, and could therefore present possible interactors (Table 1).
The comparison of reproducibly detected candidates in the four different experimental setups demonstrates that the results received in one approach could not be repeatedly observed across the others (Table 1). This finding indicates rather approach-specific results and thus revealed no compelling candidates for specific ADAM17 metalloproteinase binding. Moreover, these proteins did not show any changes in their binding properties upon LPA treatment, which might be an indication that they are not involved in the transactivation process (Table 1).

Table 1: Potential ADAM17 interaction partners reproducibly found in biological replicate experiments of four different experimental setups. Ratios of protein abundances of differentially treated cell populations are presented for ADAM17 and potential candidates.

	Protein Names	Gene Names	Ratio (ADAM17 siRNA, LPA) / (control siRNA, unstimulated) exp. 1	Ratio (ADAM17 siRNA, LPA) / (control siRNA, LPA) exp. 1	Ratio (control siRNA, LPA) / (control siRNA, unstimulated) exp. 1	Ratio (ADAM17 siRNA, LPA) / (control siRNA, unstimulated) exp. 2	Ratio (ADAM17 siRNA, LPA) / (control siRNA, LPA) exp. 2	Ratio (control siRNA, LPA) / (control siRNA, unstimulated) exp. 2
1st setup	Disintegrin and metalloproteinase domain-containing protein 17	ADAM17	0.44	0.37	0.82	0.51	0.39	1.28
	Laminin subunit beta -3	LAMB3	0.35	0.40	0.62	0.61	0.49	1.14
2nd setup	Disintegrin and metalloproteinase domain-containing protein 17	ADAM17	0.54	0.45	1.21	0.42	0.41	0.95
	Heterogeneous nuclear ribonucleoprotein A3	HNRNPA3	0.50	0.34	1.69	0.18	0.52	1.75
3rd setup	Disintegrin and metalloproteinase domain-containing protein 17	ADAM17	0.32	0.30	1.08	0.27	0.25	0.98
	Plasminogen activator inhibitor 1	SERPINE1	0.48	0.47	1.06	0.43	0.40	1.01
	Thrombospondin-1	THBS1	0.29	0.22	1.45	0.19	0.27	1.54

	Protein Names	Gene Names	Ratio (eluate 2, LPA) / (eluate 1, unstimulated) exp. 1	Ratio (eluate 2, LPA) / (eluate 1, LPA) exp. 1	Ratio (eluate 1, LPA) / (eluate 1, unstimulated) exp. 1	Ratio (eluate 2, LPA) / (eluate 1, unstimulated) exp. 2	Ratio (eluate 2, LPA) / (eluate 1, LPA) exp. 2	Ratio (eluate 1, LPA) / (eluate 1, unstimulated) exp. 2
4th setup	Disintegrin and metalloproteinase domain-containing protein 17	ADAM17	0.17	0.17	0.88	0.19	0.19	0.95
	52 kDa Ro protein	TRIM21	0.12	0.23	0.55	0.09	0.10	0.93
	Isoform 1 of Granulins precursor	GRN	0.29	0.45	0.82	0.21	0.17	0.90

3.2 Glycoprotein capture and quantitative phosphoproteomics indicate coordinated regulation of cell surface proteins upon lysophosphatidic acid stimulation

In LPA-induced signal transmission protein phosphorylation plays a key role. Especially, time-dependent phosphorylation changes provide insights into multifunctional regulation mechanisms triggered by such an external stimulus. Hence, the exploration of phosphorylation alterations on ADAM17 and the EGFR upon short-term LPA stimulation might be one step further in understanding the mechanism underlying the EGFR transactivation process. Furthermore, as EGFR transactivation is only one pathway through which the LPA-generated signals traverse the cell and trigger a variety of cell processes, the aim was now to survey time-resolved LPA-induced phosphorylation changes on plasma membrane proteins and their interaction partners. Proteins located at the plasma membrane are of major interest as they fulfill many functions that range from the initial recognition of environmental signals to the final execution of cell signalling information to modulate interactions with surrounding cells or extracellular matrix components.

3.2.1 Experimental strategy for quantitative glycoproteome analysis

To analyse the phosphoregulation of plasma membrane proteins in response to the serum-derived growth factor LPA, a proteomics approach based on glycoprotein capture and SILAC quantification was performed. SCC-9 cells were labelled with combinations of different amino acid isotopes as indicated in Figure 9A, starved for 48 h and afterwards stimulated with externally added LPA. In a first SILAC experiment, Arg0/Lys0-labelled cells were left untreated, whereas the Arg6/Lys4- and Arg10/Lys8-encoded SCC-9 cells were stimulated for 1.5 and 5 min with LPA, respectively. Total cell lysates were then prepared from the differently treated cell populations and subjected to separate *in vitro* associations with a mixture of the three lectin affinity resins lentil, WGA and concanavalin A agarose to enrich for glycosylated proteins such as plasma membrane proteins. The elution fractions from the three lectin pull-downs were pooled prior to further MS sample preparation. 80% of the lectin-purified material was resolved by gel electrophoresis and then trypsin digested in gel slices followed by phosphopeptide affinity enrichment with TiO_2 beads. In addition, total peptide samples were prepared from small aliquots of these in-gel digests for protein identification and quantification. The remaining 20% of lectin-enriched material was digested in-solution with trypsin followed by three consecutive enrichments in which the initial

phosphopeptide amount was in excess of the binding capacity of the TiO_2 microspheres. In this phosphopeptide fractionation strategy, phosphopeptides with high affinity are preferentially retained in the first incubation step, whereas those with a by comparison lower affinity for TiO_2 remain in the supernatant and are retained in the subsequent purifications with fresh beads. Thus, as the focus was on protein phosphorylation events in the glycoproteome and not on the glycosylation sites themselves, lectin-purification was performed for intact proteins instead of proteolytically derived glycopeptides.

Overall, the fractionation strategy resulted in 27 peptide samples that were measured as already described for the other approaches. To be able to detect phosphorylation modifications in this project the MaxQuant software was used to additionally perform phosphorylation site localisation by computational PTM scoring. Furthermore, to assess reproducibility of quantitative data, a second SILAC experiment with modified labels regarding cell treatment conditions was performed (Figure 9A).

The rapid phosphorylation of EGFR upon 1.5 and 5 min of LPA treatment was detected by immunoblotting for both experiments (Figure 9B). These modification changes could further be recapitulated by SILAC MS data as exemplified by increased ion intensities of the EGFR phosphopeptide harbouring the autophosphorylation site Tyr-1197 from LPA-treated cells. Notably, relative signal intensities changed according to the different SILAC scheme in the second experiment (Figure 9C). This illustrates the assessment of biological reproducibility in replicate SILAC experiments. Moreover, phosphopeptide changes did not result from altered protein amounts in lectin-purified fractions upon LPA treatment, as evident from similar levels of a representative, non-phosphorylated EGFR peptide in both replicate SILAC experiments (Figure 9D).

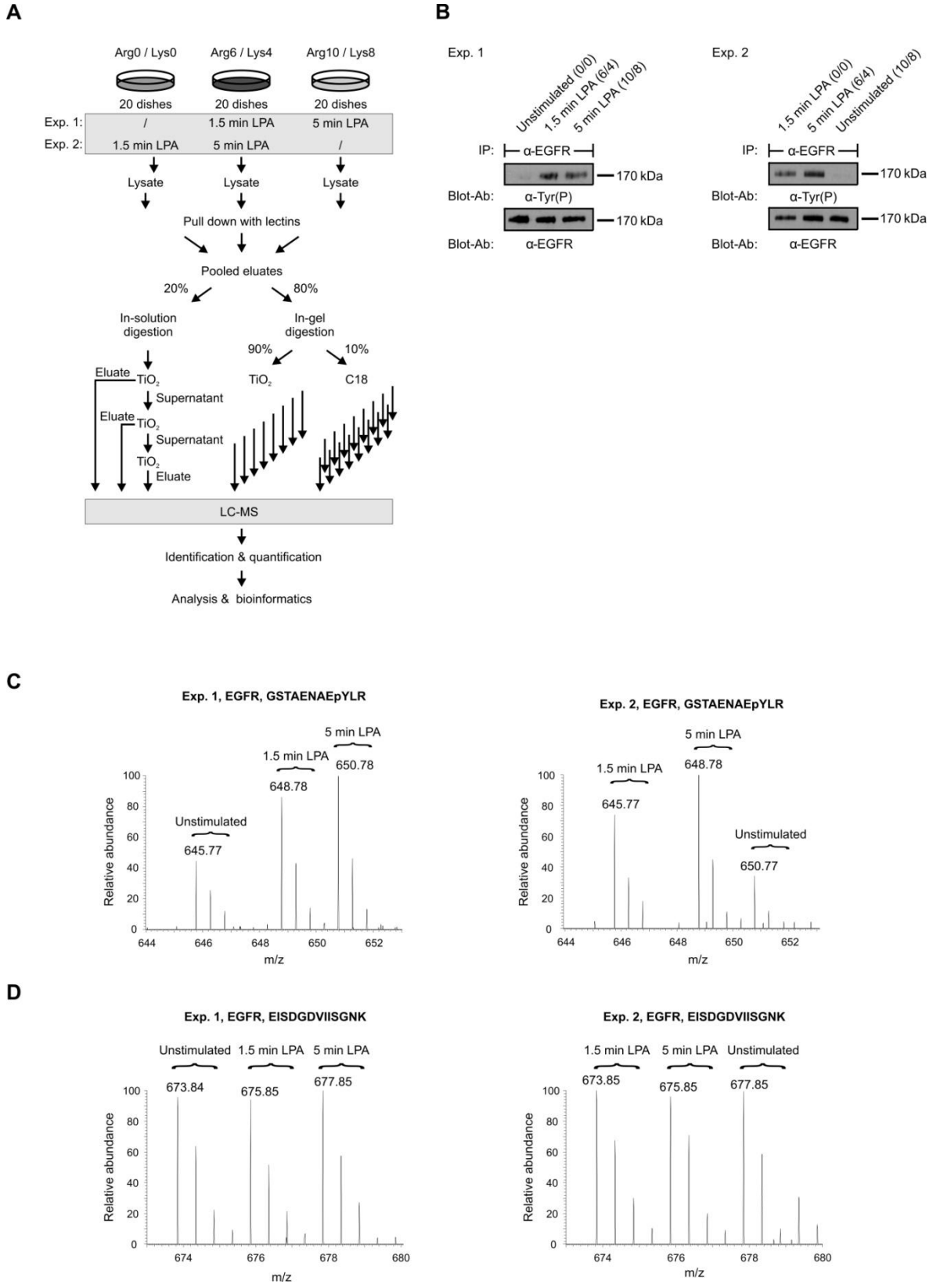

Figure 9: Quantitative phosphoproteomics approach to identify phosphorylation changes in lectin-purified proteins upon LPA stimulation. A, Experimental workflow showing SILAC labelling and

stimulation schemes in biological replicate experiments and the protein enrichment and MS sample preparation strategy (TiO_2, phosphopeptide purification with TiO_2 beads; C18, peptide desalting by C_{18} StageTips) followed by MS data acquisition and analysis. The numbers of arrows indicate how many samples were analysed by LC-MS per biological replicate analysis. B, SILAC-encoded and serum-starved SCC-9 cells were stimulated with LPA before lysis as indicated. EGFR was immunoprecipitated and analysed by immunoblotting with anti-phosphotyrosine and EGFR-specific antibodies. C, MS spectra of the EGFR phosphopeptide harbouring LPA-induced Tyr(P)-1197 from SILAC experiments 1 and 2. D, MS spectra of the unmodified EGFR peptide EISDGDVIISGNK from SILAC experiments 1 and 2.

To confirm plasma membrane protein enrichment by lectin-based affinity purification, a gel-based proteome analysis of total cell extract was performed with the same MS sample preparation strategy as used for protein identification from lectin-enriched fractions. Comparative analysis of gene ontology (GO) molecular function terms annotated to identified proteins revealed several-fold enrichment for protein families such as GPCRs, RTKs, metalloproteases and ion transporters upon lectin affinity purification, indicating pre-fractionation of integral plasma membrane proteins with rather diverse topologies and functions (Figure 10).

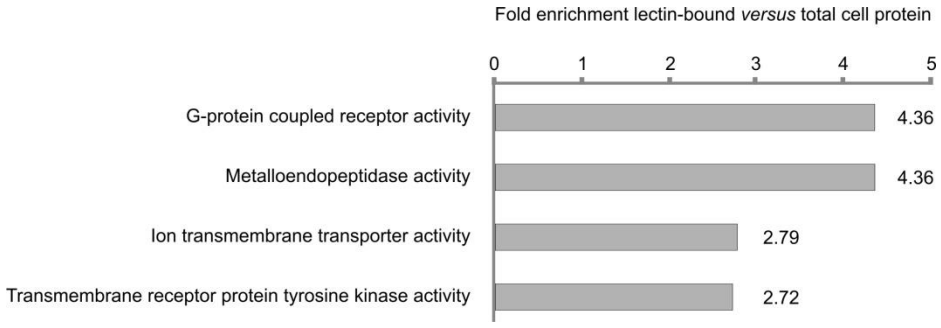

Figure 10: Enrichment for selected GO molecular function terms upon lectin resin purification. Fold enrichment of the indicated molecular functions is shown based on the fraction of annotated proteins identified upon lectin-based fractionation compared to the fraction of annotated proteins identified from total cell lysate analysis.

3.2.2 Quantitative analysis of LPA-induced regulation

Overall, the analysis of lectin-enriched SCC-9 cell fractions resulted in the identification and quantification of more than 1,000 distinct proteins and nearly 1,700 distinct phosphopeptides, which in both cases represented highly confident assignments due to data filtering for protein and peptide FDRs of less than 1%. Moreover, more than 1,600 distinct site-specific phosphorylation events could be pinpointed on quantified peptides with localisation probabilities of at least 0.75 by PTM scoring (class I sites). The overlap between the two biological replicate analyses was 67% on the protein, 51% on the phosphopeptide, and 45% on the phosphorylation site level (Figure 11). Serine, threonine and tyrosine modifications accounted for 84.1%, 13.5% and 2.4% of all quantified phosphorylation sites, respectively.

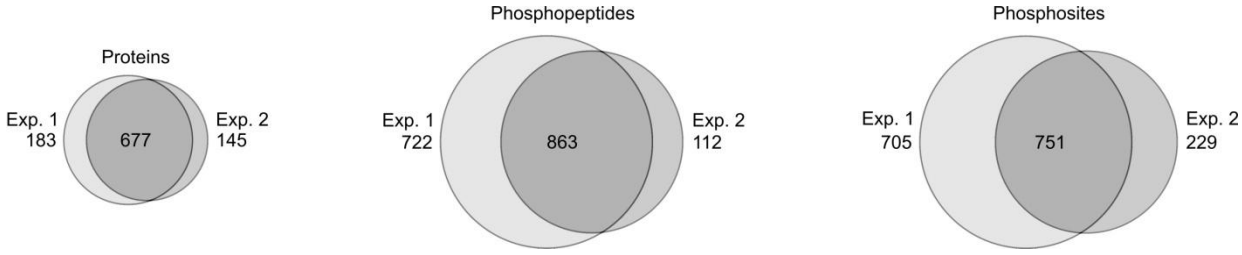

Figure 11: Comparison of protein groups, phosphopeptides and class I phosphosites quantified in two biological replicate analyses.

At first, the extent to which LPA affected protein abundance in lectin-purified fractions was analysed. To identify significant changes over inherent inter-experimental variability, protein ratios determined in the first experiment were devided by those measured in the second experiment and the distribution characteristics of the resulting ratios-of-ratios were analysed (Figure 12A). Threshold values of significant regulation were set to 2.5 σ of the ratios-of-ratios distribution, and this criterion had to be met in both replicate analyses for at least one LPA time point to identify a protein as regulated. Out of 677 proteins quantified in both experiments, only glycogen phosphorylase and calpain-2 catalytic subunit precursor exhibited significant and reproducible increase in abundance in lectin-purified fractions while six proteins (alpha-enolase, desmoplakin, desmoglein-2 precursor, 40S ribosomal protein S3, zinc finger RNA-binding protein, epiplakin) were found in reduced levels upon LPA treatment (Figure 12B). As only about 1% of all reproducibly quantified proteins

significantly changed, we conclude that LPA stimulation did not affect protein abundance for the vast majority of lectin-enriched proteins.

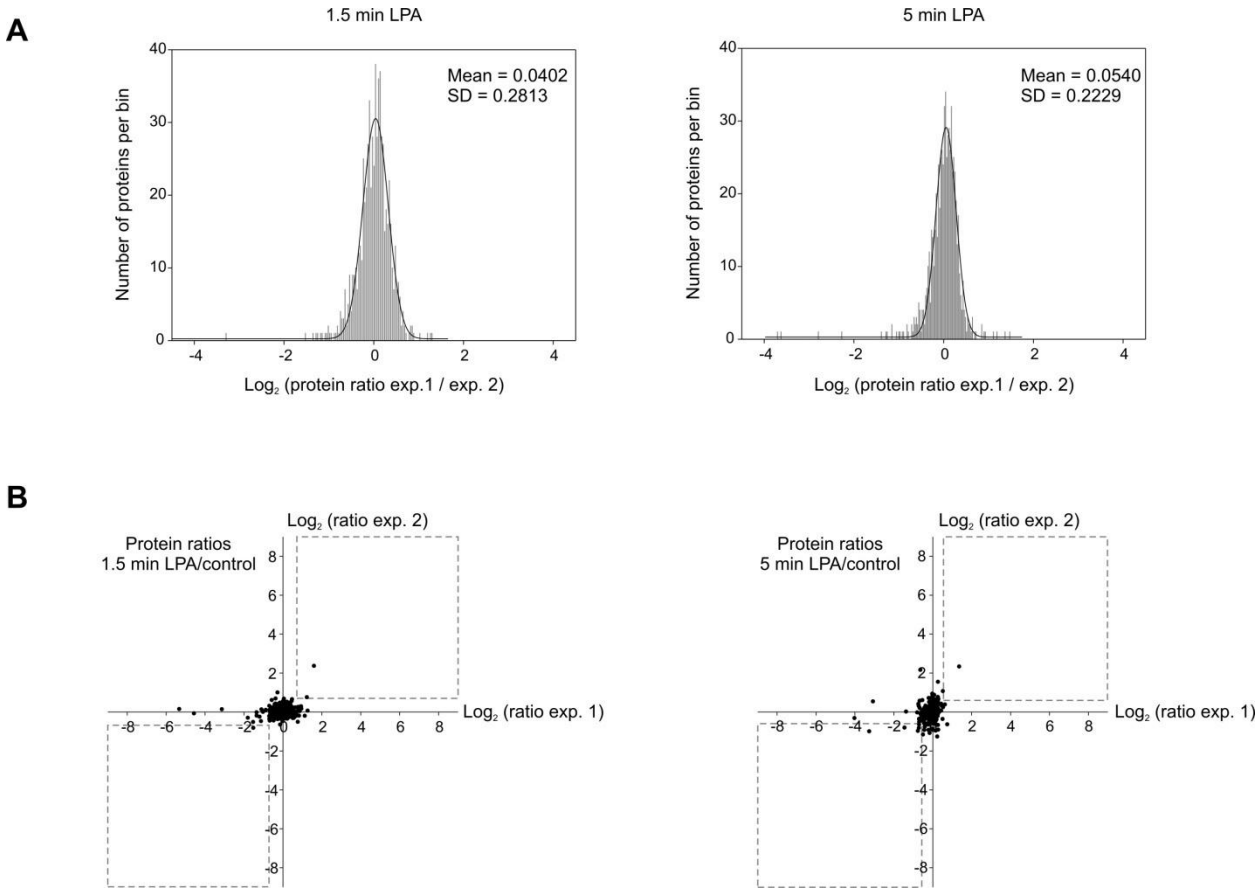

Figure 12: Statistical analysis based on replicate protein quantifications. A, Quantified proteins were binned according to their log_2-transformed ratios of their 1.5 min or 5 min LPA *versus* control ratios obtained from the biological replicate experiments 1 and 2. The mean and standard deviation of each of the two ratios-of-ratios distributions is indicated. B, Scatter plot comparison of log_2-transformed LPA *versus* control protein ratios measured in experiment 1 and 2 for the 1.5 and 5 min time points. The squares indicate reproducible up- and downregulation, corresponding to ratios greater than 1.63 and 1.47 or ratios less than 0.61 and 0.67 for the 1.5 and 5 min time points, respectively.

For comprehensive analysis of phosphoregulation, LPA-mediated phosphorylation changes were quantified both on the level of phosphopeptides, which were specified by the amino acid sequence and number of phosphate groups, and on the level of confidently assigned class I phosphorylation sites, for which MaxQuant computes a ratio based on all quantified phosphopeptides bearing an identified site. As LPA treatment affected only two

phosphoproteins in their abundance in lectin-enriched fractions, measured phosphopeptide and phosphosite ratios were highly similar to the corresponding ratios normalised for protein abundance (Figure 13). Herein, quantification of non-phosphorylated peptide species from phosphoproteins enabled normalisation for protein abundance (Daub, Olsen *et al.*, 2008). Therefore, phosphopeptide and -site ratios without normalisation were considered for further analysis as this strategy ensures consistent analysis of phosphorylation changes irrespective of whether protein abundance ratios were measured.

Figure 13 (next page): Comparison of phosphopeptide and phosphosite ratios with or without normalisation for protein abundance. Phosphopeptides and -sites derived from proteins for which abundance ratios could be determined (based on the quantification of non-phosphorylated peptides) were considered. Scatter plots are shown for 1.5 min LPA *versus* control and 5 min LPA *versus* control ratios for both experiments. The diagonal line indicates maximum correlation for phosphorylation ratios.

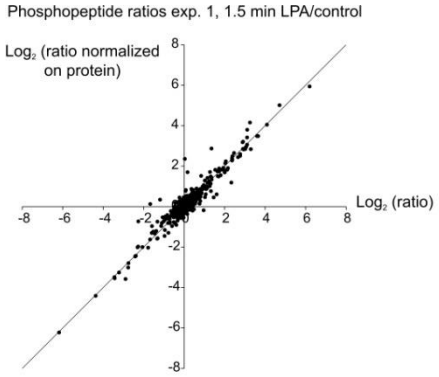
Phosphopeptide ratios exp. 1, 1.5 min LPA/control
Log2 (ratio normalized on protein)
Log2 (ratio)

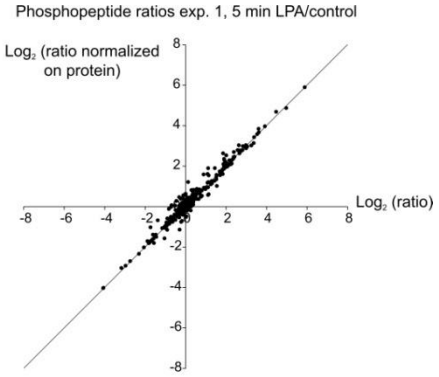
Phosphopeptide ratios exp. 1, 5 min LPA/control
Log2 (ratio normalized on protein)
Log2 (ratio)

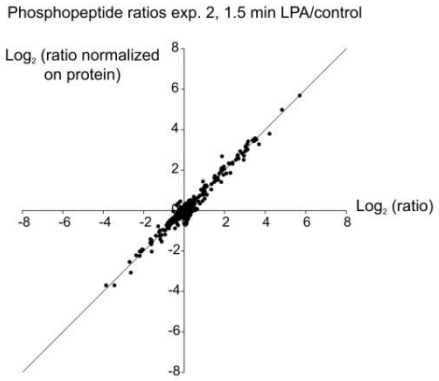
Phosphopeptide ratios exp. 2, 1.5 min LPA/control
Log2 (ratio normalized on protein)
Log2 (ratio)

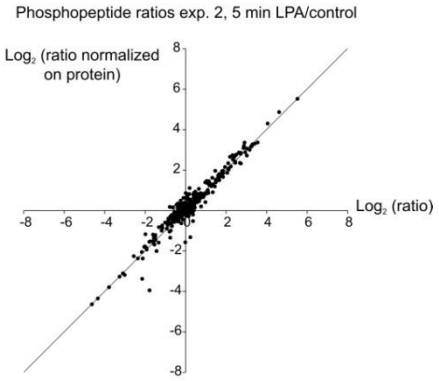
Phosphopeptide ratios exp. 2, 5 min LPA/control
Log2 (ratio normalized on protein)
Log2 (ratio)

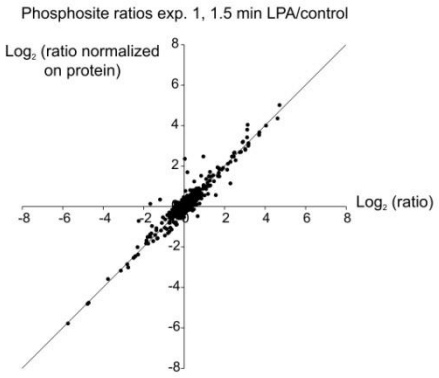
Phosphosite ratios exp. 1, 1.5 min LPA/control
Log2 (ratio normalized on protein)
Log2 (ratio)

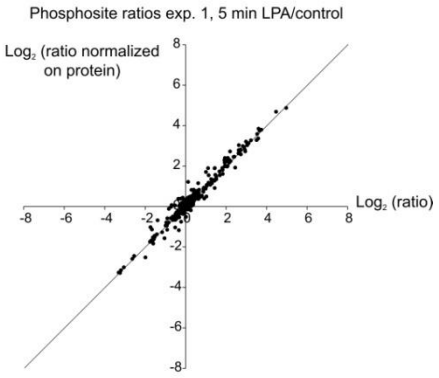
Phosphosite ratios exp. 1, 5 min LPA/control
Log2 (ratio normalized on protein)
Log2 (ratio)

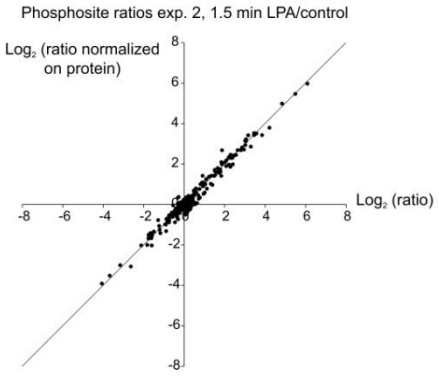
Phosphosite ratios exp. 2, 1.5 min LPA/control
Log2 (ratio normalized on protein)
Log2 (ratio)

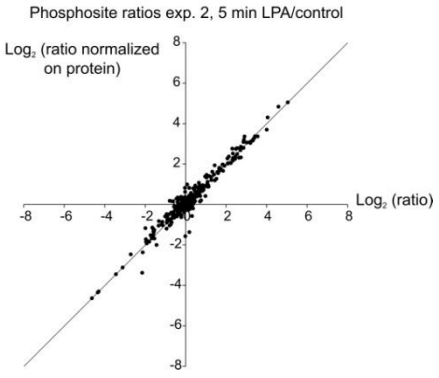
Phosphosite ratios exp. 2, 5 min LPA/control
Log2 (ratio normalized on protein)
Log2 (ratio)

To assess the reproducibility of these datasets phosphopeptide and –site ratios that were quantified in both biological replicate analyses were compared. As visualized in x-y scatter plot comparisons of the two independent SILAC experiments we observed a high concordance of measured ratios for both the 1.5 and 5 min LPA stimulation times (Figure 14).

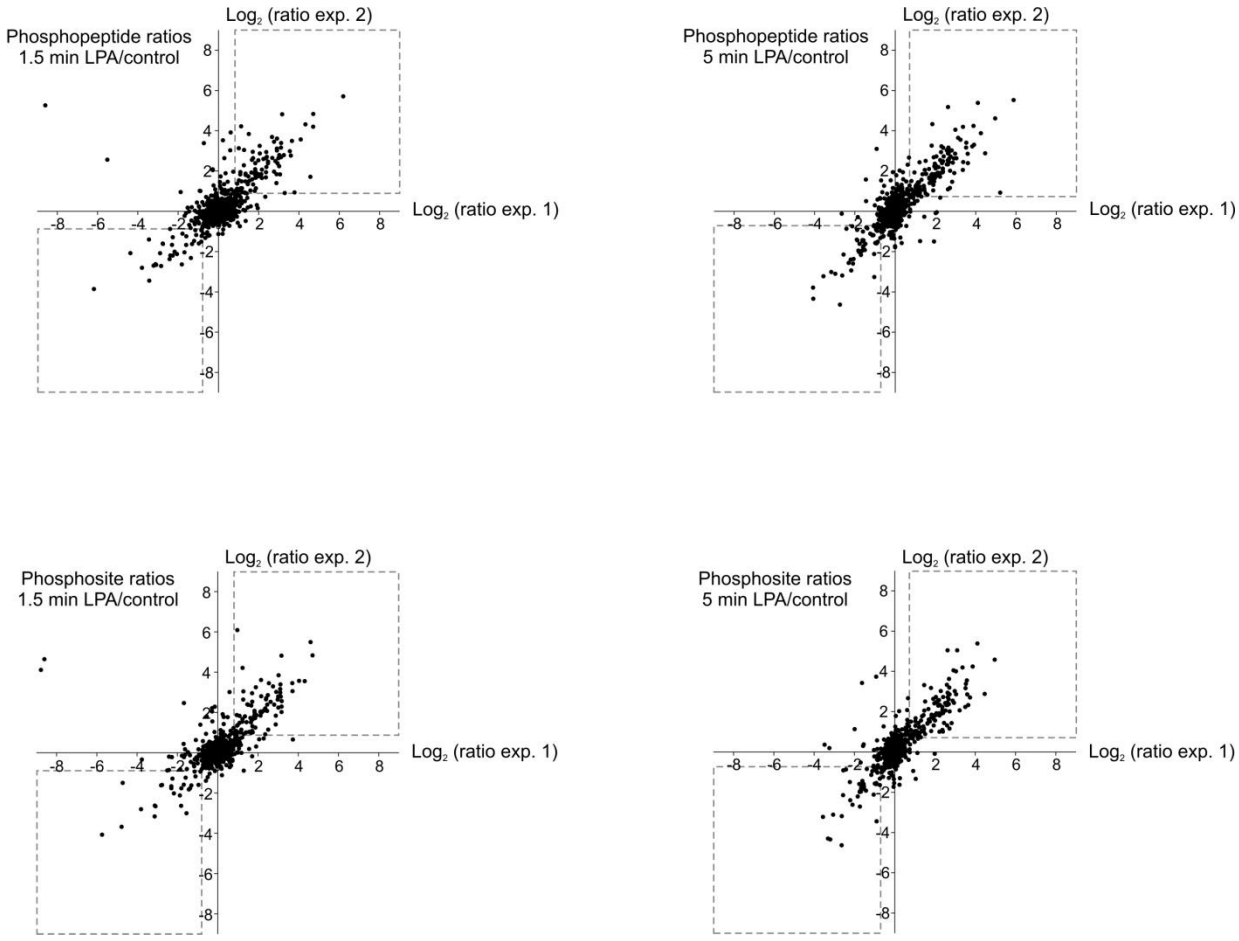

Figure 14: Comparison of log_2- transformed LPA *versus* control phosphopeptide and –site ratios from experiments 1 and 2 for 1.5 and 5 min treatment. The squares indicate significant and reproducible up- and downregulation, corresponding to ratios of greater than 1.77 and 1.65 or ratios of less than 0.57 and 0.61 for the 1.5 and 5 min time points, respectively.

To define thresholds for significantly regulated peptides, the same strategy as described for protein quantification was used and, accordingly, ratios-of-ratios distribution of peptides quantified in both replicate experiments were analysed. The log_2-transformed values followed a Gaussian distribution with the mean close to zero and standard deviations (σ) of around 0.3

for both time points in the two experiments (Figure 15). Changes of more than 2.5 σ were considered as significant, corresponding to ratios of more than 1.77 and 1.65 or ratios of less than 0.57 and 0.61 for the 1.5 min and 5 min LPA time points, respectively. Additionally, significantly regulated phosphopeptide or -site ratios were required to be consistently above or below these values in both experiments (Figure 14).

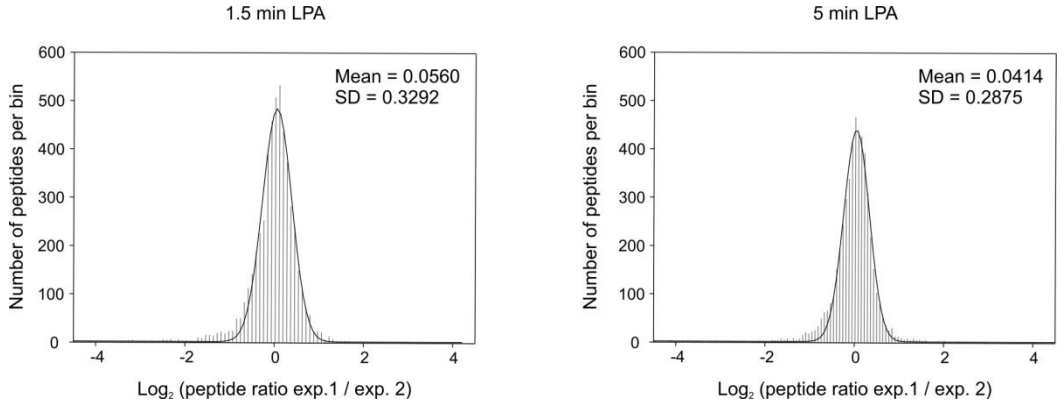

Figure 15: Statistical analysis based on replicate peptide quantifications. Quantified peptides were binned according to their log_2-transformed ratios of their 1.5 min or 5 min LPA versus control ratios obtained in the biological replicate experiments 1 and 2. Gaussian regression analysis was used to calculate the mean and standard deviation of each of the two ratios-of-ratios distributions.

According to these stringent criteria, about one fifth of the more than 700 repeatedly quantified phosphopeptides and –sites were reproducibly regulated after LPA treatment at one or both time points (Figure 16). Notably, the number of regulated sites and peptides only slightly increased from the 1.5 min to the 5 min time point of LPA stimulation, indicating rapid induction of phosphorylation changes that were found in the lectin-purified sub-proteome. Upregulation was detected in case of more than 70% of the LPA-triggered phosphorylation changes. The remaining regulated phosphopeptides were found in reduced abundance, which suggests a considerable number of rapid de-phosphorylation events on the analysed proteins.

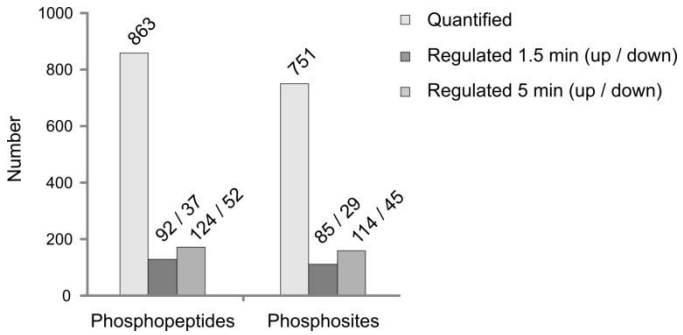

Figure 16: Numbers of repeatedly quantified and reproducibly regulated phosphopeptides and phosphosites.

3.2.3 Bioinformatics analysis of LPA-induced phosphoregulation

The focus was then on reproducibly and significantly upregulated phosphosites found in lectin-enriched proteins to extract phosphorylation motifs reflecting preferential substrate requirements of LPA-activated protein kinases. Due to the small number of regulated phosphorylation events on tyrosine residues, only confidently assigned (class I) serine and threonine sites in the context of their 12 surrounding residues were considered. These upregulated sites after 1.5 and/or 5 min LPA treatment were analysed with the Motif-X software against the background of all other localized phosphorylation events, to identify combinations of amino acids that are significantly over-represented in proximity of LPA-induced phosphoacceptor sites. Besides two motifs with hydrophobic residues in the +1 position (pS/pT-L and pS/pT-V) this iterative analysis extracted R-X-X-pS/pT (where X denotes any amino acid) as most prominent motif found in the subset of LPA-stimulated phosphorylation sites (Figure 17). This matches a known kinase substrate motif shared by protein kinase A, protein kinase C and calmodulin-dependent protein kinase (Pearson and Kemp, 1991; Schwartz and Gygi, 2005), with the latter two representing prominent signal transducers upon LPA stimulation (Radeff-Huang, Seasholtz *et al.*, 2004; Rozengurt, 2007).

Ser/Thr motifs	Score	Foreground dataset		Background dataset	
		Matches	Size	Matches	Size
1) ...R..s/t.....	8.69	40	115	76	585
2) .....s/tL.....	4.66	17	75	37	509
3) .....s/tV.....	4.23	8	58	11	472

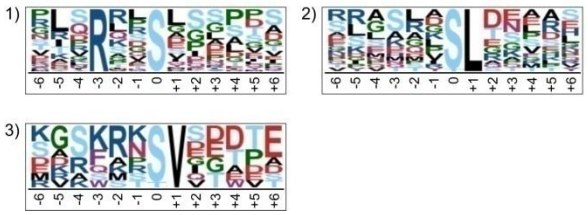

Figure 17: Kinase substrate motifs extracted from LPA-induced phosphorylation sites. The Motif-X algorithm was used to extract significant motifs from all significantly and reproducibly LPA-induced class I Ser(P) and Thr(P) sites (foreground dataset) using all other quantified Ser(P) and Thr(P) sites as background dataset. Sequence logo presentations and a table listing motif scores and counts are shown for all extracted significant motifs.

To explore which biological processes in the glycoproteome may be preferably phosphoregulated upon short-term LPA treatment, gene ontology (GO) annotations were used to identify over-represented GO biological process terms for proteins with reproducibly regulated phosphorylation events (Figure 18). Compared to all phosphoproteins quantified in both experiments, GO analysis not only revealed the expected categories relating to functions in signal transduction, but also showed significant enrichment for cell migration and ion transport across the plasma membrane, with the latter exhibiting the highest ratio among all over-represented GO terms.

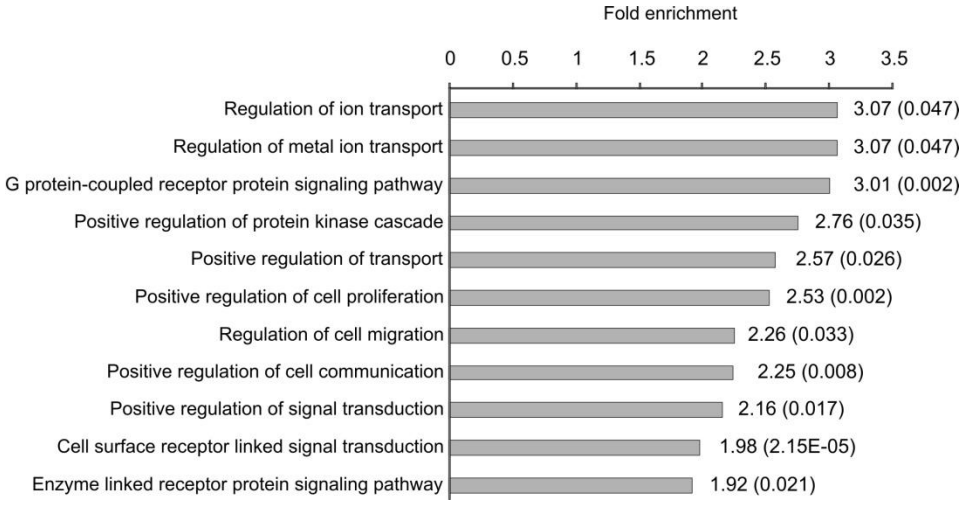

Figure 18: GO analysis of LPA-induced phosphoproteins. Proteins identified with phosphopeptides reproducibly regulated upon LPA were compared to all phosphoproteins quantified in lectin-enriched fractions. For significantly overrepresented GO biological process terms fold-enrichment is shown. The DAVID EASE score, which was required to be less than 0.05, is shown in parentheses for all biological process terms.

Next, the protein interaction properties of all quantified phosphoproteins were investigated. Therefore, the data was submitted to the STRING database to retrieve functional and physical interactions of high confidence (Jensen, Kuhn *et al.*, 2009). Interestingly, STRING analysis revealed that parts of the network were highly enriched for proteins with known plasma membrane localisation (Figure 19). These phosphoproteins formed sub-networks containing, for example, cell adhesion molecules and plasma membrane receptors together with some associated cytosolic partners. In particular, we found two prominent cell adhesion modules, one composed of hemidesmosomal and the other of adherence junction and desmosomal proteins. In Figure 19, it is further indicated which nodes were found with reproducible phosphorylation changes in both experiments, which were additional candidates for LPA regulation due to quantifications in only one of the two experiments, and which were either unregulated or not consistently regulated according to the aforementioned ratio thresholds. While more than half of all plasma membrane phosphoproteins were LPA-regulated in one or both experiments, less than one third of all other network components exhibited phosphorylation changes. Notably, many of those constituted additional modules which related to functions such as nuclear transport and RNA processing.

Figure 19 (next page): Phosphoprotein interaction network. The network is based on all quantified phosphoproteins in lectin-enriched fractions and was generated by querying the STRING database for high confidence interactions. Proteins detected with reproducible and significant phosphorylation changes in both experiments are highlighted in red, additional candidates for LPA regulation based on phosphopeptide quantification in only one of the two experiments are depicted in orange, and phosphoproteins that were either not regulated or not consistently regulated are shown in blue. Square-shaped nodes indicate proteins localising to the plasma membrane.

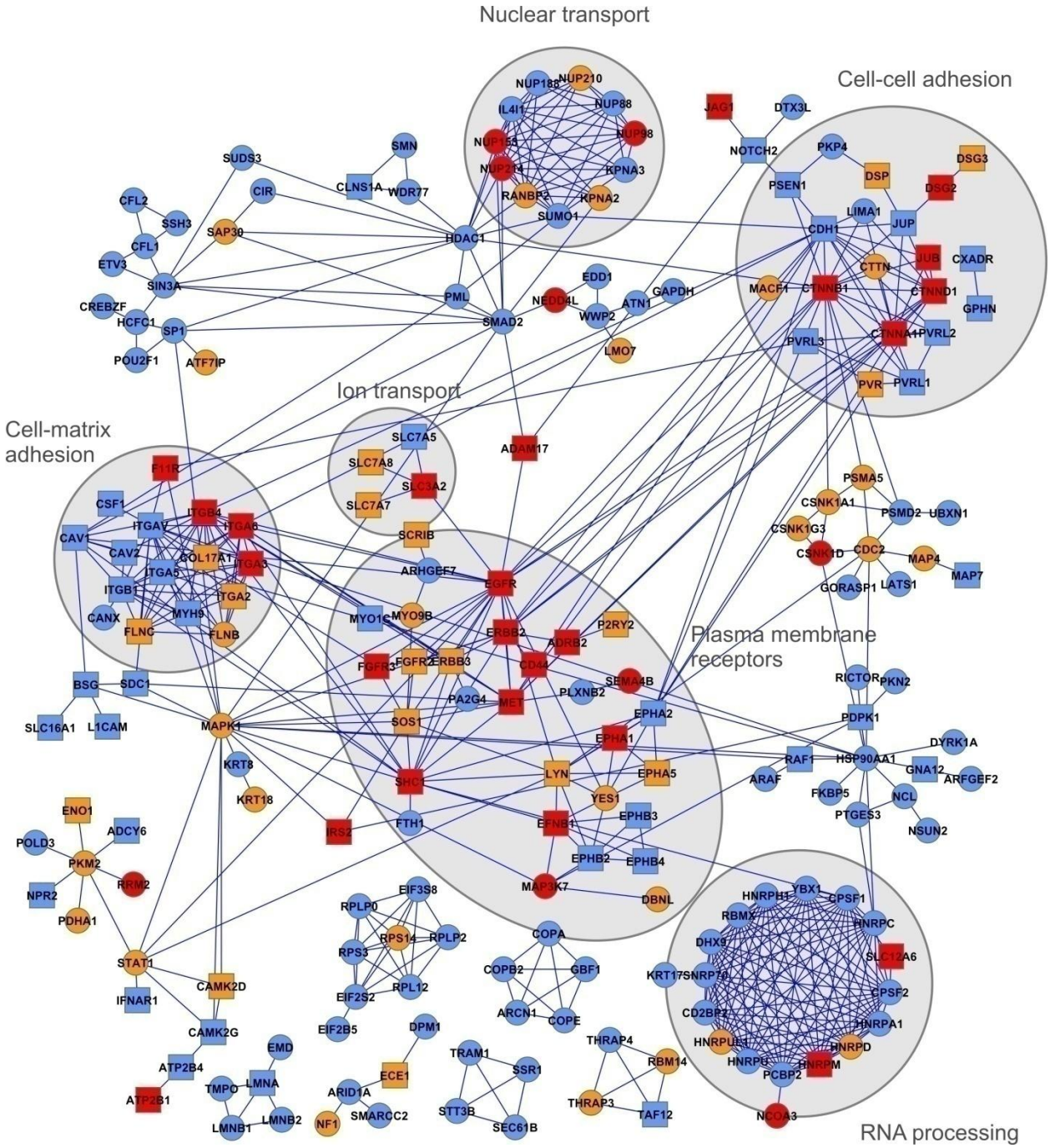
Nuclear transport
Cell-cell adhesion
Ion transport
Cell-matrix adhesion
Plasma membrane receptors
RNA processing
NUP210
NUP188
NUP88
IL4I1
NUP98
NUP155
NUP214
KPNA3
RANBP2
KPNA2
SUMO1
SMN
CLNS1A
WDR77
SUDS3
CIR
SAP30
HDAC1
CFL2
SSH3
CFL1
ETV3
SIN3A
CREBZF
HCFC1
SP1
POU2F1
ATF7IP
PML
SMAD2
EDD1
NEDD4L
WWP2
ATN1
GAPDH
LMO7
JAG1
DTX3L
NOTCH2
PKP4
DSG3
PSEN1
DSP
DSG2
LIMA1
JUP
CDH1
JUB
CXADR
CTTN
MACF1
CTNNB1
CTNND1
GPHN
CTNNA1
PVRL2
PVRL3
PVR
PVRL1
SLC7A5
SLC7A8
SLC3A2
SLC7A7
ADAM17
F11R
CSF1
ITGB4
ITGAV
ITGA6
CAV1
CAV2
COL17A1
ITGA3
ITGA5
ITGB1
ITGA2
CANX
MYH9
FLNC
FLNB
SCRIB
ARHGEF7
EGFR
MYO1C
MYO9B
ERBB2
ADRB2
P2RY2
FGFR3
FGFR2
ERBB3
CD44
SEMA4B
PLXNB2
PA2G4
MET
BSG
SDC1
SLC16A1
L1CAM
MAPK1
SOS1
EPHA2
EPHA1
LYN
EPHA5
SHC1
YES1
EPHB3
EFNB1
FTH1
IRS2
EPHB2
EPHB4
MAP3K7
DBNL
KRT8
KRT18
PSMA5
CSNK1A1
PSMD2
UBXN1
CSNK1G3
CSNK1D
CDC2
MAP4
MAP7
GORASP1
LATS1
RICTOR
PKN2
PDPK1
DYRK1A
RAF1
HSP90AA1
GNA12
ARFGEF2
ARAF
FKBP5
NCL
PTGES3
NSUN2
ENO1
POLD3
ADCY6
PKM2
RRM2
NPR2
PDHA1
STAT1
IFNAR1
CAMK2D
CAMK2G
EIF3S8
RPLP0
RPS14
RPLP2
RPS3
RPL12
EIF2S2
EIF2B5
DPM1
ECE1
ARID1A
SMARCC2
NF1
TRAM1
SSR1
STT3B
SEC61B
COPA
COPB2
GBF1
ARCN1
COPE
THRAP4
RBM14
THRAP3
TAF12
ATP2B4
ATP2B1
EMD
TMPO
LMNA
LMNB1
LMNB2
YBX1
HNRPH1
CPSF1
RBMX
HNRPC
DHX9
SLC12A6
KRT17
SNRPA1
CPSF2
CD2BP2
HNRPA1
HNRPU
HNRPD
HNRPR
HNRPM
PCBP2
NCOA3

3.2.4 Time-dependent phosphorylation profiles of lectin-enriched proteins upon LPA stimulation

Finally, to categorise the observed phosphorylation changes, temporal profiles of reproducibly LPA-regulated class I serine, threonine and tyrosine sites were clustered with the self organising tree algorithm (SOTA). Phosphorylation profiles were assigned to five clusters that were representative of the distinct phosphorylation kinetics observed in our study (Figure 20). Clusters 1 to 3 contained upregulated, while clusters 4 and 5 comprised downregulated phosphorylation sites. Notably, almost half of all regulated phosphorylation sites were rapidly induced and constituted cluster 1 (Figure 20).

Figure 20 (next page): Clustering of time-dependent profiles of LPA-regulated phosphosites. The self organizing tree algorithm (SOTA) was used to cluster significantly and reproducibly regulated class I phosphosites (localisation probability ≥ 0.75) according to their temporal profiles. Phosphorylation ratios at the different time points were log_{10} transformed and normalised ratios (y-axis). Phosphosite numbers and selected phosphorylation sites are indicated for each cluster.

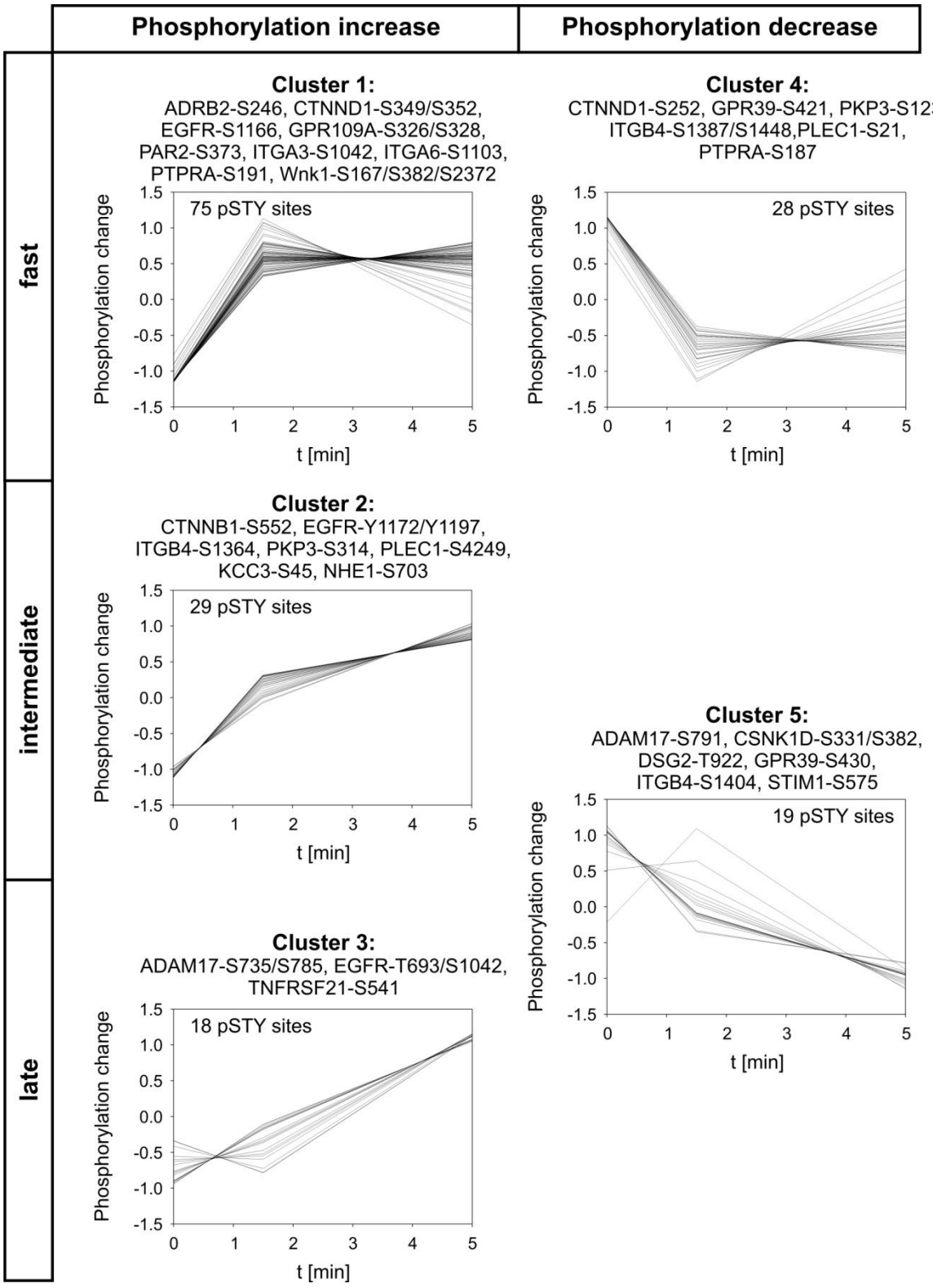
Phosphorylation increase
Phosphorylation decrease
fast
intermediate
late
Cluster 1:
ADRB2-S246, CTNND1-S349/S352, EGFR-S1166, GPR109A-S326/S328, PAR2-S373, ITGA3-S1042, ITGA6-S1103, PTPRA-S191, Wnk1-S167/S382/S2372
75 pSTY sites
Cluster 4:
CTNND1-S252, GPR39-S421, PKP3-S123, ITGB4-S1387/S1448,PLEC1-S21, PTPRA-S187
28 pSTY sites
Cluster 2:
CTNNB1-S552, EGFR-Y1172/Y1197, ITGB4-S1364, PKP3-S314, PLEC1-S4249, KCC3-S45, NHE1-S703
29 pSTY sites
Cluster 5:
ADAM17-S791, CSNK1D-S331/S382, DSG2-T922, GPR39-S430, ITGB4-S1404, STIM1-S575
19 pSTY sites
Cluster 3:
ADAM17-S735/S785, EGFR-T693/S1042, TNFRSF21-S541
18 pSTY sites
Phosphorylation change
t [min]

3.2.4.1 LPA-triggered phosphoregulation of the EGFR and ADAM17

The glycoproteome fraction strategy enabled the sensitive analysis of LPA-induced phosphorylation changes on the EGFR and ADAM17, the metalloproteinase implicated in EGFR transactivation mediated by amphiregulin shedding in SCC-9 cells (Gschwind, Hart *et al.*, 2003) (Table 2, Figure 21A). On ADAM17 significant and reproducible phosphorylation changes were detected at Ser-785, Thr-735 and Thr-791. Phosphorylation of Thr-735, which was found induced upon LPA, was shown to positively regulate metalloproteinase activity (Diaz-Rodriguez, Montero *et al.*, 2002). This might be further enhanced by LPA-triggered downregulation of Thr(P)-791 due to the reported negative role of this site-specific phosphorylation on ADAM17 activity (Xu and Derynck, 2010). However, both sites were more slowly modulated than EGFR phosphorylation at Tyr-1172 and Tyr-1197 (Figure 21B), which are major autophosphorylation sites induced upon extracellular ligand binding (Sorkin, Waters *et al.*, 1991; Sorkin, Helin *et al.*, 1992). In one of the two biological replicate experiments, the previously unknown ADAM17 phosphorylation site Thr-761 was identified and quantified. The corresponding MS and MS/MS spectra are shown in Figure 21C. Interestingly, this site was as rapidly LPA-induced as EGFR tyrosine phosphorylation (Figure 21B and C). Although biological replicate quantification was not achieved for Thr(P)-761, an about four-fold induction after 1.5 min LPA treatment was reproducibly found in three independent quantifications of differently methionine-oxidized peptide species in the second experiment. Additionally, the three dimensional elution profile of these peptide species is presented in Figure 21D.

Furthermore, LPA-induced Ser/Thr phosphorylation sites were monitored on the EGFR, with Ser(P)-1166 being highly upregulated after 1.5 min LPA treatment, and Thr(P)-693 and Ser(P)-1042 exhibiting slower induction (Figure 20 and Figure 21B). Notably, EGFR phosphorylation at Thr-693 is implicated in receptor desensitisation, based on studies showing that mutational inactivation of this site results in impaired EGFR endocytosis (Heisermann, Wiley *et al.*, 1990). Moreover, in addition to the EGFR, LPA-regulated Ser/Thr phosphorylation was found on a variety of other RTKs, such as fibroblast growth factor receptor 3, receptor tyrosine-protein kinase erbB-2, ephrin type-A receptor 1 and hepatocyte growth factor receptor (Figure 19, Table 2).

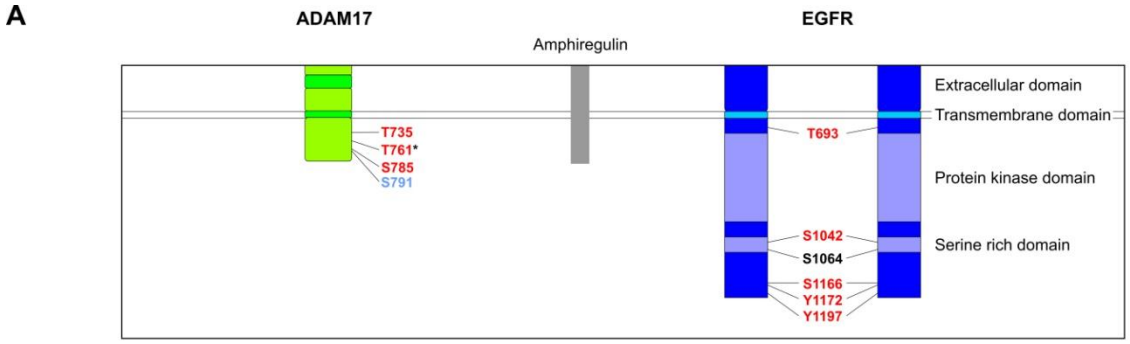

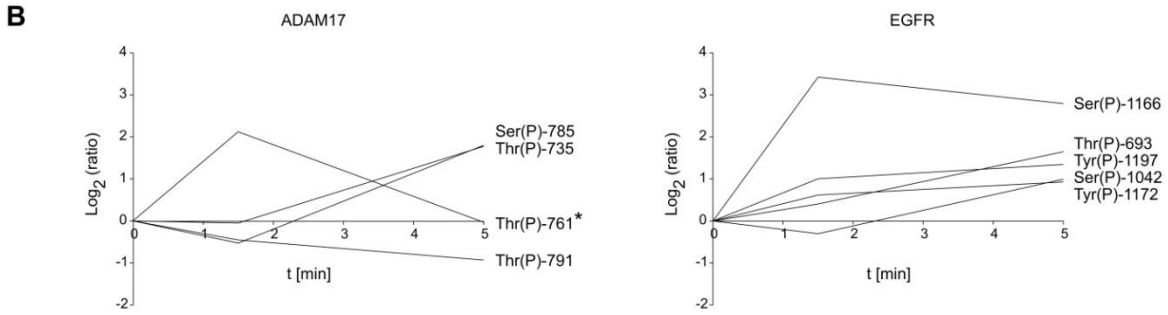

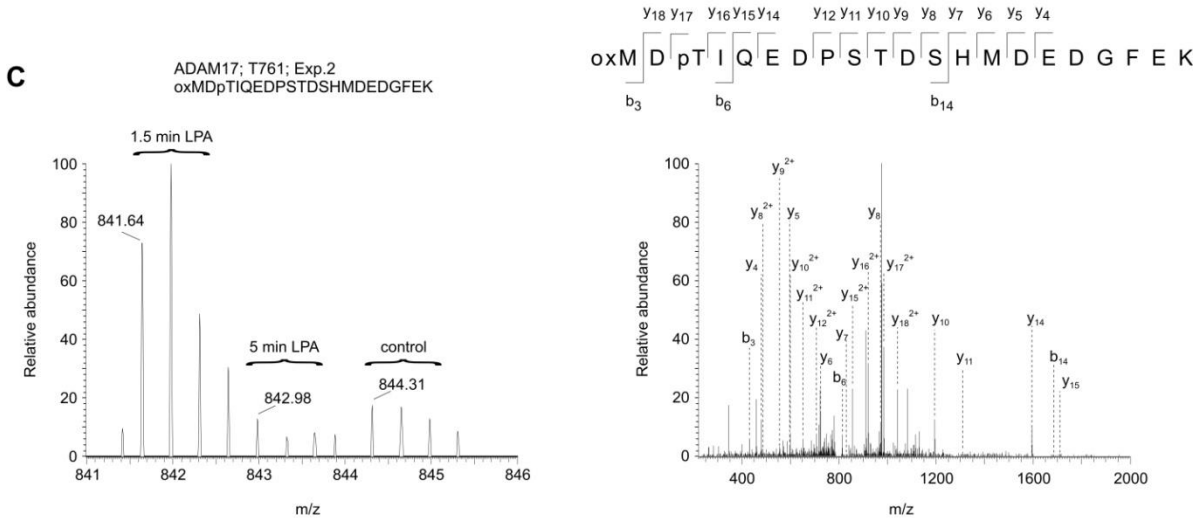

D

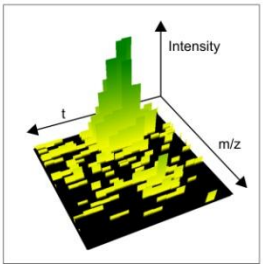

Evidence ID	*Modified Sequence*	*Ratio 1.5 min LPA/ control*	*Ratio 5 min LPA/ control*
28837	_M(ox)DT(ph)IQEDPSTDSHM(ox)DEDGFEK_	3.99	1.84
28838	_MDT(ph)IQEDPSTDSHM(ox)DEDGFEK_	4.40	0.91
28839	_M(ox)DT(ph)IQEDPSTDSHMDEDGFEK_	4.33	0.98

Figure 21: LPA-induced phosphorylation events on ADAM17 and the EGFR. A, Schematic representation showing reproducibly quantified phosphorylation sites located in the intracellular parts of the metalloproteinase ADAM17 and the EGFR. Phosphosites highlighted in red were significantly upregulated upon LPA treatment. B, Time-dependent profiles of LPA-triggered phosphorylation events on ADAM17 and the EGFR. C, MS and MS/MS spectra of the ADAM17 peptide M(ox)DT(ph)IQEDPSTDSHMDEDGFEK harbouring the phosphosite Thr(P)-761. D, 3D elution profile of ADAM17 peptide M(ox)DT(ph)IQEDPSTDSHMDEDGFEK and table showing ratios from independent quantifications of different methionine-oxidized phosphopeptide species. Asterik indicates a non-reproducibly detected phosphosite.

3.2.4.2 Phosphoregulation of GPCRs, ion co-transporters and exchangers

Besides RTKs GPCRs and ion transporters constitute a major class of integral membrane proteins, which were enriched in lectin-purified SCC-9 fractions and thus amenable to sensitive phosphorylation site analysis (Figure 10).

Several rapid modifications were found on non-LPA GPCRs that were assigned to cluster 1. These included phosphorylations on β2 adrenergic receptor, prostaglandin E2 receptor, proteinase-activated receptor 2 and nicotinic acid receptor 1 (Table 2). Moreover, GPR39A exhibited a rapid phosphorylation decrease at one site assigned to cluster 4.

Interestingly, LPA-regulated site-specific phosphorylations were further detected on proteins with ion transmembrane transporter activity (Table 2) (Chen, Sun *et al.*, 2008). The natrium/hydrogen exchanger 1 (NHE1) was regulated on two distinct phosphorylation sites Ser(P)-703 and Ser(P)-796 upon LPA treatment which were assigned to clusters 2 and 1, respectively (Figure 20). Phosphorylation at Ser-703 is mediated by p90 ribosomal S6 protein kinases (RSKs) and known to enhance NHE1 exchange activity upon serum stimulation, resulting in proton efflux coupled to the influx of sodium ions (Takahashi, Abe *et al.*, 1999). This regulatory mechanism was here observed in response to a specific ligand, the bioactive lipid LPA.

Moreover, the potassium/chloride cotransporter KCC3, which is another major determinant of osmotic homeostasis, was found phosphorylated on Ser-45 upon LPA treatment. Ser(P)-45 is an unreported phosphorylation site located in the N-terminal domain of the cotransporter. Additional LPA-regulated phosphorylation events were detected e.g. on multidrug resistance-associated protein 1 and sodium-coupled neutral amino acid transporter 1.

3.2.4.3 Regulation of cell adhesion proteins

The bioactive lipid LPA potently induces cell migration in SCC-9 and other cancer cells, which requires the coordinated modulation of integrin-mediated interactions with the ECM. Integrins are composed of α and β subunits to form heterodimeric transmembrane proteins with bidirectional signalling properties, in a way that either intracellular signals can regulate binding to ECM proteins such as fibronectin, laminin or collagen or, *vice versa*, ECM proteins act as extracellular ligands to evoke integrin-mediated signals on the cytoplasmic side. Integrins are glycosylated and therefore as many as 12 different subunits were detected upon lectin-based enrichment from SCC-9 extracts. Notably, LPA-induced phosphorylation changes were monitored on several of these cell adhesion molecules. LPA induced rapid and sustained phosphorylation of Ser-1042 in integrin α3 and Ser-1103 in integrin α6 (Table 2). These phosphorylation changes were both assigned to cluster 1 (Figure 20) due to their kinetics and occurred within a shared QPpSxxE motif. Interestingly, phosphorylation of that particular motif was implicated in integrin-mediated regulation of cytoskeletal organisation (Zhang, Bontrager *et al.*, 2001). Although both sites were regulated with a similar temporal profile, upregulation of Ser(P)-1103 on the α6 integrin subunit was more pronounced with a seven- and ten-fold induction measured after 1.5 and 5 min LPA treatment, respectively. This strong increase preceded LPA-induced phosphorylation of Ser-1364 on the associated β4 integrin subunit assigned to cluster 2 (Figure 20). Notably, phosphorylation of this site is known to disrupt intracellular binding to plectin 1, which links the β4 integrin to keratin intermediate filaments (Wilhelmsen, Litjens *et al.*, 2007). The heterodimeric α6/β4 integrin is a key component of hemidesmosomes, which link cytoskeletal structures in epithelial cells with ECM components of the basement membrane. Furthermore, in contrast to increased phosphorylation of Ser-1364, rapid LPA-induced downregulation was detected on a number of sites located in the connective segment of integrin β4. LPA-induced reciprocal regulation as on intergrin β4 was also observed on its aforementioned interactor plectin 1 (Table 2).

Analyses also revealed LPA-induced phosphoregulation of many proteins involved in the formation of cell-cell contacts, including δ-catenin and β-catenin associated with adherence functions as well as desmoglein and plakophilins involved in desmosome assembly. Interestingly, the amino-terminal domain of δ-catenin contains regulatory sequences which have been implicated in adherens junction disassembly upon dephosphorylation of this protein region (Xia, Mariner *et al.*, 2003). Although LPA was reported to reduce the overall

phosphorylation level in the amino-terminal domain of δ-catenin (Ratcliffe, Smales *et al.*, 1999), the corresponding phosphorylation sites have not been mapped in the context of GPCR signalling. Rapid loss of phosphorylation was recorded on Ser-252, which was decreased by four-fold within only 1.5 min LPA treatment and assigned to cluster 4 due its temporal profile (Figure 20). Moreover, δ-catenin was reciprocally regulated on the phosphorylation level, as evident from two upregulated phosphorylation sites located at Ser-349 and Ser-352, both of which exhibited fast and sustained induction upon LPA stimulation (Figure 20, cluster 1). Interestingly, phosphorylation was also observed of the δ-catenin-interacting protein β-catenin on Ser-552 upon LPA treatment (Table 2). This β-catenin site is a known Akt kinase substrate site. Its phosphorylation releases β-catenin from the cell-cell contacts, which is a pre-requisite for the protein to translocate into the nucleus for transcriptional control (Fang, Hawke *et al.*, 2007).

Although not all significant phosphoregulations on several adherens junction proteins could be detected in both biological replicate experiments, reproducible phosporylation events were found on two components of desmosomes: desmoglein 2 and plakophilin 3. Both adherens junctions and desmosomes form stable extracellular cell-cell contacts, but interact with distinct cytoskeletal structures (actin filaments and cytokeratin filaments, respectively) on the intracellular side of the plasma membrane. LPA treatment resulted in the gradual downregulation on Thr(P)-922 of desmoglein 2 and the reciprocal regulation of the plakophilin 3 phosphorylation sites Ser-123 and Ser-314. These results identify desmosomes as additional cellular components targeted by LPA-induced signalling.

3.2.4.4 LPA-dependent regulation of Wnk1 and its role in cell migration

In addition to the EGFR tyrosine kinase the serine/threonine protein kinase Wnk1 was detected as a prominent phosphoprotein in lectin-enriched fractions. This suggests that Wnk1 either associates with transmembrane glycoproteins or, alternatively, bound to immobilized lectin molecules due to O-linked GlcNAc modification (Hart, Haltiwanger *et al.*, 1989). Seven phosphorylation sites were identified that could be quantified in both replicate experiments and confidently assigned to specific residues (Figure 22A). Four of these sites were significantly upregulated and exhibited more than two-fold induction already after 1.5 min LPA treatment (Figure 22B). These included the functionally characterised site Ser(P)-382, which is a known autophosphorylation site of Wnk1 that stabilizes the active

kinase state due to its location in the activation loop region of the Wnk1 kinase domain (Xu, Min *et al.*, 2002; Zagorska, Pozo-Guisado *et al.*, 2007). Owing to this biochemical evidence for rapid induction of cellular Wnk1 signalling activity a knock-down protocol was established, which is based on RNA interference with duplex siRNAs, to further explore Wnk1 function in LPA signalling. As phosphorylation changes on Wnk1 followed a similar kinetics as EGFR autophosphorylation on tyrosine residues it was tested whether Wnk1 acts upstream of the EGFR in the transactivation process. Therefore, cells were transfected with either control siRNA or siRNAs directed against Wnk1, starved for 48 h and then either treated with 10 µM LPA for 3 min or left untreated. However, despite efficient downregulation of Wnk1 protein in SCC-9 cells, LPA-induced autophosphorylation of EGFR was rather similar in Wnk1-depleted cells compared to control-transfected cells (Figure 22C). Thus Wnk1 does not act as an intermediate signal transducer in LPA-evoked EGFR transactivation. As the induction of cell migration and cell proliferation represent major biological outcomes in LPA-treated SCC-9 cancer cells, the RNAi knock-down approach was further used to test for possible Wnk1 functions in these biological processes. Therefore, wound closure assays were performed in SCC-9 cells to examine the migratory behavior. In control-transfected cells LPA treatment induced a pronounced migratory response that was measured after 22 h (Gschwind, Prenzel *et al.*, 2002). Notably, RNAi-mediated Wnk1 ablation resulted in strong impairment of LPA-induced migration in SCC-9 cells, which was consistently observed with two distinct Wnk1 siRNAs (Figure 22D). In contrast, Wnk1 protein knock-down had only a minor effect on SCC-9 cell proliferation measured in parallel to migration (Figure 22E).

Figure 22 (next page): Regulation and function of Wnk1 in LPA signalling. A, Schematic illustration of Wnk1. Reproducibly upregulated phosphosites upon LPA stimulation are shown in bold. B, Temporal profiles of LPA-regulated phosphosites. C, Immunoblot analysis of LPA-induced EGFR transactivation in Wnk1 knock-down cells. Detection was done in parallel with antibodies recognizing Tyr(P)-1173 in the EGFR, Wnk1 and tubulin. D, Effect of Wnk1 protein knock-down by siRNA transfection on LPA-induced cell migration of SCC-9 cells. Wound closure rates measured in scratch assays were determined and the results are shown as the mean ± SD (*p < 0.001 according to Student's t-test). Protein knock-down of Wnk1 was verified by immunoblot analysis. E, LPA-dependent cell proliferation was analysed in parallel to the wound closure assay.**

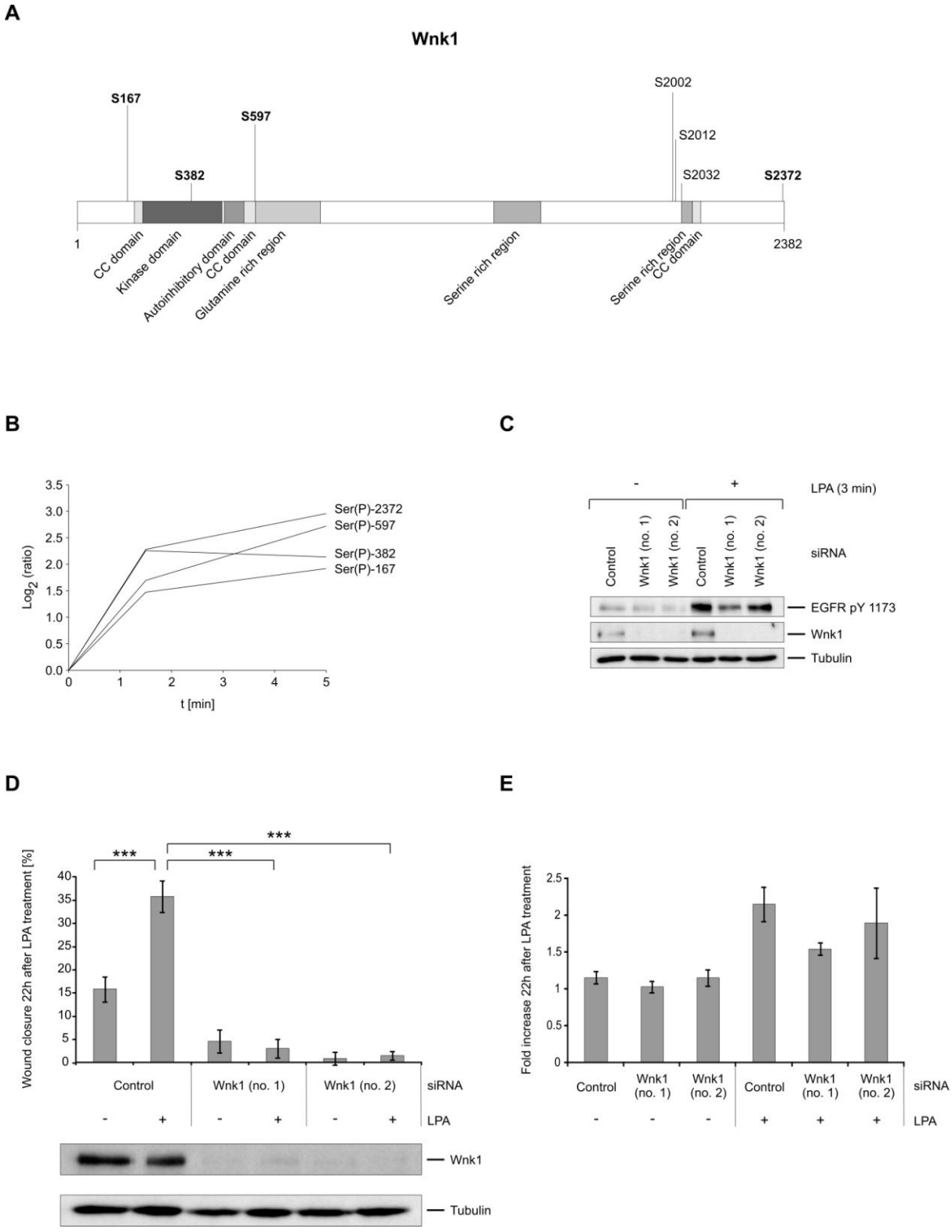
A
Wnk1
S167
S597
S382
S2002
S2012
S2032
S2372
1
2382
CC domain
Kinase domain
Autoinhibitory domain
CC domain
Glutamine rich region
Serine rich region
Serine rich region
CC domain
B
Log2 (ratio)
t [min]
Ser(P)-2372
Ser(P)-597
Ser(P)-382
Ser(P)-167
C
LPA (3 min)
siRNA
Control
Wnk1 (no. 1)
Wnk1 (no. 2)
EGFR pY 1173
Wnk1
Tubulin
D
Wound closure 22h after LPA treatment [%]
***
Control
Wnk1 (no. 1)
Wnk1 (no. 2)
siRNA
LPA
Wnk1
Tubulin
E
Fold increase 22h after LPA treatment
Control
Wnk1 (no. 1)
Wnk1 (no. 2)
siRNA
LPA

Table 2: Selected LPA-stimulated phosphorylation sites

Protein	IPI	Position	Sequence	Ratio 1.5 min LPA / control	Ratio 5 min LPA / control
G protein-coupled receptors					
Beta-2 adrenergic receptor	IPI00465066	246	FHVQNL**S**QVEQDG	18.57	14.29
CD97 antigen precursor	IPI00397229	831	TRALRA**S**ESGI	2.90	4.70
Nicotinic acid receptor 1	IPI00157746	326	EPDNNR**S**TSVELT	2.11	1.84
Nicotinic acid receptor 1	IPI00157746	328	DNNRST**S**VELTGD	3.01	2.33
Prostaglandin E2 receptor EP2 subtype	IPI00016314	240	CGPSLG**S**GRGGPG	5.90	6.27
Proteinase-activated receptor 2 precursor	IPI00296446	373	VKQMQV**S**LTSKKH	7.47	4.89
Cell adhesion molecules					
Catenin alpha-1	IPI00215948	655	DVRSRT**S**VQTEDD	6.43	8.00
Catenin beta-1	IPI00017292	552[a]	DTQRRT**S**MGGTQQ	2.46	3.48
Catenin beta-1	IPI00017292	556	RTSMGG**T**QQQFVE	2.76	3.82
Catenin delta-1	IPI00182540	349	ERGSLA**S**LDSLRK	2.67	2.45
Catenin delta-1	IPI00182540	352	SLASLD**S**LRKGGP	2.89	4.08
CD44 antigen precursor	IPI00305064	697[b]	VEDRKP**S**GLNGEA	3.71	6.38
Integrin alpha-3 precursor	IPI00215995	1042[c]	EMKSQP**S**ETERLT	2.24	2.35
Integrin alpha-6 precursor	IPI00216225	1103	EIHAQP**S**DKERLT	6.95	9.93
Integrin beta-4 precursor	IPI00220845	1364[d]	SGSQRP**S**VSDDTE	2.69	4.19
Junctional adhesion molecule A precursor	IPI00001754	284	VIYSQP**S**ARSEGE	8.37	2.62
Junctional adhesion molecule A precursor	IPI00001754	287	SQPSAR**S**EGEFKQ	34.67	20.80
Plakophilin-3	IPI00026952	314	TLQRLS**S**GFDDID	2.73	6.76
Plectin-1	IPI00398779	4249	FRSRSS**S**VGSSSS	1.50	2.03
Protein ajuba	IPI00063605	119	PTAPAL**S**PRSSFA	1.84	2.29
Transporters					
Wolframin	IPI00008711	32	RLNATA**S**LEQERS	27.31	27.59
Solute carrier organic anion transporter family member 4A1	IPI00100858	43	TPLSPG**S**LRSAAH	8.33	2.99
Solute carrier family 12 member 6	IPI00220151	45	PDLSQN**S**ITGEHS	1.47	2.11
Sodium-coupled neutral amino acid transporter 1	IPI00871279	52	DRESRR**S**LTNSHL	4.20	4.09
Metal transporter CNNM4	IPI00418426	657	RSPAHP**T**PLSRSA	1.68	2.38
Metal transporter CNNM4	IPI00418426	660	AHPTPL**S**RSASLS	1.59	2.36
Metal transporter CNNM4	IPI00418426	664	PLSRSA**S**LSYPDR	2.99	3.15
Sodium/hydrogen exchanger 1	IPI00020060	703[e]	SRARIG**S**DPLAYE	1.76	3.47
Sodium/hydrogen exchanger 1	IPI00020060	796	RIQRCL**S**DPGPHP	4.31	5.95
Multidrug resistance-associated protein 1	IPI00719178	925	QLQRQL**S**SSSSYS	4.56	5.13
Inositol 1,4,5-trisphosphate receptor type 3	IPI00291607	934	VLSRKQ**S**VFSAPS	10.43	8.01
Inositol 1,4,5-trisphosphate receptor type 3	IPI00291607	1832	TKGRVA**S**FSIPGS	11.25	11.86
Inositol 1,4,5-trisphosphate receptor type 3	IPI00291607	1834	GRVASF**S**IPGSSS	4.02	6.55
Inositol 1,4,5-trisphosphate receptor type 3	IPI00291607	1843	GSSSRY**S**LGPSLR	2.84	3.58

Kinases and phosphatases					
Ephrin type-A receptor 1 precursor	IPI00294250	906	VTLRLP**S**LSGSDG	4.26	5.28
Epidermal growth factor receptor precursor	IPI00018274	693[f]	ELVEPL**T**PSGEAP	1.32	3.13
Epidermal growth factor receptor precursor	IPI00018274	1042	SSLSAT**S**NNSTVA	0.81	1.99
Epidermal growth factor receptor precursor	IPI00018274	1166	KGSHQI**S**LDNPDY	10.70	6.92
Epidermal growth factor receptor precursor	IPI00018274	1172	SLDNPD**Y**QQDFFP	1.53	1.90
Epidermal growth factor receptor precursor	IPI00018274	1197[g]	TAENAE**Y**LRVAPQ	2.00	2.54
Fibroblast growth factor receptor 3 isoform 1 variant	IPI00556575	538	SSGEGP**T**LANVSE	3.25	3.12
Macrophage-stimulating protein receptor precursor	IPI00030273	1056	PLLRKE**S**IQLRDL	7.80	9.68
Pantothenate kinase 2, mitochondrial precursor	IPI00171176	189	RRDRLG**S**YSGPTS	2.23	3.64
Receptor tyrosine-protein kinase erbB-2 precursor	IPI00300384	701	ELVEPL**T**PSGAMP	1.37	4.45
Receptor tyrosine-protein kinase erbB-2 precursor	IPI00300384	998	EDLGPA**S**PLDSTF	2.49	10.20
Receptor tyrosine-protein kinase erbB-2 precursor	IPI00300384	1073	EEEAPR**S**PLAPSE	1.61	5.82
Receptor-type tyrosine-protein phosphatase alpha precursor	IPI00743698	191	AGSHSN**S**FRLSNG	4.83	4.80
Septin-9	IPI00784614	30	GPALKR**S**FEVEEV	5.50	5.37
Serine/threonine-protein kinase D2	IPI00009334	710[h]	EKSFRR**S**VVGTPA	15.83	19.59
Serine/threonine-protein kinase WNK1	IPI00004472	167	SKDRPV**S**QPSLVG	2.78	3.78
Serine/threonine-protein kinase WNK1	IPI00004472	382[i]	RASFAK**S**VIGTPE	4.78	4.40
Serine/threonine-protein kinase WNK1	IPI00004472	597	QQVEQS**S**ASQTGI	3.24	6.59
Serine/threonine-protein kinase WNK1	IPI00004472	2372	NLQKSI**S**NPPGSN	4.86	7.77
Others					
ADAM 17 precursor	IPI00288894	735[j]	PFPAPQ**T**PGRLQP	0.97	3.42
ADAM 17 precursor	IPI00288894	785	KDPFPN**S**STAAKS	0.69	3.48
Heat shock protein beta-1	IPI00025512	82[k]	ALSRQL**S**SGVSEI	3.46	4.99
Nuclear receptor coactivator 3	IPI00748532	860[l]	PYNRAV**S**LDSPVS	3.02	2.48
Oncostatin-M specific receptor subunit beta precursor	IPI00022674	826	FLGTRK**S**LTETEL	2.56	2.48
Prostaglandin F2 receptor negative regulator precursor	IPI00871938	922	ERRRLM**S**MEMD	14.15	10.99
Rhotekin	IPI00029834	106	KTSRRP**S**DSGPPA	1.64	2.09
Semaphorin-4B precursor	IPI00419724	830	PRVRLG**S**EIRDSV	1.44	2.08
SHC-transforming protein 1	IPI00021326	428[m]	LFDDPS**Y**VNVQNL	3.17	8.05
Tissue factor precursor	IPI00010338	285[n]	KAGVGQ**S**WKENSP	6.10	12.05
Tumor necrosis factor receptor superfamily member 21 precursor	IPI00004413	541	LLTVEP**S**PQDKNK	0.87	2.01

[a] Increase of transcriptional activity; dissociation of catenin β from cell-cell contacts (Fang, Hawke *et al.*, 2007)

[b] Regulation of cell motility (Tzircotis, Thorne *et al.*, 2006)

[c] Regulation of signalling, motility and cytoskeletal engagement (Zhang, Bontrager *et al.*, 2001)

[d] Inhibition of interaction with plectin 1 and induction of hemidesmosome disruption (Wilhelmsen, Litjens *et al.*, 2007)

[e] Enhancement of NHE1 exchange activity (Takahashi, Abe *et al.*, 1999)

[f] Receptor internalisation (Heisermann, Wiley *et al.*, 1990; Gamou and Shimizu, 1994; Winograd-Katz and Levitzki, 2006)

[g] Enzymatic activation (Sorkin, Waters *et al.*, 1991; Sorkin, Helin *et al.*, 1992)

[h] Activation of PKD2 (Sturany, Van Lint *et al.*, 2002)

[i] Activation of Wnk1 kinase activity (Xu, Min *et al.*, 2002; Zagorska, Pozo-Guisado *et al.*, 2007)

[j] Activation of ADAM17 shedding activity (Diaz-Rodriguez, Montero *et al.*, 2002)

[k] Cytoskeletal reorganisation (Butt, Immler *et al.*, 2001)

[l] Inhibition of interaction with estrogen receptor α (Wu, Qin *et al.*, 2004)

[m] Induction of interaction with Grb2 (Ugi, Imamura *et al.*, 2002; Patrussi, Savino *et al.*, 2005)

[n] Regulation of cell growth and cell motility (Ahamed and Ruf, 2004; Siegbahn, Johnell *et al.*, 2005; Li, Collier *et al.*, 2008)

3.3 Time-resolved phosphorylation site analysis in the entire SCC-9 cell proteome upon LPA treatment

The glycoproteome analysis described in the previous sections provided interesting results about short-term LPA-induced regulations on plasma membrane proteins such as cell surface receptors, ion transporters and cell adhesion molecules. To gain a more comprehensive view of global phosphorylation events in response to LPA treatment, an additional approach was used to monitor the phosphoproteome of SCC-9 cells on a more global scale across five stimulation intervals covering the initial 90 min after stimulation. Thus, the following experiments not only aimed to identify phosphorylation regulations upon LPA stimulation but also to capture time-dependent changes in phosphoprotein interaction networks that underly the signalling phases of signal initiation, propagation and terminal effector regulation.

3.3.1 Experimental design for LPA-induced time-resolved phosphorylation analysis

SILAC-based phosphoproteomics was used for the time-resolved quantification of LPA-induced phosphorylation events. The combination of two triple labelling experiments (part A and B) enabled the quantitative comparison of site-specific phosphorylations at five different time points (Figure 23). LPA stimulation times of 3, 10, 30 and 90 min were chosen and compared with respect to the unstimulated control. The two triple labelling SILAC experiments were coupled through the common 10 min stimulation condition, which was selected as biological and technical variances were assumed to be minimal at this particular time point. After SILAC-labelled SCC-9 cells had been stimulated with 10 µM LPA for the indicated times cells were lysed. Total cell lysates from the unstimulated cells, 3 min and 10 min LPA-treated cells, corresponding to part A of the experiment, and likewise cell lysates derived from the 10 min, 30 min and 90 min LPA-stimulated cells, corresponding to part B, were combined in equal protein amounts, respectively. All subsequent sample processing steps were carried out separately for both experimental parts. These steps encompassed tryptic in-solution digest, desalting as well as fractionation of peptide mixtures and enrichment of phosphopeptides. Herein, the fractionation of peptides relied on high-performance strong cation exchange chromatography (SCX), while phosphopeptide enrichment was based on immobilized metal ion affinity chromatography (IMAC). For each experimental part 14 SCX fractions were collected and separately subjected to further

phosphopeptide enrichment and subsequent LC-MS/MS analysis. Furthermore, to gain highly confident phosphoproteomics data based on biological reproducibility, in total three biological replicates were performed for both experimental parts, and for each replicate experiment cell labels were changed with regard to stimulation conditions as indicated in Figure 23. Due to the 14 LC-MS/MS runs per experimental part and biological replicate the final number of LC-MS measurements added up to 84 runs.

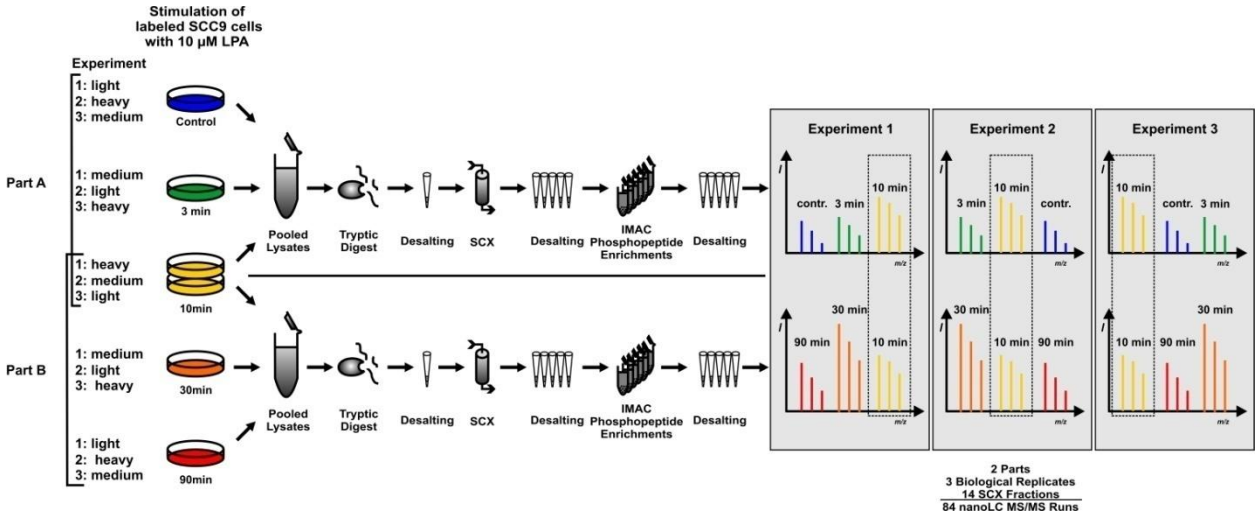

Figure 23: Quantitative phosphoproteomics approach to identify LPA-dependent temporal phosphorylation profiles. Labelling schemes and sample processing are shown for the combination of two SILAC labelling experiments (part A and B) and the three biological replicate experiments performed. After pooling of the respective lysates proteins were tryptically digested in solution and the resulting peptides were fractionated by strong cation exchange chromatography (SCX). Phosphopeptides were then enriched by immobilized ion metal affinity chromatography (IMAC) and analysed on an Orbitrap mass spectrometer. Acquired MS data were merged through the common reference condition of 10 min LPA stimulation.

Identification of peptides and quantification of phosphopeptides and discrete phosphorylation sites were then performed with the algorithms implemented in the MaxQuant software suite as already described above. In total, 3,840 distinct phosphoproteins could be identified that harboured as many as 17,190 high-confidence phosphorylation sites with a localisation probability of more than 0.75 (class I). Notably, more than 95% of these sites were quantified in at least one of the three biological replicate experiments. Comparitive analysis of the quantified phosphosites revealed a high degree of similarity between all three experiments as demonstrated by their remarkable overlap (Figure 24A). 7,587 phosphorylation sites were quantified in all three biological replicates, and more than 3,700 additional sites were found

in two replicates, with quantification performed for at least one of the five LPA stimulation times. The observed high overlap between the three experiments was also reflected on the phosphopeptide level (Figure 24B). Again, phosphopeptides were defined by their amino acid sequence and number of phosphate groups.

Further analysis was performed for distinct phosphosites, and only those 6,841 phosphosites were considered that were quantified for all five time points in at least two of the biological replicate analyses. To generate individual time-dependent profiles for these sites MS-derived ratios of the 30 and 90 min time point from experimental part B were related to the unstimulated control condition of experimental part A. In a final step averages across the biological replicates were calculated for every time point. The main focus of this project lied on phosphorylation alterations upon LPA stimulation and the criteria for regulated sites were set as follows: Phosphorylation sites were defined to be regulated in case of a more than two-fold average change upon LPA treatment, corresponding to a ratio of more than 2 for upregulated sites and less than 0.5 for downregulated sites. Furthermore, to ensure minimal variance of quantitative data only those phosphosites were extracted for further analysis that exhibited at one or more regulated time points a coefficient of variation smaller than 0.3 across biological replicates. Astonishingly, almost one third of the profiled phosphorylation sites, 2,095, matched these stringent filter criteria and was used for subsequent bioinformatic analysis.

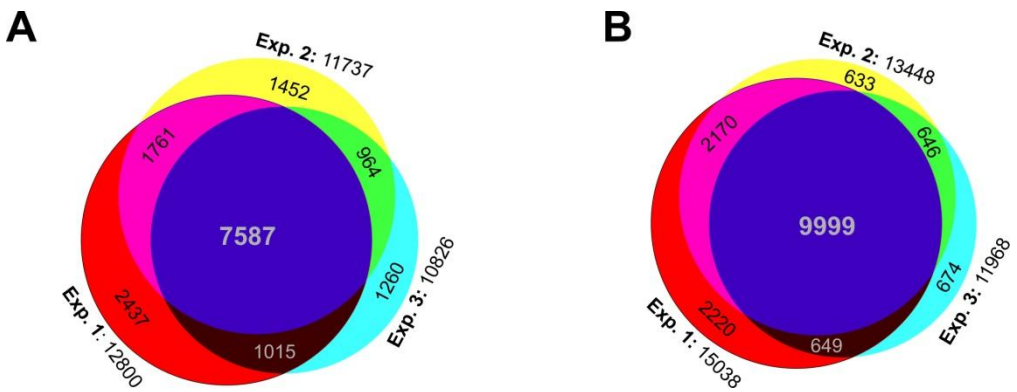

Figure 24: Overlap of quantified class I phosphosites (A) and phosphopeptides (B) between three biological replicate experiments. The overlap of two and three biological replicates is presented in Venn diagrams.

3.3.2 Interaction network of LPA-regulated phosphoproteins

In a first step protein-protein interactions among LPA-regulated phosphoproteins were analysed. The interconnectivity of proteins responding to the same stimulus can provide insights into which proteins might be regulated in a complex or as part of a functional module and therefore contribute to a certain biological process in a coordinated manner. Consequently, all proteins harbouring regulated phosphorylation sites were submitted to the STRING protein-interaction database in order to map LPA signalling data on reported high confidence ($p > 0.7$) protein-protein interactions based on experimental and database knowledge. The resulting network comprised a heterogenous main module containing proteins involved in the biological processes such as cell adhesion, transcription and MAPK signalling (Figure 25). The latter two categories were mainly represented by transcription factors and kinases as seen in Figure 25 and showed a high degree of internal connectivity. The class of cell adhesion proteins is represented by components of different adhesion structures like tight junctions (F11R, TJP1, TJP2), adherens junctions (CTNNB1, CTNNA, CTNND1), hemidesmosomes (ITGB4) and focal adhesions (PXN, PARVA). Remarkably, a central position in the main module is occupied by the EGFR with a high number of directly interacting partners involved in a variety of biological processes. In addition to the central module of the network several submodules emerged from the STRING analysis. The MAPK signalling components are for example linked to one submodule consisting of translation initiation factors and ribosomal proteins and to a second submodule of RNA splicing proteins, both via the ribosomal protein S6 kinase (RPS6K). Furthermore, both submodules are interconnected with each other by protein-protein interactions of the two members nuclear cap-binding protein subunit 1 (NCBP1) and the eukaryotic translation initiation factor G1 (EIFG1). Notably, LPA not only affects the phosphomodification of the aforementioned proteins, but has also an impact on the phosphorylation of a remarkable number of nuclear pore proteins forming a separate submodule. This particular submodule encompasses also proteins involved in nuclear division and has extraordinary high internal connectivity. Extensive LPA-induced phosphorylation was further detected on G-protein regulatory elements such as GTPase-activating proteins (GAPs), guanine nucleotide exchange factors (GEFs) and a GDP dissociation inhibitor (GDI), which build the fourth and most prominent submodule with a high number of members that were all connected amonst each other.

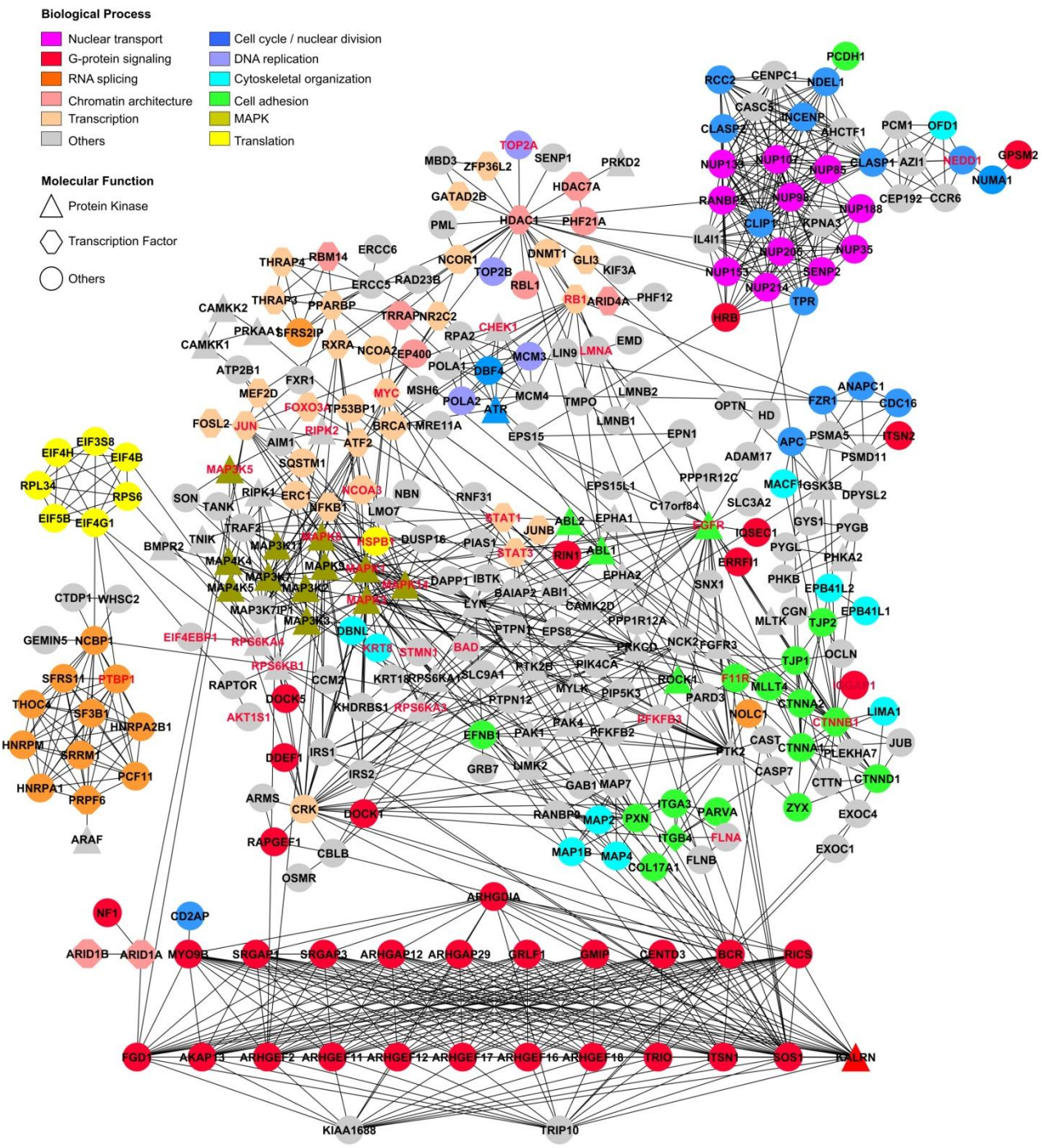

Figure 25: Phosphoprotein interaction network. Highly confident (p > 0.7) interactions between LPA-regulated phosphoproteins are shown as retrieved from the STRING database. Molecular functions and biological processes are encoded by shape and colour based on the respective Gene Ontology annotations. Proteins harbouring regulated phosphosites that have been functionally characterised previously are depicted in red font (Table 3).

3.3.3 Hierarchical clustering of time-dependent phosphorylation profiles

Many proteins in the interaction network contain multiple phosphosites with different time-dependent phosporylation patterns. To analyse LPA-induced profiles of detected phosphosites heatmaps were generated for proteins of selected functional categories (Figure 26). Only phosphorylation sites originating from singly phosphorylated peptides were considered in this analysis. Besides cateogories such as G protein-coupled signalling, G protein-coupled receptor regulation or protein kinase activation, which are very prominent in the context of LPA signalling, the focus was here on the initiation of processes which phenotypic effects might become evident at later time points.

Hierarchical clustering of transcription factor phosphorylation sites revealed similar temporal regulation of multiple sites lying in proximity within the same protein. For example, rapid and sustained decrease in phosphorylation was observed on the neighbouring sites Ser-104 and Tyr-106 of the tripartite motif-containing protein 29 (TRIM29). Furthermore, Ser(P)-98 and Tyr(P)-544 of this protein were downregulated, whereas Ser(P)-152 was highly upregulated at all time points upon LPA treatment. Although multiple regulated phosphosites were observed for TRIM29 none of these sites has been functionally characterised in earlier studies. Furthermore, the phosphorylation profiles of the two neighbouring sites Ser-90 and Ser-92 within the butyrate response factor (ZFP36L1) clustered together as both phosphosites were rapidly modified with a further gradual increase of their phosphorylation levels detected from 3 to 90 min of LPA stimulation. A gradual increase in phosphorylation could also be observed for Ser(P)-125 and Ser(P)-334 of this transcription factor. While the mentioned phosphosites responded rather fast upon LPA stimulation, nearly half of all phosphosites detected on transcription factors exhibited temporal profiles with a by comparison delayed onset of phosphorylation at the 10 or 30 min time point. For example, the phosphosites Ser(P)-63 and Ser(P)-73 of AP-1 (JUN), which indicate transcriptional activity of this factor, were induced upon LPA after 10 and 30 min, respectively. Interestingly, in parallel to the LPA-dependent activation of several transcription factors, such as AP-1 (JUN), signal transducer and activator of transcription 1 and 3 (STAT1 and 3), regulation of chromatin-modifying enzymes could also be observed.

For example, demethylases or histone acteylases, which are involved in the modulation of DNA accessibility, were found regulated upon LPA. Histone acetyltransferase MYST3 was phosphorylated at Ser-1089 already at the 3 min time point and the phosphorylation level gradually increased until it peaked at the 30 min time point. In contrast, the lysine-specific

demethylase 5C phosphosite (KDM5C) Ser(P)-301 was not modified before 10 min of LPA treatment, however this site exhibited sustained upregulation over the remaining treatment period. Moreover, histone deacteylases, which possess a functional activity antoagonistic to acteyltransferases, were also found regulated but to a by comparison lower extent, e.g. as evident from Ser(P)-220 of histone deacetylase 7 (HDAC7), or were more slowly induced with significant changes first seen after 30 min LPA stimulation, as e.g. monitored for Ser(P)-406 of histone deacteylase 1 (HDAC1). These enzymes probably influence chromatin architecture, although their functional relevant phosphosites are still unknown and await further characterisation.

Interestingly, while chromatin architecture and transcription were affected by LPA treatment, a regulatory effect was also observed for RNA splicing processes. Proteins falling in this category furthermore formed a separate submodule in the interaction network. Phosphorylation on RNA splicing-associated phosphoproteins was mainly observed after 10 and 30 min of LPA stimulation and reverted to basal levels after 90 min. For example, heterogeneous nuclear ribonucleoprotein A2/B1 (HNRAPA2B1) was strongly phosphorylated on Ser-212 at 10 and 30 mins after LPA treatment. The same profile but with a lower overall phosphorylation level was detected for Ser(P)-383 of zinc finger protein 638 (ZNF638) as well as for Ser(P)-2272 and Ser (P)-2289 of serine/arginine repetitive matrix protein 2 (SRRM2). Due to the similarity of their time-dependent phosphorylation profiles these sites clustered together in the generated heatmap (Figure 26). Moreover, a very conspicuous phosphorylation profile was detected on the THO complex protein 4 (THOC4) which is part of dynamic complexes involved in mRNA processing and export. Ser(P)-101 of this protein showed high and sustained upregulation in the time span from 3 to 30 min of LPA stimulation but was strongly counterregulated at the 90 min time point. At this time point even a decrease of phosphorylation in comparison to basal levels could be observed.

As LPA is known to trigger proliferation and migration in SCC-9 cells heatmaps were also generated for phosphosites of proteins representing the Gene Ontology categories nuclear division and cell adhesion. For nuclear division a variety of distinct different phosphorylation profiles were observed upon LPA treatment, although SCC-9 cells had not been sychronised before treatment. Rapid and transient upregulation for the first 10 min of LPA stimulation was detected for Ser(P)-241 of microtubule-stabilising protein CLIP-associating protein 2 (CLASP2) and Ser (P)-404 of the protein NEDD1. Interestingly, phosphorylation of the latter site has been described to promote the binding of NEDD1 to γ-tubulin and is important for

microtubule nucleation and spindle formation during mitosis (Zhang, Chen *et al.*, 2009). Strong and sustained upregulation was observed on distinct phosphosites of the actin-binding protein annilin (ANLN1), the CAP-Gly domain-containing linker protein 1 (CLIP1), the probable E3 ubiquitin-protein ligase MYCBP2 and the large proline-rich protein BAT2. Interestingly, besides the strongly and sustained upregulated site Ser(P)-486 the actin binding protein annilin is regulated on several sites exhibiting very different phosphorylation profiles. Thus, Ser(P)-659 shows increased phosphorylation during the first ten minutes and decreased phosphorylation below basal levels at the 30 and 90 min time points of LPA treatment. In contrast, Ser(P)-450 was found regulated late upon LPA stimulation with its dephosphorylation evident after 90 min.

The heatmap entitled cell adhesion not only consists of phosphosites from cell adhesion molecules but also harbours phosphosites from various other proteins implicated in the modulation of cellular adhesion. Therefore, phosphosites were included for the LPA-phosphorylated GPCRs CD97 and GPR56 as well as for the G-Protein regulatory protein Neurofibromin 1 (NF1). Moreover, the EGFR autophosphorylation sites Tyr(P)-1172 and Tyr(P)-1197 are listed with their time-dependent profiles demonstrating induction of phosphorylation at the 3 and 10 min time points, respectively, which then decreased to basal levels and below at later LPA time points. For the matrix metalloproteinase ADAM17, which is involved in the EGFR transactivation, the two phosphosites Ser(P)-785 and Ser(P)-791 were observed with high LPA-induced up- and downregulation, respectively. Notably, maximal regulation for both sites was achieved at the 10 and 30 min time points and regulation was slightly decreased at the 90 min time point. Upon 3 min LPA treatment, Ser(P)-785 and Ser(P)-791 did not and just matched the regulation criteria, respectively.

In stark contrast to all other heatmaps the hierarchical clustering of phosphorylation profiles of cell adhesion molecules and related proteins revealed that nearly half of all phoshosites in this category were downregulated upon LPA. Notably, the temporal profiles of multiple phosphorylation sites within particular proteins were strongly correlated. For example, the phosphorylation profiles of Ser(P)-115, Ser(P)-118 and Ser(P)-313 on the desmosomal cell adhesion molecule plakophilin 3 (PKP3) co-clustered as their phosphorylation status was reduced following a slow kinetic profile. In contrast, phosphorylation on the three sites Ser(P)-1384, Ser(P)-1385, Ser(P)-1443 of the hemidesmosomal protein integrin beta 4 (ITGB4) was rapidly and strongly reduced already after 3 min of LPA treatment. Dephosphorylation profiles of these sites followed very similar kinetics, and LPA treatment had a long-lasting effect during the whole measuring period. Moreover, dephosphorylation

events were also detected on distinct sites of adherens junction proteins such as catenin α and δ.

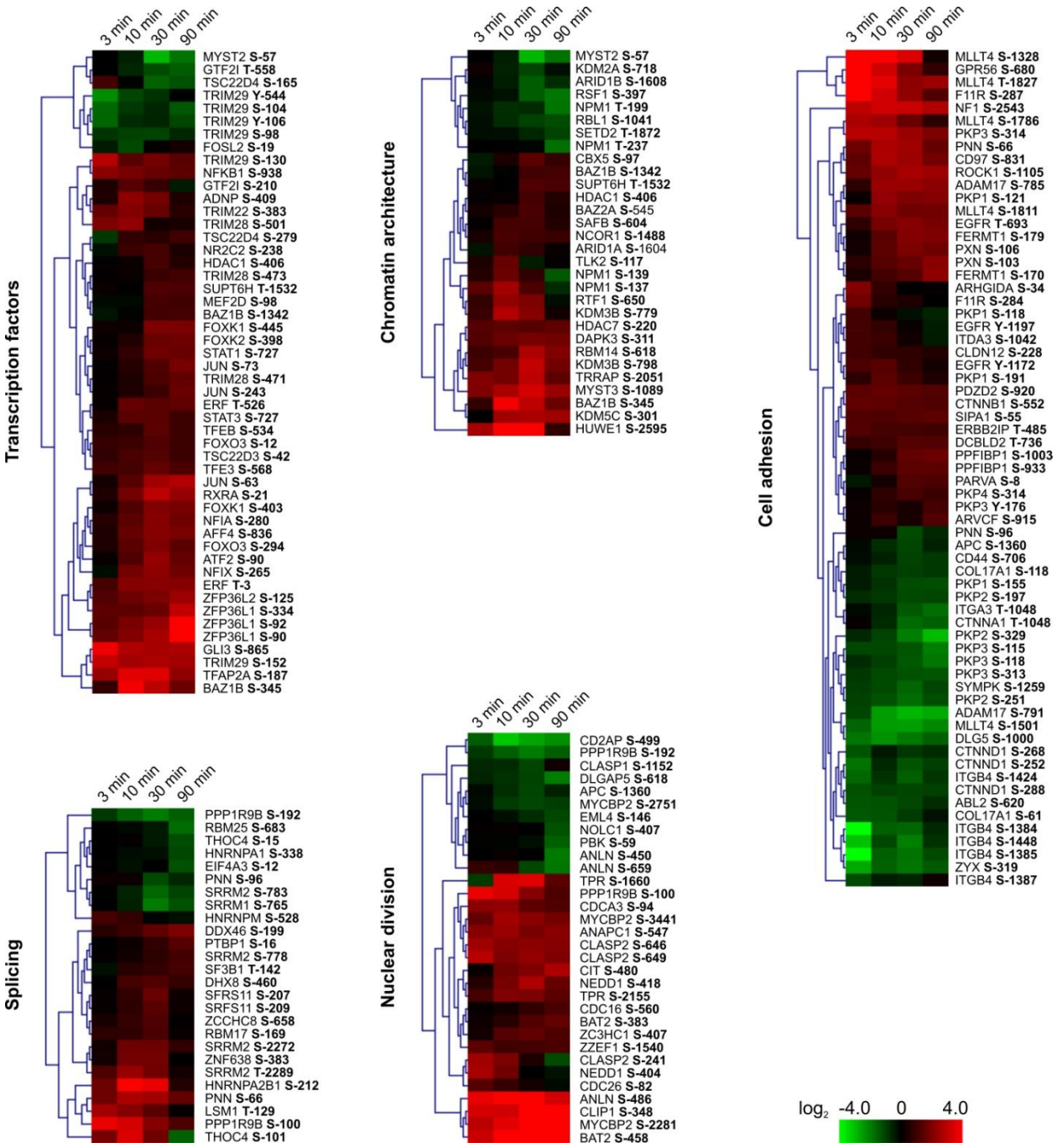

Figure 26: Hierarchical clustering of temporal phosphorylation profiles of distinct proteins belonging to the categories transcription factors, splicing, chromatin architecture, nuclear division and cell adhesion. For heatmap generation only those phosphosite ratios deriving from the quantification of singly phosphorylated peptides were considered.

3.3.4 Clustering of time-dependent phosphorylation profiles and analysis of resulting phosphoprotein networks

In order to group regulated phosphorylation sites according to their temporal profiles, fuzzy-c means clustering was performed as initially described by Olsen *et al* (Olsen, Blagoev *et al.*, 2006). Therefore, each regulated phosphorylation profile was logarithmised and normalised to yield a mean of zero and a standard deviation of one, thus reflecting the relative phosphorylation changes upon LPA stimulation. By fuzzy-c means clustering the normalised temporal profiles were assigned to eight clusters, of which five comprised the about 1,500 upregulated phosphosites and three were formed by the smaller fraction of the almost 500 downregulated phosphosites (Figure 27). Notably, the consensus profiles of the distinct clusters present signalling kinetics covering four temporal phases from signal initiation to terminal effector modulation. Hence, the clusters can be grouped into early, intermediate early, intermediate and late responders to LPA. To further explore associations among similarly regulated proteins cluster-specific interaction networks were generated (Figure 27). Remarkably, G-protein regulators were rarely or not found in interaction networks of downregulated clusters, whereas all early to intermediate upregulated clusters contained prominent submodules of these proteins. These submodules consisted of at least six G-protein regulators that exhibited high intraconnectivity among each other, while simultaneously regulated interaction partners varied between the different networks. While the Rho guanine nucleotide exchange factor FGD1 was linked to the Rho GTPase activating proteins SLIT-ROBO Rho GTPase-activating protein 3 (SRGAP3) and Rho GTPase-activating protein 29 (ARHGAP29) in the early transient and intermediate upregulated cluster, FGD1 was connected to the SLIT-ROBO Rho GTPase-activating protein 1 (SRGAP1) and Rho GTPase-activating protein 12 (ARHGAP12) in the early sustained cluster. Moreover, while FGD1 is exclusively connected to other G-protein regulators in early LPA responsive clusters this protein interacts with other protein classes, namely the transcription activator AT-rich interactive domain-containing protein 1A (ARID1A) and the endocytotic-relevant proteins Cdc42-interacting protein 4 (TRIP10) and cortactin (CTTN), in the intermediate regulated cluster. Interestingly, proteins involved in endocytotic processes almost exclusively mapped to the intermediate upregulated network. Among them the EGFR interactors epidermal growth factor receptor substrate 15 (EPS15), epidermal growth factor receptor substrate 15-like 1 (EPS15L1) and epsin (EPN1) were linked to each other and to the EGFR. These proteins play a major role in EGFR internalisation via the assembly of clathrin-coated,

endocytotic vesicles (Morinaka, Koyama *et al.*, 1999; Roxrud, Raiborg *et al.*, 2008). The presence of EGFR in this network is due to the phosphorylation profile of its functional site Thr(P)-693 which was assigned to the intermediate regulated cluster and triggers receptor internalisation upon phosphorylation (Heisermann, Wiley *et al.*, 1990; Gamou and Shimizu, 1994; Winograd-Katz and Levitzki, 2006).

In this network harbouring phosphoproteins with intermediate LPA-regulated sites EGFR is further linked to a small number of cell adhesion molecules. Interestingly, submodules of strongly connected cell adhesion molecules were very prominent in the interaction networks of the early sustained and early downregulated cluster. Herein, simultaneously regulated phosphosites from proteins constituting different adhesive structures, such as adherens junctions, focal adhesions, hemidesmosomes, desmosomes and tight junctions, were prominent. For example, in the early downregulated cluster tight junction proteins 1 and 2 (TJP 1 and 2) are linked to each other and to the adherens junction proteins catenin α 1 and 2 (CTNNA 1 and 2), catenin δ (CTNND1) and afadin (MLLT4). Furthermore, tight junction protein 1 is linked to the hemidesmosomsal subunits integrin β4 (ITGB4) and collagen 17 α chain (COL17A1) via the direct integrin beta 4 interactor plectin 1 (PLEC1). Moreover, the focal adhesion proteins zyxin (ZYX) and focal adhesion kinase 1 (PTK2) are integrated into this submodule via their connections to catenins and integrin β4 (ITGB4). In contrast to cell adhesion proteins harbouring rapidly regulated phosphosites, desmosomal proteins were mainly found in the interaction network based on intermediate downregulated phosphosites. Desmosomal structures were represented by plakophilins 1 to 3 (PKP 1-3), desmoplakin (DSP) and periplakin (PPL). Additionally, a small submodule of intraconnecting cell adhesion molecules could be even detected for phosphoproteins harbouring late upregulated phosphosites.

In the aforementioned submodule of cell adhesion molecules with early sustained phosphorylation sites catenin β is represented through its rapidly regulated site Ser(P)-552. Phosphorylation of this site is known to initiate the removal of catenin β from adherens junctions and further permits the transcriptional activity of this protein. Notably, such a phosphorylation event on proteins implicated in transcriptional processes was very rare among early regulated phosphoproteins. Hence, modulators of transcription and transcription factors formed distinct subgroups in the networks of intermediate and late regulated clusters. Remarkably, the phosphosites of transcription factors indicating their transcriptional activity were for example assigned to the late cluster for signal transducer and activator of

transcription 1 (STAT1), AP-1 (JUN) and Myc proto-oncogene protein (MYC). Late activation of these proteins was accompanied by phosphorylation events of their interaction partners fos-related antigen 2 (FOSL2), transcription factor jun-B (JUNB), myocyte-specific enhancer factor 2D (MEF2D), histone deacetylase 1 (HDAC1) and DNA (cytosine-5)-methyltransferase 1 (DNMT1).

Figure 27 (next page): Clusters of temporal phosphorylation profiles and corresponding networks of simultaneously regulated phosphoproteins. Eight clusters with distinct phosphorylation profiles were generated by fuzzy c-means clustering. The X-axis shows the time of LPA stimulation, while the Y-axis shows relative phosphorylation changes upon LPA treatment. The number of phosphosites forming one cluster is given in the upper right corner of the diagrams. Phosphoproteins deriving from one cluster were used to generate confident interaction networks (p > 0.4) and proteins were colour-coded according to Gene Ontology annotations. Triangle and octagonale forms represent kinases and transcription factors, respectively. Names in red fond indicate proteins with functionally characterised phosphosites that are assigned to the respective temporal clusters.

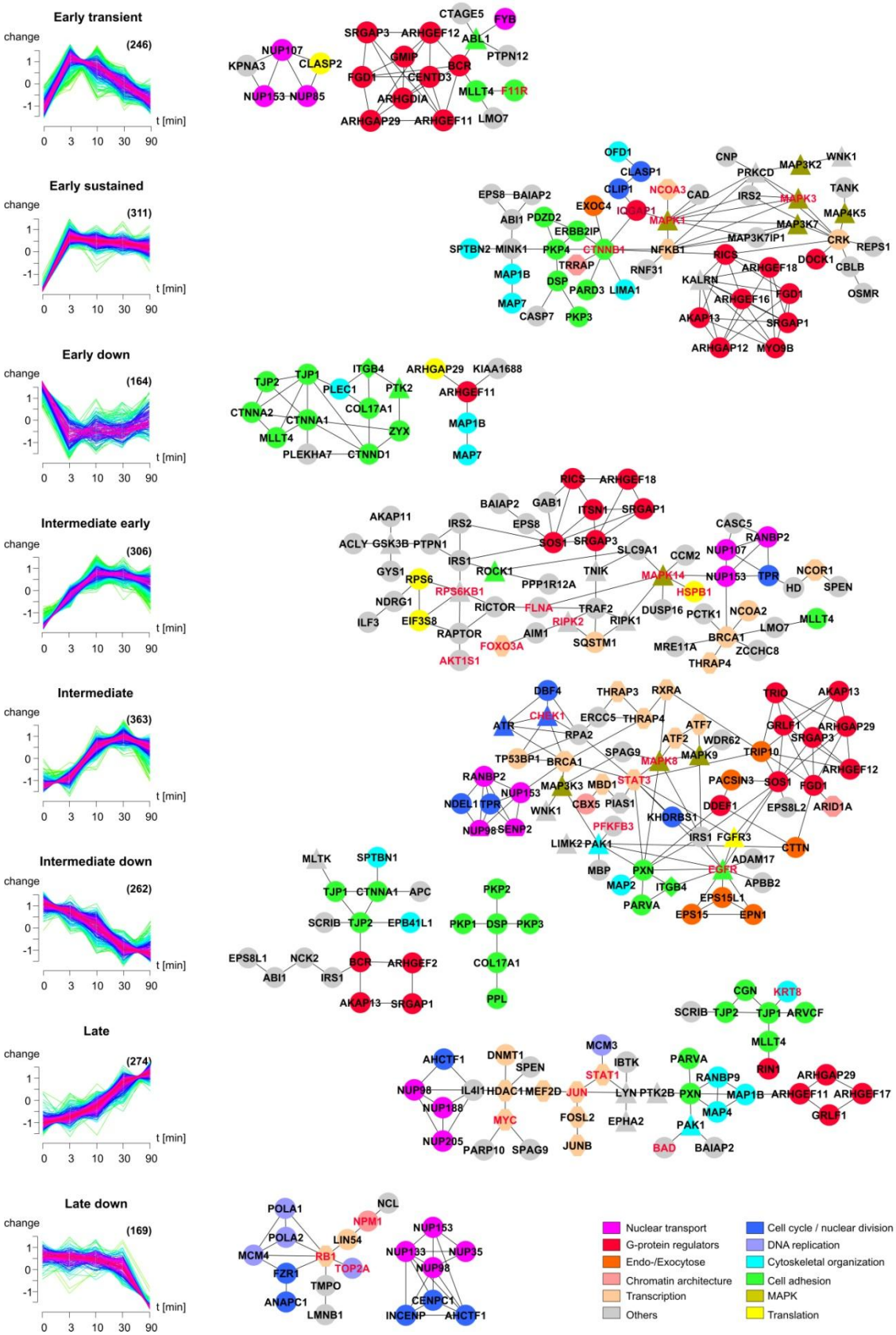
Early transient
(246)
Early sustained
(311)
Early down
(164)
Intermediate early
(306)
Intermediate
(363)
Intermediate down
(262)
Late
(274)
Late down
(169)
change
t [min]
0 3 10 30 90
Nuclear transport
G-protein regulators
Endo-/Exocytose
Chromatin architecture
Transcription
Others
Cell cycle / nuclear division
DNA replication
Cytoskeletal organization
Cell adhesion
MAPK
Translation

Table 3: Temporal profiles of functionally characterised phosphosites.

Protein Name	IPI	Position	Sequence	3 min	10 min	30 min	90 min	Effect of Phosphorylation*
40S ribosomal protein S6	IPI00021840	236	KRRRLS **S** LRASTS	1.35	2.01	0.51	0.16	Induces interaction with RNA; translation pre-initiation complex
6-phosphofructo-2-kinase/fructose-2,6-biphosphatase 2	IPI00305589	483	RRPRNY **S** VGSRPL	2.23	2.46	3.49	2.55	Induces interaction with 14-3-3; stimulates glycolysis
6-phosphofructo-2-kinase/fructose-2,6-biphosphatase 3	IPI00645153	461	PLMRRN **S** VTPLAS	2.29	6.23	8.35	5.33	Enzymatic activation
Adenomatous polyposis coli protein	IPI00012391	1360	FSSGAK **S** PSKSGA	0.91	0.60	0.47	0.69	Cell cycle regulation; mitotic spindle anchoring to the cell cortex
Bcl2 antagonist of cell death	IPI00024291	118	RELRRM **S** DEFVDS	1.86	3.07	9.93	15.12	Anti-apoptotic effect
Butyrate response factor 1	IPI00016635	92	FRDRSF **S** EGGERL	2.64	3.77	5.16	18.37	Regulates association with 14-3-3 beta; increases RNA stability
CAD protein	IPI00301263	1406	AGGRRL **S** SFVTKG	7.99	8.06	13.13	12.19	Inhibits phosphorylation on T456 and activates MAP kinases
Calcium/calmodulin-dependent protein kinase kinase 1	IPI00792960	74	LSARKL **S** LQERPA	9.75	6.96	7.90	6.58	Enzymatic activation
Caldesmon	IPI00333771	528	SVDKVT **S** PTKV__	1.05	0.98	1.36	2.11	Cytoskeletal reorganization (actin stress fibre disassembly, postmitotic spreading)
Catenin beta-1	IPI00017292	552	DTQRRT **S** MGGTQQ	2.95	2.79	2.55	2.42	Alters intracellular localization, regulates transcription and cell motility
CD44 antigen	IPI00305064	706	NGEASK **S** QEMVHL	0.89	0.70	0.48	0.54	Associates with MMP9; regulates cell motility
Desmoplakin	IPI00013933	2849	SGSRRG **S** FDATGN	2.11	1.78	1.51	1.68	Associates with intermediate keratin filaments
DNA topoisomerase 2-alpha	IPI00178667	1297	MAEVLP **S** PRGQRV	1.16	0.92	0.95	0.42	Alters intracellular localization
Endosulfine alpha	IPI00410177	125	LPQRKS **S** LVTSKL	12.90	6.73	9.54	7.72	Alters conformation and regulates molecular association
Epidermal growth factor receptor	IPI00018274	693	ELVEPL **T** PSGEAP	1.65	3.74	4.29	3.79	Receptor internalization
Epidermal growth factor receptor	IPI00018274	1172	SLDNPD **Y** QQDFFP	2.34	2.65	1.74	1.28	Enzymatic activation,, regulates cell growth
Epidermal growth factor receptor	IPI00018274	1197	TAENAE **Y** LRVAPQ	2.13	1.79	1.13	0.73	Enzymatic activation; regulates cell growth
ETS domain-containing transcription factor ERF	IPI00032936	526	EAGGPL **T** PRRVSS	1.08	3.05	2.67	2.95	Inhibits transcriptional repression, essential for G0/G1 transition
Eukaryotic translation initiation factor 4E-binding protein 1	IPI00002569	65	LMECRN **S** PVTKTP	1.28	2.07	2.32	1.87	Repressor dissociation from the eIF4E complex; translation initiation
Eukaryotic translation initiation factor 4E-binding protein 1	IPI00002569	70	NSPVTK **T** PPRDLP	1.09	1.12	1.79	2.07	Repressor dissociation from the eIF4E complex; translation initiation
Filamin-A	IPI00333541	2152	RRRRAP **S** VANVGS	1.96	2.74	3.72	3.76	Cytoskeletal

								reorganization
Forkhead box protein O3	IPI00012856	294	LSKWPG **S** PTSRSS	1.44	2.69	4.02	2.71	Induces interaction with and degradation of MDM2; regulates cell growth
Glycogen synthase kinase-3 beta	IPI00216190	9	GRPRTT **S** FAESCK	1.97	2.44	2.63	2.76	Enzymatic inhibition, transcription, cytoskeletal reorganization and others
GRB2-associated-binding protein 1	IPI00410383	657	GDKQVE **Y** LDLDLD	11.84	9.45	2.53	2.59	Regulates molecular association and cell cycle
Heat shock protein beta-1	IPI00025512	15	SLLRGP **S** WDPFRD	2.53	5.56	7.40	5.31	Regulates sumoylation of HSF1, transcription, cell cycle , cell growth
Heat shock protein beta-1	IPI00025512	78	AYSRAL **S** RQLSSG	3.79	8.60	8.53	5.25	Activation; Regulates sumoylation of HSF1, transcription, cell cycle , cell growth
Heat shock protein beta-1	IPI00025512	82	ALSRQL **S** SGVSEI	3.58	5.89	5.62	4.67	Enzymatic activation, regulates sumoylation, ubiquitinylation, cytoskeletal reorganisation, transcription and cell growth
Histone acetyltransferase MYST2	IPI00180764	57	QSSQDS **S** PVRNLQ	0.99	0.71	0.13	0.28	Regulates cell cycle
Insulin receptor substrate 1	IPI00019471	629	PSGRKG **S** GDYMPM	4.18	6.55	8.50	5.77	Regulates molecular association
Insulin receptor substrate 1	IPI00019471	636	GDYMPM **S** PKSVSA	2.22	5.95	6.57	6.38	Alters intracellular localization
Junctional adhesion molecule A	IPI00001754	284	VIYSQP **S** ARSEGE	3.53	1.59	1.44	1.01	Altered intracellular localization
Keratin, type II cytoskeletal 8	IPI00554648	432	AYGGLT **S** PGLSYS	1.03	1.48	1.92	2.19	Cytoskeletal reorganization, regulates cell motility, altered intracellular location
Lamin-A/C	IPI00021405	404	SRGRAS **S** HSSQTQ	1.19	1.22	2.06	2.95	Alters intracellular localization
Lamin-A/C	IPI00021405	652	YLLGNS **S** PRTQSP	1.30	2.39	3.44	3.56	Activation of nuclear lamin disassembly
Mitogen-activated protein kinase 14	IPI00002857	180	HTDDEM **T** GYVATR	4.10	16.03	10.16	7.87	Enzymatic activation; induces interaction with Fyn, Nck1 and p38-alpha; regulates cytoskeletal reorganization, cell adhesion, motility, cell cycle and apoptosis
Mitogen-activated protein kinase 14	IPI00002857	182	DDEMTG **Y** VATRWY	2.21	5.31	3.84	2.79	Enzymatic activation; induces interaction with p38-alpha; regulates cell adhesion, cytoskeletal reorganization, motility, cell cycle and apoptosis
Myelin protein zero-like protein 1	IPI00022558	263	KSESVV **Y** ADIRKN	1.27	1.50	2.03	1.90	Induces interaction with SHP-2 and cell adhesion
Neural cell expressed, developmentally down-regulated gene 1	IPI00791509	404	KNQDFS **S** FDDTGK	6.34	3.47	0.99	0.81	Regulates mitosis by localizing the □-tubulin ring complex to the centrosome
Nuclear receptor coactivator 3	IPI00748532	860	PYNRAV **S** LDSPVS	4.42	4.16	3.30	2.05	inhibits interaction with ER-alpha
Nucleophosmin	IPI00549248	199	KKSIRD **T** PAKNAQ	0.80	0.59	0.62	0.28	Inhibition, regulates molecular association and

									transcription
Nucleophosmin	IPI00549248	237	QEKTPK	**T**	PKGPSS	1.02	0.97	0.94	0.29	Altered intracellular localization, inhibits interaction with RNA, regulates cell cycle
PEA15 protein	IPI00643342	137	DIIRQP	**S**	EEEIIK	3.79	3.36	2.62	1.35	Protein stabilization, regulates apoptosis
Plastin-2	IPI00010471	5	__MARG	**S**	VSDEEM	3.87	12.41	24.13	14.15	Alters intracellular localization, regulates cell adhesion and molecular association
Polypyrimidine tract binding protein 1	IPI00183626	16	VGTKRG	**S**	DELFST	1.00	1.18	1.71	2.63	Induces translocation to the cytosol
Programmed cell death protein 4	IPI00290110	67	RRLRKN	**S**	SRDSGR	3.09	9.82	14.45	5.60	Induces interaction with BTRC, regulates cell cycle, increases cell growth, translation and protein degradation
Proline-rich AKT1 substrate 1	IPI00306195	203	TQQYAK	**S**	LPVSVP	1.33	1.83	2.02	1.98	Regulates molecular association
Proline-rich AKT1 substrate 1	IPI00306195	266	PRPRLN	**T**	SDFQKL	1.46	2.01	2.09	2.05	Decreases inhibitory effect towards mTORC1, induces molecular association with 14-3-3 beta
Protein FAM59A	IPI00171499	453	GKSELP	**Y**	EELWLE	0.65	2.56	3.98	1.58	Induces association with grb2 and shp-2 leading to enzymatic activation, regulates cell growth
Putative uncharacterised protein DKFZp686P03159	IPI00418169	30	EILCKL	**S**	LEGDHS	2.20	2.25	2.13	1.50	Alters intracellular localization, regulates molecular association
Pyruvate dehydrogenase E1 component subunit alpha, somatic form, mitochondrial	IPI00306301	270	RYGMGT	**S**	VERAAA	0.18	0.37	0.58	0.76	Inhibition
Ras GTPase-activating-like protein IQGAP1	IPI00009342	1443	KMKKSK	**S**	VKEDSN	23.32	22.64	15.97	8.95	Alters conformation, regulates molecular association, cytoskeletal reorganisation
Receptor-interacting serine/threonine-protein kinase 2	IPI00021917	176	WRMMSL	**S**	QSRSSK	1.50	3.86	2.61	1.71	Enzymatic activation
Ribosomal protein S6 kinase alpha-4	IPI00022536	687	SSPPLR	**T**	PDVLES	1.27	5.61	6.35	6.56	Enzymatic activation
Serine/threonine-protein kinase Chk1	IPI00023664	280	KRPRVT	**S**	GGVSES	0.98	4.60	5.31	2.60	Enzymatic inhibition, alters intracellular localization, regulates cell cycle
Serine/threonine-protein kinase Chk1	IPI00023664	317	NVKYSS	**S**	QPEPRT	1.44	2.16	1.08	0.84	Enzymatic activation, regulates molecular association and cell cycle
Serine/threonine-protein kinase D2	IPI00009334	706	RIIGEK	**S**	FRRSVV	34.17	30.76	13.41	7.06	Enzymatic activation
Serine/threonine-protein kinase TAO3	IPI00410485	324	NGPLNE	**S**	QEDEED	6.12	4.72	3.28	1.61	Activation, regulates cell cycle
Signal transducer and activator of transcription 1-alpha/beta	IPI00030781	727	DNLLPM	**S**	PEEFDE	1.18	1.71	3.47	3.13	Activation, induces interaction with PIAS1, regulates transcription, sumoylation, cell growth and apoptosis
Signal transducer and activator of transcription 3	IPI00784414	727	TIDLPM	**S**	PRTLDS	1.36	2.70	2.67	1.99	Activation; induces interaction with DNA and p300, regulates transcription, cell

									differentiation and cell growth
Sodium/hydrogen exchanger 1	IPI00020060	703	SRARIG	**S**	DPLAYE	2.28	5.47	5.69	5.05	Activation, regulates transcription
Sodium/hydrogen exchanger 1	IPI00020060	796	RIQRCL	**S**	DPGPHP	4.41	7.12	6.67	4.18	Regulates molecular association
Solute carrier family 12 member 2	IPI00022649	217	RTFGHN	**T**	MDAVPR	2.29	2.43	1.45	0.94	Activation
Stathmin	IPI00479997	25	AFELIL	**S**	PRSKES	2.41	8.48	8.09	4.49	Inhibition, cytoskeletal reorganization, regulates molecular association and cell cycle
STE20-like serine/threonine-protein kinase	IPI00022827	347	SDLSIA	**S**	SEEDKL	1.32	1.65	2.89	2.85	Enzymatic inhibition
Transcription factor AP-1	IPI00008965	63	NSDLLT	**S**	PDVGLL	1.28	2.61	5.74	7.16	Activation; protein stabilization; regulates transcription, molecular association, cell growth and apoptosis
Transcription factor AP-1	IPI00008965	73	GLLKLA	**S**	PELERL	1.07	1.52	2.45	3.79	Activation; protein stabilization; regulates transcription, molecular association, cell growth
Transcription factor AP-1	IPI00008965	243	GETPPL	**S**	PIDMES	1.11	1.44	1.99	3.18	Inhibition, regulates molecular association and transcription

*functional effect of phosphorylation according to phosphosite.org that provides further detailed information to the phosphosites as well as links to all corresponding publications.

4. Discussion

4.1 LPA-induced transactivation process in SCC-9 cells

The transactivation of the EGFR upon LPA treatment is one key pathway through which the LPA signal propagates in a cell and triggers a variety of different cellular processes. This mechanism is G protein-coupled and requires ligand shedding by an activated metalloproteinase. The cell type and the stimulus strongly determine which cleaving enzyme is functionally active. Although the metalloproteinase ADAM17 has been implicated in GPCR-mediated EGFR transactivation in SCC-9 cells several years ago (Gschwind, Hart *et al.*, 2003), the underlying molecular mechanisms are still enigmatic. Therefore, this work aimed first to establish an experimental workflow with which interaction partners of ADAM17 could be identified and, second, to monitor phosphorylation changes on ADAM17 and EGFR upon LPA treatment. As the highly sensitive and rather unbiased quantitative comparison of different conditions has become possible by mass spectrometric analysis in recent years, this analytical approach was chosen for evaluation of the transactivation process.

4.1.1 ADAM17 interaction partners

To identify LPA-regulated interaction partners of ADAM17 as many as four different approaches were evaluated and reflected the efforts in this study to further improve experimental designs. To gain confident results each approach consisted of two biological replicate experiments. In the first and second approach ADAM17 was immunoprecipitated with the homemade 343 antibody directed against the extracellular matrix metalloproteinase domain. Lysates were prepared from unstimulated cells as well as LPA-treated control and ADAM17 knock-down cells. As evident from immunoblot analysis of total cell lysate, three distinct bands could be detected with a commercial ADAM17 antibody, which represent the pro-domain containing inactive precursor, a not yet fully glycosylated, cleaved form of the precursor and the active, fully glycosylated ADAM17 protein. As neither glycomodifications were considered in MS analysis nor total protein coverage was required for protein identification, these three ADAM17 forms could not be distinguished on the basis of MS data acquired in this study. Upon immunoprecipitation with the 343 antibody the active form of the metalloproteinase was highly enriched and the analysis strategy should therefore be able to reveal interaction partners involved in the transactivation process. The first two approaches

were different regarding when the three differentially labelled cell lysates were combined to one sample. While precipitates were pooled in the first approach, cell lysates were combined before immunoprecipitation reactions in the second approach. Through this change in the experimental procedure a more stable background should be achieved. The extent of background can be defined by the number of proteins binding unspecifically to sepharose G beads or the used antibody. Such proteins should occur in all three labels with the same abundance independent of ADAM17 downregulation. In contrast, specific ADAM17 interaction partners should be reduced in ADAM17 knock-down cells, and can be ideally identified against a stable background due to such a specificity criterion. Notably, no improvement could be achieved in the second approach indicating that possible background variability due to the separate incubations in the first approach was not the reason for apparent regulations of unspecific binders. Many such background binders that seemed to conform with selectivity criteria in one experiment could be effectively eliminated due their inconsistent binding characteristics in the biological replicate experiment. However, laminin subunit beta 3 (LAMB3) and heterogenous nuclear ribonucleoprotein A3 (HNRNPA3) were detected with similar abundance profiles as ADAM17 in biological replicates of approach 1 and 2, respectively. LAMB3 is part of the extracellular matrix laminin structures that are strongly interacting with other matrix proteins and can not serve as cytoplasmic ADAM17 binding protein. HNRNPA3 has a described function as mRNA processing protein and predominantly locates to spliceosomal complexes (Ma, Moran-Jones *et al.*, 2002). Thus, these two proteins seem to be rather unlikely candidates for a key regulatory role in the EGFR transactivation process, although some modulatory influence cannot be excluded either. However, LAMB3 and HNRNPA3could not be confirmed in the remaining two ADAM17 analysis approaches.

In the next step, the lectin-bound subfraction was analysed to identify proteins that locate to the plasma membrane upon LPA treatment. ADAM17 and EGFR are glycosylated on multiple sites and thus exhibited affinities towards all three lectin resins used as demonstrated in pre-experiments (data not shown). Not surprisingly, this experimental design resulted in the identification of far more proteins compared to ADAM17 immunoprecipitation. Nevertheless, only few LPA or ADAM17 related apparent changes were seen and such interactions of ADAM17 with potential candidates have to be confirmed in further experiments. In addition, it has to be mentioned that lectin-bound subfractions consist of proteins with different glycosylation patterns including cell surface as well as, to a certain extent, also cytosolic O-linked N-acetyl-glucosamine (O-GlcNAc) modifications. However, the lectin-based

fractionation procedure enriches for plasma membrane proteins (see point 3.2.1) and appeared therefore initially as a viable strategy to address which proteins might be involved in the transactivation process. Though, a comparison of the lectin-bound subfraction with total cell lysate of SCC-9 cells revealed that lectin-bound proteins, which were less abundant in ADAM17 knock-down cells, exhibited equally reduced protein levels in the same cell population of total cell lysate. This observation indicates that several of these changes in protein abundance after lectin pull-down did not rely on ADAM17 interactions but were likely differential off-target effects of the used ADAM17 and "control" siRNAs. The unspecific silencing of non-target proteins is a common problem of this technique and, although this method is therefore not specific enough to unambiguously identify true interaction proteins against a large background, the application of siRNA-mediated silencing is definitely very useful to monitor specific proteins, e.g. by immunoblot analysis, in case they behave consistently for different siRNAs targeting the same protein-of-interest. For a large scale analysis as performed in this project, stable knock-out cell lines might be more advantageous, even though complete knock-out of ADAM17 bears the risk to alter cell behaviour to a major extent as ADAM17 is described to be of great importance in development and knock-out in mice led to perinatal lethality (Killar, White *et al.*, 1999). The two reproducibly found candidates plasminogen activator inhibitor 1 (SERPINE 1) and thrombospondin-1 (THBS1) could not be verified as equally expressed in total cell lysate. Both are extracellular matrix proteins and can therefore be excluded as ADAM17 cytoplasmic binders. Besides their implication in a variety of biological processes, interestingly, SERPINE 1 and THBS1 are involved in the negative regulation of cell adhesion mediated by integrins and the negative regulation of focal adhesion assembly, respectively.

The fourth approach sought to omit ADAM17 downregulation via siRNA and was based on two consecutive ADAM17 immunoprecipitations, in which cell lysates derived from LPA-treated SCC-9 cells and an untreated cell population. In this strategy, ADAM17 interaction partners can be identified as they are ideally co-depleted with similar ratios as ADAM17 by binding to the anti-ADAM17 343 antibody in a first immunoprecipitation. The obvious advantage is that cells are not perturbed by treatment with siRNAs and transfection reagents. Moreover, an internal replicate is included in the experimental setup. The two reproducibly detected, potential ADAM17 interaction partners granulin precursor (GRN) and 52 kDa Ro (TRIM21) protein were found by this approach. Granulin precursor could also be identified in one biological replicate of approach 1 and 2 as well as in both replicate experiments of approach 3. Quantification in all these experiments revealed that granulin exhibited a constant

protein level independent of ADAM17 knock-down or LPA treatment. Hence, the result of granulin regulation in the fourth approach seemed to be rather an approach-specific observation. The 52 kDa Ro protein was detected with highly similar ratios as ADAM17 and therefore matched the criteria of an ADAM17 interactor. However, literature search revealed that 52 kDa Ro, a ribonucleoprotein particle with E3 ubiquitin ligase activity, binds to the F_c region of IgG antibodies (Rhodes and Trowsdale, 2007; Keeble, Khan *et al.*, 2008; Takahata, Bohgaki *et al.*, 2008). IgG receptor activity of 52 kDa Ro explains the highly similar ratios of this protein and ADAM17 in the performed experiments and indicates an equally high affinity for both proteins towards the anti-ADAM17 343 antibody. Notably, the different binding sites, F_{ab} region for ADAM17 and F_c region for 52 kDa Ro, indicate an uncompetitive and non-allosteric binding of the two proteins. Due to the aforementioned reasons, the reproducibly detected proteins granulin precursor and 52 kDa Ro protein were excluded as potential ADAM17 interactors.

Although no interaction partners of ADAM17 that might play a role in the transactivation process could be identified, a series of experimental designs was established that not only revealed the complex problems inherent to the combination of molecular biology techniques and mass spectrometry, but that also should be highly useful to address these critical issues in a systematic way in other protein interaction studies. Remarkably, the established approaches, especially the approach based on two consecutive immunoprecipitations was shown to work with other proteins-of-interest (Bezler, 2010). Furthermore, the problems might not have a technical basis but lie in the biochemical properties of the assumed ADAM17 complex. This complex of interacting proteins could be very instable or moreover be only intact when integrated in the plasma membrane, while disruption of the plasma membrane during cell lysis resolves the complex. Cooperating molecules might as well be localized in near proximity to each other in the intact membrane but can not be purified as a complex upon breaking up the membrane. Most importantly, interactions playing a role in signal transduction pathways are very transient and modifiying enzymes such as kinases bind to their substrates in a short time-window with often low affinities. As ADAM17 is described to be activated by phosphorylation, phosphorylation changes that were observed on ADAM17 and EGFR in the lectin-purified subfraction as well as in the cellular phosphoproteome provided further insights into potential regulatory mechanisms of the transactivation process.

4.1.2 Time-dependent phosphorylation profiles of ADAM17 and the EGFR

Analysis of the lectin-purified subfraction from SCC-9 cells revealed the three reproducibly LPA-regulated phosphosites Ser(P)-785, Thr(P)-735 and Thr(P)-791 on ADAM17. Phosphorylation modifications on these sites were pinpointed with high confidence localisation probabilities of more than 0.99. The latter two sites are known to mediate and support shedding activity of the metalloproteinase upon their phosphorylation and dephosphorylation, respectively (Diaz-Rodriguez, Montero *et al.*, 2002, Xu and Derynck, 2010). Thr(P)-735 was 3.5-fold upregulated upon 5 min LPA treatment, whereas no regulation could be observed at the 1.5 min time point indicating a slow induction of this site. Similary, Thr(P)-791 was detected downregulated upon 5 min and 3 min of LPA treatment in the lectin pull-down experiment and the whole cell phosphoproteome analysis, respectively, but not at the earliest measured time point of 1.5 min. Whole cell phosphoproteome analysis demonstrated that phosphorylation at this site is 2-fold decreased after 3 min as well as more than 5-fold reduced over the whole interval from 10 min to 90 min of LPA stimulation, indicating a long-lasting regulation of Thr (P)-791. An equally long-lasting regulation was observed on the so far unknown ADAM17 phosphosite Ser(P)-785 that could be reproducibly detected in both approaches. Ser(P)-785 was phosphorylated after 5, 10, 30 and 90 min of LPA incubation wheras this site was not yet regulated at the 1.5 and 3 min time point in the respective experiments. In stark contrast to the slow induction but long-lasting regulation of these ADAM17 sites, Tyr-phosphorylation on the EGFR indicative of its enzymatic activity appeared faster with Tyr(P)-1172 and Tyr(P)-1197 being already upregulated at the 1.5 and 3 min time point in the lectin-purified subfraction and the phosphoproteome analysis, respectively. Taking together the information of both experiments, phosphorylation profiles point to induced EGFR kinase activity in the time frame between 1.5 to 10 min LPA stimulation. Phosphorylation on Tyr-sites are already reduced to basal level after 30 min at which Thr(P)-693, a site involved in EGFR internalization, peaks with respect to its upregulation (Heisermann, Wiley *et al.*, 1990). This site also fulfilled regulation criteria at the 10 and 90 min time points. However, the fact that EGFR autophosphorylation sites are modulated faster than phosphosites indicating the shedding activity of ADAM17 argues against a functional role of ADAM17 Thr(P)-735 and Thr(P)-791 in early EGFR transactivation, albeit these LPA-induced signalling events might prolong the active state of ADAM17. More likely, the rapidly regulated ADAM17 phosphosite Thr(P)-761 could be involved in fast ADAM17 metalloproteinase activation preceding EGFR ligand shedding in

the transactivation process. Thr(P)-761 could be confidently detected in one of two biological replicates in the lectin-purified subfraction and exhibited a rapid and transient phosphorylation profile at the 1.5 min time point. This temporal profile is of great interest as it suggests an early on-off switch that might be responsible for the initial induction of the transactivation process, which then triggers the onset of a second longer lasting regulation mechanism that involves the already known activation sites Thr(P)-735 and Ser(P)-791 on ADAM17. Furthermore, the possible long-lasting shedding activity of ADAM17 of more than 90 min as depicted in the phosphorylation profiles indicates that the transactivation process might not be downregulated on the level of ADAM17 but, as expected, rather at the EGFR as indicated by a temporal limitation of autophosphorylation to the first 10 min and the induction of receptor internalisation after 10 min. This tight regulation, which might include two time-shifted mechanisms, suggests that ADAM17 could interact with different proteins in a time-dependent manner. Therefore, it might be an improvement to choose 1.5 and 10 min stimulation intervals for the identification of early and time-delayed ADAM17 interacting regulators rather than the chosen 3 min of LPA treatment in this study. Furthermore, it would be interesting to confirm yet unknown or functionally uncharacterised sites with conspicuous phosphorylation profiles and elucidate their functions in the transactivation process. These are e.g. the singly detected Thr(P)-787 on ADAM17, which exhibits a 4-fold and 5-fold upregulation upon 1.5 and 5 min of LPA treatment, and Ser(P)-1166, which is nearly 11-fold upregulated after 1.5 min. Notably, the ADAM17 phosphosite Ser(P)-819, which was recently described to positively regulate enzymatic activation of ADAM17 in addition to Ser(P)-735 (Xu and Derynck, 2010) has not been detected in any of the performed experiments, including data of the differentially prepared samples as well as data from all replicates in different experimental subparts. No peptides have been measured that harboured this specific site, possibly indicating that the corresponding position was not phosphorylated upon LPA in SCC-9 cells.

Collectively, the results of ADAM17 and EGFR phosphoregulation reveal potential mechanisms involved in LPA-triggered EGFR transactivation and desensitisation and therefore especially validate lectin-based pre-fractionation as a strategy for sensitive analysis of these central signal transducers.

4.2 Discussion of the glycoproteome study

4.2.1 Lectin pull-down strategy and changes in protein abundance upon LPA treatment in the enriched subfraction

Due to the overall high glycosylation of plasma membrane proteins, the lectin pull-down with a mixture of three different resins was a useful strategy to enrich these proteins as part of the cellular glycoproteome. The purified subfraction further consisted of non-membrane proteins, which might have bound to the lectins due to cytosolic O-linked N-acetyl-glucosamine (O-GlcNAc) modifications as these groups are described to exhibit weak affinity for the lectin WGA (Vosseller, Trinidad *et al.*, 2006). This cytosolic modification could be an explanation for the binding of e.g. the Ser/Thr protein kinase Wnk1 that was shown to positively regulate migration, or proteins related to functions such as nuclear transport and RNA processing, which were observed as additional modules in the network analysis. However, it can not be excluded that their presence is due to physical interactions with highly glycosylated plasma membrane proteins, as might be true e.g. for several RNA processing proteins interacting with glycosylated potassium/chloride cotransporter KCC3 (Figure 19).

Upon LPA stimulation, protein changes observed in this approach might generally result from regulated protein-protein interactions, altered distribution to lysis buffer-insoluble compartments, rapid proteolytic processing or even regulated glycosylation events such as cytosolic O-GlcNAc modification of serine or threonine residues. Notably, the few regulated proteins upon LPA treatment included three proteins, calpain-2, desmoglein-2 and desmoplakin, that could be implicated in LPA-triggered migration. Calpain-2 activity is known to be required for de-adhesion processes in cell migration, and upregulation upon LPA treatment might reflect cellular re-localisation of this protease (Shao, Chou *et al.*, 2006). Moreover, the desmosomal proteins desmoglein-2 and desmoplakin were downregulated, possibly suggesting a re-localisation or degradation upon LPA treatment. As in desmosomes these two proteins constitute the connection to the neighbouring cell on the extracellular side and the linker to intermediate filaments on the cytoplasmic side, respectively, a decrease in protein abundances might be associated with desmosome disruption as a prerequisite of cell migration. Thus, these observations highlight the importance of LPA-induced regulation on protein level.

4.2.2 LPA-dependent regulation of the phosphoproteins implicated in a variety of functions including cell migration

Gene ontology analysis of proteins harbouring LPA-regulated phosphosites revealed an enrichment of these proteins in categories related to signal transduction, proliferation, migration and, interestingly, ion transport. The overrepresentation of LPA-affected phosphoproteins in the first three biological processes supports experimental observations demonstrating distinct signalling events and migration as well as proliferation increase in the analysed SCC-9 cell line upon LPA treatment (Gschwind, Prenzel *et al.*, 2002; Gschwind, Hart *et al.*, 2003). In contrast, the influence of LPA on ion transporters, which were 3-fold overrepresented in this analysis and thus exhibited the highest enrichment, has not been expected to such an extent.

Among ion transporters e.g. the natrium/hydrogen exchanger 1 (NHE1) was positively regulated in response to LPA by phosphorylation on the crucial site Ser-703 known to increase transporter activity. The so far unknown LPA-regulated phosphorylation event on Ser-796 might as well be involved in the molecular control of NHE1 functions, which, in addition to ion transport, include the recruitment of signalling proteins and regulation of cytoskeletal dynamics (Meima, Mackley *et al.*, 2007). The potassium/chloride cotransporter KCC3 is another integral membrane protein involved in osmotic homeostasis of the cell, which was found upregulated on its unreported site Ser-45 upon LPA treatment. KCC3 was recently described to be activated in hypotonic conditions due to cooperative dephosphorylation of Thr(P)-991 and Thr(P)-1048 (Rinehart, Maksimova *et al.*, 2009). These two sites have not been detected in this study, however it will be interesting to explore whether phosphorylation of Ser-45 has functional consequences or if this site is even functionally associated with the two dephosphorylation events. Taken together, the glycoproteome capture approach identified GPCR-regulated phosphorylation events on diverse ion transporters and hence the influence of LPA on osmotic homeostasis, which can serve as a basis for further functional studies.

Furthermore, a variety of different plasma membrane receptors was found sensitive to LPA stimulation and was accessible for analysis due to the lectin purification strategy. In addition to the EGFR, several other receptor tyrosine kinases such as ephrin receptors and fibroblast growth factor receptors exhibited LPA-regulated Ser/Thr phosphorylations pointing to inter-receptor communication as a rather prominent aspect in early LPA signalling. Moreover, analysis of this dataset provided evidence of signalling crosstalk within the GPCR

superfamily. LPA-regulated GPCRs including e.g. the β2 adrenergic receptor or nicotinic acid receptor 1, were rapidly upregulated, or downregulated in case of GPR39A, upon LPA treatment. Although there is some evidence that phosphorylation events are involved in GPCR regulation the functional implications of such modifications are in most cases not known so far (Luttrell and Lefkowitz, 2002). Nevertheless, these observations point to fairly extensive inter-receptor communication among distinct members of the GPCR superfamily, which may indicate receptor desensitisation processes as non-LPA GPCRs were affected.

LPA-induced regulation was observed on receptors as well as on effector molecules such as cell adhesion proteins already after 1.5 min of LPA stimulation. Interestingly, phosphorylation changes occurred on several substructures of adhesion complexes, which are either involved in the establishment of cell-matrix or cell-cell interactions. In hemidesmosomes both subunits of the integrin heterodimer α6 and β4 were regulated in a coordinated way, and the regulated Ser-1364 of integrin β4 is a functionally known site that upon phosphorylation triggers the loss of interaction with plectin-1. The missing link between extracellular and cytoplasmic hemidesmosomal proteins consequently leads to the disruption of these adhesive structures. In this context it would be interesting to explore the functional impact of rapidly downregulated sites in near proximity to Ser(P)-1364 in the connective segment of integrin β4 and whether they could influence the three dimensional structure of the protein and thereby the connection to plectin-1. Moreover, it could be possible that the downregulation of phosphorylation on site Ser(P)-21 at the very N-terminus and the concomitant upregulation of site Ser(P)-4249 at the C-terminus of plectin-1 modulate its binding properties to integrin β4. The loss of integrin β4 affinity has e.g. been observed by deletion of plectin-1 sequences preceding the active binding site around Q131, R138 and N149 (Litjens, Koster *et al.*, 2003). It could as well be possible that the mutually exclusive binding of plectin-1 to either integrin β4 or F-actin is regulated by such a phosphorylation-based mechanism.

Concerted phosphorylation/dephosphorylation reactions on functionally relevant sites of adherens junction proteins further indicated an interplay of mechanisms by which LPA-triggered signals modulate cell-cell contacts. Dephosphorylation events in the N-terminal region of δ-catenin upon LPA treatment have been shown to result in adherens junction disassembly, which is supported by removal of β-catenin from these adhesive structures upon phosphorylation of the functional site Ser(P)-552 (Xia, Mariner *et al.*, 2003; Fang, Hawke *et al.*, 2007). By phosphorylation-dependent destabilisation of adherens junctions the LPA-

triggered mechanism facilitates cell migration, however the underlying regulations of phosphosites, including the yet unknown increase of phosphorylation on Ser(P)-349 and Ser(P)-352 of δ-catenin, have to be further elucidated. This reciprocal phospho-regulation on δ-catenin, a known regulator of cell adhesion properties, may also have an impact on its interaction to E-cadherin and β-catenin or other adherens junction proteins, such as α-catenin that has also been found regulated.

Regulation on desmosomal proteins has so far not been observed in response to LPA and none of the already detected phosphosites on these proteins have been functionally characterised in previous studies. Therefore, it will be interesting to explore whether their modification status controls desmosomal architecture and adhesive properties. Upon LPA treatment phosphorylation regulation was found on the two interactors plakophilin 3 and desmoglein 2. As the latter protein of desmosomal cell-cell contacts has been found with reduced protein abundance and additionally harboured downregulated sites upon LPA treatment one could speculate that there is a functional link between dephosphorylation and protein degradation in this specific case. Although such assumptions are speculative it is worth to find out if phosphorylation generally plays a role in the maintenance or disruption of desmosomes.

Collectively, short-term stimulation of SCC-9 cells with LPA provided evidence of phospho-regulation events on plasma membrane proteins, most importantly on ion transporters, as well as different classes of receptors and a variety of cell adhesion structures, as depicted in Figure 28. Above all, modification on substructures of hemidesmosomes, adherens junctions and desmosomes in regard to already known functional sites, point to or in case of desmosomes suggest a molecular mechanism by which LPA-induced signals dissolve cell-matrix and cell-cell contacts to initiate cell migration.

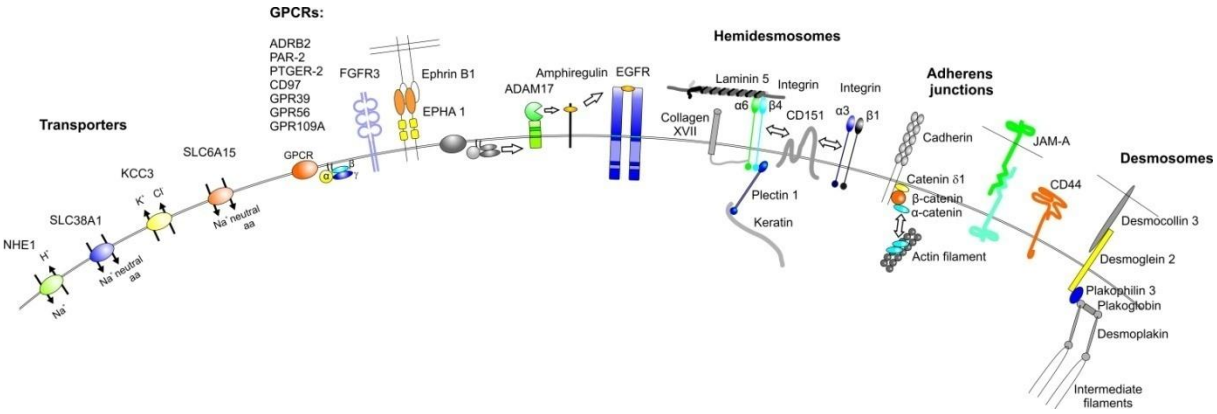

Figure 28: Schematic overview of cell surface proteins that undergo phosphoregulation upon LPA treatment. ADAM17, a disintegrin and metalloprotease domain 17; ADRB2, β2 adrenergic receptor; CD151, CD151 antigen; CD44, CD44 antigen precursor; CD97, CD97 antigen precursor; EPHA1, ephrin type-A receptor 1 precursor; FGFR3, fibroblast growth factor receptor 3; GPR39, probable G protein-coupled receptor 39; GPR56, G protein-coupled receptor 56; GPR109A, nicotinic acid receptor 1; JAM-A, junctional adhesion molecule A precursor; PAR-2, proteinase-activated receptor 2 precursor; PTGER-2, prostaglandin E2 receptor; SLC12A6, solute carrier family 12 member 6; SLC38A1, solute carrier family 38 member 1; SLC6A15, solute carrier family 6 member 15.

Furthermore, experimental data indicate a pro-migratory effect of the serine/threonine protein kinase Wnk1 which might be due to LPA-induced upregulation of Wnk1 signalling activity. Cellular activation of the kinase was evident from the rapid phosphorylation of the functionally characterised site Ser-382. Possible functional implications of the upregulated sites Ser(P)-167, Ser(P)-597 and Ser(P)-2372 have not been analysed until now and might be involved in kinase activity control as well as other proposed functions of this protein. Results of this study provide the first evidence for Wnk1 regulation and functional relevance in GPCR-mediated signalling. In the light of earlier data showing Wnk1 involvement in both cell migration and proliferation in EGF-treated neural progenitor cells (Sun, Gao *et al.*, 2006), it appears that the overall repertoire of Wnk1 functions might differ in a cell context- or growth factor-dependent manner. Moreover, previous studies reported Wnk1 activation upon cell treatments such as osmotic stress as well as membrane depolarization (Xu, English *et al.*, 2000; Xu, Min *et al.*, 2002; Lenertz, Lee *et al.*, 2005; Moriguchi, Urushiyama *et al.*, 2005; Zagorska, Pozo-Guisado *et al.*, 2007; Richardson and Alessi, 2008). Thus, data of this study further support the notion that rather diverse external stimuli converge on Wnk1 to regulate cellular responses such as ion transport regulation, cell migration and others.

4.2.3 Regulation mechanisms of LPA-induced phosphosites

The analysis of LPA-regulated phosphorylation events on glycoproteins revealed not only new phosphorylation sites but also characterised phosphosites that so far have not been known to be modified upon LPA treatment. Some of the phosphorylation changes provide insight into possible regulation mechanisms involved in the initiation or execution of LPA-triggered biological responses.

Time-resolved monitoring of phosphorylation changes in response to LPA showed which sites are transiently induced to e.g. initiate a process or protein activation and which sites are regulated over a longer period of time to possibly mediate rather long-lasting activation or repression phases. For example, it is more likely that the rapidly and transiently regulated site Ser(P)-761 of ADAM17 plays a role in early induction, whereas the phosphorylation profile of Thr(P)-735 suggests a role in late metalloproteinase activation.

Comparison of temporal profiles of phosphosites on different proteins might shed further light on coordinated regulations of e.g. interaction partners. Such a mechanism has, amongst others, been observed for the directly interacting proteins α-catenin, β-catenin and δ-catenin on their respective sites Ser(P)-655, Thr(P)-556 and Ser(P)-349, which followed the same rapidly induced phosphorylation profiles. Furthermore, knowledge about the time-dependent regulation of distinct proteins can be helpful in understanding complex mechanisms involving multiple proteins, such as apparent in the EGFR transactivation process.

Some conclusions can also be drawn when looking at the amino acids surrounding a regulated phosphorylation site. Short sequence motifs around phosphosites may reflect substrate motifs of kinases and phosphatases in case of phosphorylation and dephosphorylation events, respectively. The two sites Ser-703 and Ser-796 of NHE1, which were both phosphorylated upon LPA treatment, reside within a shared RxxSDP motif. The functionally characterised site Ser(P)-703 is phosphorylated by p90 ribosomal S6 protein kinase, which might further phosphorylate Ser-796 due to the same substrate motif (Takahashi, Abe *et al.*, 1999). Several equivalent substrate motifs within the same protein point to a mechanism, which increases the overall phosphorylation status of a protein by several similar sites targeted by the same kinase.

Phosphorylation sites embedded in the same motif and moreover exhibiting the same temporal phosphorylation profile upon LPA stimulation have also be found on different integrin α-subunits, namely Ser(P)-1042 of integrin α3 and Ser(P)-1103 of integrin α6. As these two subunits are engaged in heterodimers with distinct functions, namely the α3/β1 and

α6/β4 integrins, the data indicate coordinated regulation of different cell adhesion complexes by an LPA-induced kinase targeting a shared substrate motif on the α subunits. Interestingly, the shared QPpSxxE motif is evolutionary conserved across vertebrate species from frog to man, further highlighting the functional importance of the corresponding serine phosphorylation site (Zhang, Bontrager *et al.*, 2001).

Phosphorylation changes on functionally characterised sites are probably the most informative regarding biochemical mechanisms that may underlie biological responses to a new stimulus, which was e.g. the case for the observed phosphorylation on the activation site Ser-382 of Wnk1 upon LPA treatment. Furthermore, predictions can be made based on the functional domain in which regulated phosphosites are located. For example, the LPA-induced site Ser(P)-382 of Wnk1 is located in the activation loop of this kinase, whereas no changes could be observed in its autoinhibitory region. Similarly, phosphorylation data of integrin β4 indicate massive regulation in its connective segment probably suggesting a functional role for this domain (Figure 29). And indeed, de Pereda *et al* have recently shown that parts of the integrin β4 connective segment contribute to the binding interface with plectin 1 in hemidesmosomes (de Pereda, Lillo *et al.*, 2009). Moreover, by comparing integrin β4 in a complex with plectin 1 *versus* free integrin β4 molecules the authors demonstrated that the connective segment undergoes a conformational change by binding to its interaction partner. These data have been raised without considering possible phosphoregulation. The phosphorylation data of the glycoproteome analysis thus identifies a likely additional level of regulation that involves drastic and rapid change of the phosphorylation status in the connective segment region that may influence the static interface on which the interaction of integrin β4 and plectin 1 is based.

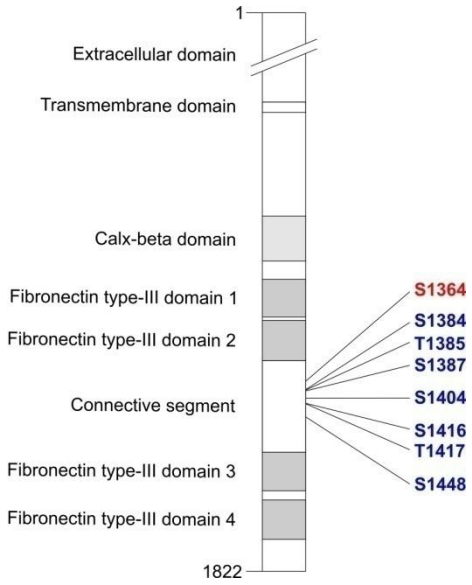

Figure 29: Schematic illustration of integrin β4 showing reproducibly LPA-regulated phosphosites. Red and blue colouring indicates up- and downregulation of phosphorylation upon LPA treatment, respectively.

LPA-mediated regulation mechanisms have not only been observed on distinct proteins or interactors but also on several subunits belonging to the same higher order structure. Hence, as already mentioned, different subunits of a distinct adhesive structure were regulated in a tightly concerted way upon LPA stimulation, which was observed for hemidesmosomes, adherens junctions and desmosomes. Notably, these simultaneously regulated structures could contribute to a common biological process, in which disruption of adhesive connections facilitate migration. Although not every detected phosphorylation change might have a direct consequence, monitoring and comparing these events may provide a more comprehensive understanding of signalling mechanisms ranging from single phosphorylation modifications to global regulatory processes.

4.3 Comparison of the glycoproteome and the time-course study

The focus of the glycoproteome approach was on phosphorylation changes occuring on plasma membrane proteins upon short term stimulation of SCC-9 cells with LPA for 1.5 and 5 min. The aim was to shed light on rapidly induced processes such as the transactivation of EGFR or cell surface structures with direct effects on the cell environment. For analysing

time-dependent phosphorylation changes in the time range from 3 up to 90 min of LPA treatment, the same cell line was used, but this project further targeted the global phosphoproteome in comparison to the lectin-enriched subfraction in the first project.

Concerning sample preparation in the two projects, somewhat different techniques were applied. Lectin-purified proteins were subjected to parallel in-solution and in-gel digests, with the latter performed upon fractionation of proteins by electrophoresis based on molecular weight. In contrast, whole cell lysate in the global phosphoproteome analysis was trypsin-digested in-solution and peptides were subsequently fractionated due to their solution charge in acidic conditions by strong cation exchange chromatography. Enrichment of phosphopeptides was performed with two highly efficient metal affinity chromatographies, applying titanium beads in the first and iron ion complexed beads in the second project. Moreover, the second, global phosphoproteome project dealt with more complex samples and as many as five different time-points and three biological replicates were included that reflected the advances in experimental design throughout this PhD thesis.

As expected, the different complexity of the two projects is also reflected by the overall numbers of confident and reproducibly detected phosphosites. Glycoproteome analysis and global phosphoproteome analysis revealed 751 and 11,327 phosphosites that were found in at least two biological replicate experiments, of which 169 and 2,095 phosphosites were classified as regulated upon LPA treatment, respectively. Considering all detected class I phosphosites independent of the stimulation interval in the separate projects, each dataset reveals around 20% of the sites regulated upon LPA treatment (22.5% and 18.5% for the first and second project, respectively). However, the comparison of regulated phosphosites at time points with minimal differences between the two projects, corresponding to the 1.5 and 5 min time points of the first and the 3 min time point of the second project, shows that 22.5% of the phosphosites are regulated in the lectin-purified subproteome whereas only 8.0% can be regarded regulated in the global phosphoproteome. This observation strongly indicates that a major part of phosphoregulation occurs in the glycoproteome, mainly including plasma membrane proteins, upon short term LPA stimulation and thus validates lectin-purification for analysis of cell surface phosphorylation events in response to short LPA stimulation intervals. Notably, the lectin purification strategy improved the accessibility of plasma membrane proteins for phosphorylation analysis, which is confirmed by the fact that 55% of the phosphosites from the glycoproteome could not be detected in the global phosphoproteome analysis and were thus uniquely found in the lectin-purified subfraction. Among them are, e.g., regulated phosphosites on the GPCRs beta-2 adrenergic receptor, prostaglandin E2

receptor (PTGER2) and G protein-coupled receptor 39 (GPR39) as well as additional sites detected on various cell adhesion molecules, such as integrins and catenins, and furthermore crucial sites like the ADAM17 activation site Ser(P)-735.

The time-dependent regulation of phosphoproteins can further be seen when comparing the generated protein interaction networks. Due to the smaller number of LPA-regulated phosphoproteins in the glycoproteome dataset the network was based on all phosphoproteins, whereas the one derived from the global analysis solely consisted of regulated phosphoproteins. Regarding the lectin-enriched subset, an interconnectivity of proteins harbouring LPA-regulated phosphosites could be predominantly found for proteins exhibiting cell-adhesive, ion transport and plasma membrane receptor properties. In the network based on the global phosphoproteome analysis, proteins belonging to the categories cell adhesion and plasma membrane receptors are integrated into a tightly interconnecting main module. Notably, this network additionaly exhibits clusters for LPA-regulated phosphoproteins implicated in G protein signalling, MAPK cascades, transcription, RNA splicing, nuclear transport and translation. Whereas the first two clusters consisting of many cross-linked members contain mainly rapidly LPA-regulated phosphoproteins, the remaining clusters represent biological processes with a by comparison later regulation onset upon LPA treatment. Due to their simultaneous regulation and high interconnectivity G protein elements including GTPase activating proteins (GAPs) and guanine nucleotide exchange factors (GEFs) are also represented in time-dependent networks consisting of proteins with similar early or intermediate upregulated phosphorylation profiles. Although G protein regulators as well as MAP kinases are early LPA-regulated phosphoproteins, they have not been detected to such an extent in the lectin-purified short term stimulated phosphoproteome subset. The absence of most of these proteins in the subfraction may arise from the fact that they do not possess cytosolic glycosylation modifications or that their interaction with lectin-bound proteins is very transient and of lower affinity. In comparison to the early regulated network modules the global phosphoproteome network further points to later LPA-regulated modules, such as those formed by transcriptional or splicing proteins. As can be seen in time-resolved heatmaps of their corresponding phosphorylation sites, most of them are regulated earliest after 10 min of LPA stimulation and peak at the 30 or 90 min time point.

Although the lectin purification approach and the global phosphoproteome analysis had different focuses regarding the time frame of LPA stimulation and, moreover, different methods were applied for sample preparation, an astonishingly high congruency regarding phosphorylation profiles of proteins detected in both projects was observed. The high

reproducibility of stimulation conditions is shown by combining the different time point measurements of the two projects to receive a common phosphorylation profile as demonstrated in Figure 30 for selected phosphosites. This procedure enables predictions of phosphosite regulations covering the time span from 1.5 to 90 mins.

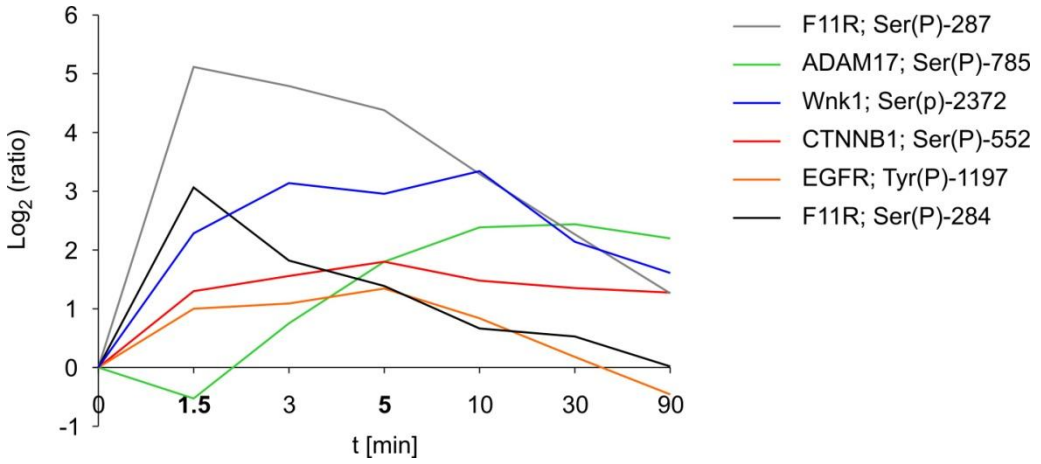

Figure 30: Time-dependent phosphorylation profiles of selected sites. Ratios of the 1.5 and 5 min time points from the lectin-purified subproteome (shown in bold) were combined with those of the 3, 10, 30 and 90 min time points of LPA stimulation from the global phosphoproteome analysis.

4.4 Outlook

This study sheds light on LPA-induced signalling events by applying SILAC-based quantitative proteomics and phosphoproteomics for both global analysis as well as analyses of enriched subfractions. The global analysis represented the so far largest study on LPA signalling in human cells and demonstrated the enormous analytical power of highly sensitive and accurate mass spectrometry applied in signal transduction reserach. In combination with refined MS sample preparation and MS data analysis startegies this enabled, for example, the time-resolved identification of phosphorylation events, the multiplexing of SILAC experiments and underpinned the upward potential of these technologies when combined with so called classical biochemical methods.

The identification of a plethora of yet unknown LPA-regulated proteins, the potentially phosphoregulated catalytic activity or function of LPA signalling targets and the still large unknown identities of kinases that are responsible for distinct phosphorylation events raise

many new questions, for which the studies reported here provide an vastly extended knowledge base. The straightforward techniques described in this study should also have considerable potential when applied to other biological questions. Furthermore, with the improvement of detection methods for e.g. glycomodifications it will be interesting to analyse the interplay between phosphorylation and cytosolic glycosylation modifications, which are reported to either inhibit or augment each other in influencing signalling events.

In conclusion, MS and subsequent bioinformatic analysis enable unbiased and rather comprehensive approaches to explore the complex interplay of proteins involved in distinct processes as well as their modification-based regulations, which together result in a precise biological outcome. Thus, quantitative MS data can not only foster the understanding of basic mechanisms, as shown for LPA signalling in this study, but can also be exploited for drug target identification in diseases caused by the misregulation of specific proteins.

5. References

Ahamed, J. and W. Ruf (2004). "Protease-activated receptor 2-dependent phosphorylation of the tissue factor cytoplasmic domain." J Biol Chem **279**(22): 23038-23044.

Barrera, N. P., B. Morales, *et al.* (2005). "Principles: mechanisms and modeling of synergism in cellular responses." Trends Pharmacol Sci **26**(10): 526-532.

Bezler, M. (2010). "The HER3 Receptor: Role as an Intervention Target in Ovarian Cancer." Dissertation.

Black, R. A., C. T. Rauch, *et al.* (1997). "A metalloproteinase disintegrin that releases tumour-necrosis factor-alpha from cells." Nature **385**(6618): 729-733.

Blobel, C. P. (2005). "ADAMs: key components in EGFR signalling and development." Nat Rev Mol Cell Biol **6**(1): 32-43.

Borrell-Pages, M., F. Rojo, *et al.* (2003). "TACE is required for the activation of the EGFR by TGF-alpha in tumors." Embo J **22**(5): 1114-1124.

Brou, C., F. Logeat, *et al.* (2000). "A novel proteolytic cleavage involved in Notch signaling: the role of the disintegrin-metalloprotease TACE." Mol Cell **5**(2): 207-216.

Butt, E., D. Immler, *et al.* (2001). "Heat shock protein 27 is a substrate of cGMP-dependent protein kinase in intact human platelets: phosphorylation-induced actin polymerization caused by HSP27 mutants." J Biol Chem **276**(10): 7108-7113.

Chen, N., W. Sun, *et al.* (2008). "Quantitative proteome analysis of HCC cell lines with different metastatic potentials by SILAC." Proteomics **8**(23-24): 5108-5118.

Choi, J. W., D. R. Herr, *et al.* (2010). "LPA receptors: subtypes and biological actions." Annu Rev Pharmacol Toxicol **50**: 157-186.

Choudhary, C., C. Kumar, *et al.* (2009). "Lysine acetylation targets protein complexes and co-regulates major cellular functions." Science **325**(5942): 834-840.

Choudhary, C. and M. Mann (2010). "Decoding signalling networks by mass spectrometry-based proteomics." Nat Rev Mol Cell Biol **11**(6): 427-439.

Christensen, G. L., C. D. Kelstrup, *et al.* (2010). "Quantitative phosphoproteomics dissection of seven-transmembrane receptor signaling using full and biased agonists." Mol Cell Proteomics **9**(7): 1540-1553.

Cox, J. and M. Mann (2008). "MaxQuant enables high peptide identification rates, individualized p.p.b.-range mass accuracies and proteome-wide protein quantification." Nat Biotechnol **26**(12): 1367-1372.

Crocker, S. J., A. Pagenstecher, *et al.* (2004). "The TIMPs tango with MMPs and more in the central nervous system." J Neurosci Res **75**(1): 1-11.

Daub, H., J. V. Olsen, *et al.* (2008). "Kinase-selective enrichment enables quantitative phosphoproteomics of the kinome across the cell cycle." Mol Cell **31**(3): 438-448.

Daub, H., F. U. Weiss, *et al.* (1996). "Role of transactivation of the EGF receptor in signalling by G-protein-coupled receptors." Nature **379**(6565): 557-560.

de Pereda, J. M., M. P. Lillo, *et al.* (2009). "Structural basis of the interaction between integrin alpha6beta4 and plectin at the hemidesmosomes." Embo J **28**(8): 1180-1190.

Dennis, G., Jr., B. T. Sherman, *et al.* (2003). "DAVID: Database for Annotation, Visualization, and Integrated Discovery." Genome Biol **4**(5): P3.

Diaz-Rodriguez, E., J. C. Montero, *et al.* (2002). "Extracellular signal-regulated kinase phosphorylates tumor necrosis factor alpha-converting enzyme at threonine 735: a potential role in regulated shedding." Mol Biol Cell **13**(6): 2031-2044.

Domon, B. and R. Aebersold (2006). "Mass spectrometry and protein analysis." Science **312**(5771): 212-217.

Dumont, J. E., F. Pecasse, *et al.* (2001). "Crosstalk and specificity in signalling. Are we crosstalking ourselves into general confusion?" Cell Signal **13**(7): 457-463.

Fang, D., D. Hawke, *et al.* (2007). "Phosphorylation of beta-catenin by AKT promotes beta-catenin transcriptional activity." J Biol Chem **282**(15): 11221-11229.

Gamou, S. and N. Shimizu (1994). "Calphostin-C stimulates epidermal growth factor receptor phosphorylation and internalization via light-dependent mechanism." J Cell Physiol **158**(1): 151-159.

Geiger, T., J. Cox, *et al.* (2010). "Super-SILAC mix for quantitative proteomics of human tumor tissue." Nat Methods **7**(5): 383-385.

Gilpin, B. J., F. Loechel, *et al.* (1998). "A novel, secreted form of human ADAM 12 (meltrin alpha) provokes myogenesis in vivo." J Biol Chem **273**(1): 157-166.

Gruhler, A., J. V. Olsen, *et al.* (2005). "Quantitative phosphoproteomics applied to the yeast pheromone signaling pathway." Mol Cell Proteomics **4**(3): 310-327.

Gschwind, A., S. Hart, *et al.* (2003). "TACE cleavage of proamphiregulin regulates GPCR-induced proliferation and motility of cancer cells." Embo J **22**(10): 2411-2421.

Gschwind, A., N. Prenzel, *et al.* (2002). "Lysophosphatidic acid-induced squamous cell carcinoma cell proliferation and motility involves epidermal growth factor receptor signal transactivation." Cancer Res **62**(21): 6329-6336.

Hart, G. W., R. S. Haltiwanger, *et al.* (1989). "Nucleoplasmic and cytoplasmic glycoproteins." Ciba Found Symp **145**: 102-112, discussion 112-108.

Hart, S. (2004). Characterisation of the Molecular Mechanisms of EGFR Signal Transactivation in Human Cancer. Dissertation.

Heisermann, G. J., H. S. Wiley, *et al.* (1990). "Mutational removal of the Thr669 and Ser671 phosphorylation sites alters substrate specificity and ligand-induced internalization of the epidermal growth factor receptor." J Biol Chem **265**(22): 12820-12827.

Hinkle, C. L., S. W. Sunnarborg, *et al.* (2004). "Selective roles for tumor necrosis factor alpha-converting enzyme/ADAM17 in the shedding of the epidermal growth factor receptor ligand family: the juxtamembrane stalk determines cleavage efficiency." J Biol Chem **279**(23): 24179-24188.

Huang da, W., B. T. Sherman, *et al.* (2009). "Systematic and integrative analysis of large gene lists using DAVID bioinformatics resources." Nat Protoc **4**(1): 44-57.

Jensen, L. J., M. Kuhn, *et al.* (2009). "STRING 8--a global view on proteins and their functional interactions in 630 organisms." Nucleic Acids Res **37**(Database issue): D412-416.

Jensen, O. N. (2006). "Interpreting the protein language using proteomics." Nat Rev Mol Cell Biol **7**(6): 391-403.

Johnson, S. A. and T. Hunter (2005). "Kinomics: methods for deciphering the kinome." Nat Methods **2**(1): 17-25.

Karan, D., F. C. Lin, *et al.* (2003). "Expression of ADAMs (a disintegrin and metalloproteases) and TIMP-3 (tissue inhibitor of metalloproteinase-3) in human prostatic adenocarcinomas." Int J Oncol **23**(5): 1365-1371.

Keeble, A. H., Z. Khan, *et al.* (2008). "TRIM21 is an IgG receptor that is structurally, thermodynamically, and kinetically conserved." Proc Natl Acad Sci U S A **105**(16): 6045-6050.

Kholodenko, B. N., J. F. Hancock, *et al.* (2010). "Signalling ballet in space and time." Nat Rev Mol Cell Biol **11**(6): 414-426.

Killar, L., J. White, *et al.* (1999). "Adamalysins. A family of metzincins including TNF-alpha converting enzyme (TACE)." Ann N Y Acad Sci **878**: 442-452.

Kishi, Y., S. Okudaira, *et al.* (2006). "Autotaxin is overexpressed in glioblastoma multiforme and contributes to cell motility of glioblastoma by converting lysophosphatidylcholine to lysophosphatidic acid." J Biol Chem **281**(25): 17492-17500.

Kristiansen, K. (2004). "Molecular mechanisms of ligand binding, signaling, and regulation within the superfamily of G-protein-coupled receptors: molecular modeling and mutagenesis approaches to receptor structure and function." Pharmacol Ther **103**(1): 21-80.

Kruger, M., M. Moser, *et al.* (2008). "SILAC mouse for quantitative proteomics uncovers kindlin-3 as an essential factor for red blood cell function." Cell **134**(2): 353-364.

Landis, C. A., S. B. Masters, *et al.* (1989). "GTPase inhibiting mutations activate the alpha chain of Gs and stimulate adenylyl cyclase in human pituitary tumours." Nature **340**(6236): 692-696.

Leitner, A. and W. Lindner (2006). "Chemistry meets proteomics: the use of chemical tagging reactions for MS-based proteomics." Proteomics **6**(20): 5418-5434.

Lenertz, L. Y., B. H. Lee, *et al.* (2005). "Properties of WNK1 and implications for other family members." J Biol Chem **280**(29): 26653-26658.

Li, C., M. E. Collier, *et al.* (2008). "Investigation of the mechanisms of tissue factor-mediated evasion of tumour cells from cellular cytotoxicity." Cancer Immunol Immunother **57**(9): 1347-1355.

Lienhard, G. E. (2008). "Non-functional phosphorylations?" Trends Biochem Sci **33**(8): 351-352.

Link, A. J., J. Eng, *et al.* (1999). "Direct analysis of protein complexes using mass spectrometry." Nat Biotechnol **17**(7): 676-682.

Litjens, S. H., J. Koster, *et al.* (2003). "Specificity of binding of the plectin actin-binding domain to beta4 integrin." Mol Biol Cell **14**(10): 4039-4050.

Luttrell, L. M. and R. J. Lefkowitz (2002). "The role of beta-arrestins in the termination and transduction of G-protein-coupled receptor signals." J Cell Sci **115**(Pt 3): 455-465.

Lyons, J., C. A. Landis, *et al.* (1990). "Two G protein oncogenes in human endocrine tumors." Science **249**(4969): 655-659.

Ma, A. S., K. Moran-Jones, *et al.* (2002). "Heterogeneous nuclear ribonucleoprotein A3, a novel RNA trafficking response element-binding protein." J Biol Chem **277**(20): 18010-18020.

Macek, B., M. Mann, *et al.* (2009). "Global and site-specific quantitative phosphoproteomics: principles and applications." Annu Rev Pharmacol Toxicol **49**: 199-221.

Mann, M. (2006). "Functional and quantitative proteomics using SILAC." Nat Rev Mol Cell Biol **7**(12): 952-958.

Manning, G., D. B. Whyte, *et al.* (2002). "The protein kinase complement of the human genome." Science **298**(5600): 1912-1934.

Masuda, A., K. Nakamura, *et al.* (2008). "Serum autotaxin measurement in haematological malignancies: a promising marker for follicular lymphoma." Br J Haematol **143**(1): 60-70.

McGowan, P. M., B. M. Ryan, *et al.* (2007). "ADAM-17 expression in breast cancer correlates with variables of tumor progression." Clin Cancer Res **13**(8): 2335-2343.

Meima, M. E., J. R. Mackley, *et al.* (2007). "Beyond ion translocation: structural functions of the sodium-hydrogen exchanger isoform-1." Curr Opin Nephrol Hypertens **16**(4): 365-372.

Merchant, N. B., I. Voskresensky, *et al.* (2008). "TACE/ADAM-17: a component of the epidermal growth factor receptor axis and a promising therapeutic target in colorectal cancer." Clin Cancer Res **14**(4): 1182-1191.

Mills, G. B. and W. H. Moolenaar (2003). "The emerging role of lysophosphatidic acid in cancer." Nat Rev Cancer **3**(8): 582-591.

Montaner, S., A. Sodhi, *et al.* (2003). "Endothelial infection with KSHV genes in vivo reveals that vGPCR initiates Kaposi's sarcomagenesis and can promote the tumorigenic potential of viral latent genes." Cancer Cell **3**(1): 23-36.

Moriguchi, T., S. Urushiyama, *et al.* (2005). "WNK1 regulates phosphorylation of cation-chloride-coupled cotransporters via the STE20-related kinases, SPAK and OSR1." J Biol Chem **280**(52): 42685-42693.

Morinaka, K., S. Koyama, *et al.* (1999). "Epsin binds to the EH domain of POB1 and regulates receptor-mediated endocytosis." Oncogene **18**(43): 5915-5922.

Moss, M. L., S. L. Jin, *et al.* (1997). "Cloning of a disintegrin metalloproteinase that processes precursor tumour-necrosis factor-alpha." Nature **385**(6618): 733-736.

Murphy, G. (2008). "The ADAMs: signalling scissors in the tumour microenvironment." Nat Rev Cancer **8**(12): 929-941.

Nam, S. W., T. Clair, *et al.* (2000). "Autotaxin (ATX), a potent tumor motogen, augments invasive and metastatic potential of ras-transformed cells." Oncogene **19**(2): 241-247.

Oldham, W. M. and H. E. Hamm (2008). "Heterotrimeric G protein activation by G-protein-coupled receptors." Nat Rev Mol Cell Biol **9**(1): 60-71.

Olsen, J. V., B. Blagoev, *et al.* (2006). "Global, in vivo, and site-specific phosphorylation dynamics in signaling networks." Cell **127**(3): 635-648.

Olsen, J. V., L. M. de Godoy, *et al.* (2005). "Parts per million mass accuracy on an Orbitrap mass spectrometer via lock mass injection into a C-trap." Mol Cell Proteomics **4**(12): 2010-2021.

Olsen, J. V., B. Macek, *et al.* (2007). "Higher-energy C-trap dissociation for peptide modification analysis." Nat Methods **4**(9): 709-712.

Olsen, J. V., J. C. Schwartz, *et al.* (2009). "A dual pressure linear ion trap Orbitrap instrument with very high sequencing speed." Mol Cell Proteomics **8**(12): 2759-2769.

Olsen, J. V., M. Vermeulen, *et al.* (2010). "Quantitative phosphoproteomics reveals widespread full phosphorylation site occupancy during mitosis." Sci Signal **3**(104): ra3.

Ong, S. E., B. Blagoev, *et al.* (2002). "Stable isotope labeling by amino acids in cell culture, SILAC, as a simple and accurate approach to expression proteomics." Mol Cell Proteomics **1**(5): 376-386.

Ong, S. E. and M. Mann (2005). "Mass spectrometry-based proteomics turns quantitative." Nat Chem Biol **1**(5): 252-262.

Ong, S. E., G. Mittler, *et al.* (2004). "Identifying and quantifying in vivo methylation sites by heavy methyl SILAC." Nat Methods **1**(2): 119-126.

Page-McCaw, A., A. J. Ewald, *et al.* (2007). "Matrix metalloproteinases and the regulation of tissue remodelling." Nat Rev Mol Cell Biol **8**(3): 221-233.

Parma, J., L. Duprez, *et al.* (1993). "Somatic mutations in the thyrotropin receptor gene cause hyperfunctioning thyroid adenomas." Nature **365**(6447): 649-651.

Patrussi, L., M. T. Savino, *et al.* (2005). "Cooperation and selectivity of the two Grb2 binding sites of p52Shc in T-cell antigen receptor signaling to Ras family GTPases and Myc-dependent survival." Oncogene **24**(13): 2218-2228.

Pearson, R. B. and B. E. Kemp (1991). "Protein kinase phosphorylation site sequences and consensus specificity motifs: tabulations." Methods Enzymol **200**: 62-81.

Peng, J., D. Schwartz, *et al.* (2003). "A proteomics approach to understanding protein ubiquitination." Nat Biotechnol **21**(8): 921-926.

Peschon, J. J., J. L. Slack, *et al.* (1998). "An essential role for ectodomain shedding in mammalian development." Science **282**(5392): 1281-1284.

Pierce, A., R. D. Unwin, *et al.* (2008). "Eight-channel iTRAQ enables comparison of the activity of six leukemogenic tyrosine kinases." Mol Cell Proteomics **7**(5): 853-863.

Powell, R. M., J. Wicks, *et al.* (2004). "The splicing and fate of ADAM33 transcripts in primary human airways fibroblasts." Am J Respir Cell Mol Biol **31**(1): 13-21.

Prenzel, N., E. Zwick, *et al.* (1999). "EGF receptor transactivation by G-protein-coupled receptors requires metalloproteinase cleavage of proHB-EGF." Nature **402**(6764): 884-888.

Radeff-Huang, J., T. M. Seasholtz, *et al.* (2004). "G protein mediated signaling pathways in lysophospholipid induced cell proliferation and survival." J Cell Biochem **92**(5): 949-966.

Ratcliffe, M. J., C. Smales, *et al.* (1999). "Dephosphorylation of the catenins p120 and p100 in endothelial cells in response to inflammatory stimuli." Biochem J **338 (Pt 2)**: 471-478.

Rhodes, D. A. and J. Trowsdale (2007). "TRIM21 is a trimeric protein that binds IgG Fc via the B30.2 domain." Mol Immunol **44**(9): 2406-2414.

Richardson, C. and D. R. Alessi (2008). "The regulation of salt transport and blood pressure by the WNK-SPAK/OSR1 signalling pathway." J Cell Sci **121**(Pt 20): 3293-3304.

Rinehart, J., Y. D. Maksimova, *et al.* (2009). "Sites of regulated phosphorylation that control K-Cl cotransporter activity." Cell **138**(3): 525-536.

Ringel, J., R. Jesnowski, *et al.* (2006). "Aberrant expression of a disintegrin and metalloproteinase 17/tumor necrosis factor-alpha converting enzyme increases the malignant potential in human pancreatic ductal adenocarcinoma." Cancer Res **66**(18): 9045-9053.

Rio, C., J. D. Buxbaum, *et al.* (2000). "Tumor necrosis factor-alpha-converting enzyme is required for cleavage of erbB4/HER4." J Biol Chem **275**(14): 10379-10387.

Ross, P. L., Y. N. Huang, *et al.* (2004). "Multiplexed protein quantitation in Saccharomyces cerevisiae using amine-reactive isobaric tagging reagents." Mol Cell Proteomics **3**(12): 1154-1169.

Roxrud, I., C. Raiborg, *et al.* (2008). "An endosomally localized isoform of Eps15 interacts with Hrs to mediate degradation of epidermal growth factor receptor." J Cell Biol **180**(6): 1205-1218.

Rozengurt, E. (2007). "Mitogenic signaling pathways induced by G protein-coupled receptors." J Cell Physiol **213**(3): 589-602.

Saeed, A. I., V. Sharov, *et al.* (2003). "TM4: a free, open-source system for microarray data management and analysis." Biotechniques **34**(2): 374-378.

Sahin, U., G. Weskamp, *et al.* (2004). "Distinct roles for ADAM10 and ADAM17 in ectodomain shedding of six EGFR ligands." J Cell Biol **164**(5): 769-779.

Schlessinger, J. (2000). "Cell signaling by receptor tyrosine kinases." Cell **103**(2): 211-225.

Schlessinger, J. and M. A. Lemmon (2003). "SH2 and PTB domains in tyrosine kinase signaling." Sci STKE **2003**(191): RE12.

Schreiber, T. B., N. Mausbacher, *et al.* (2008). "Quantitative phosphoproteomics--an emerging key technology in signal-transduction research." Proteomics **8**(21): 4416-4432.

Schroeder, M. J., J. Shabanowitz, *et al.* (2004). "A neutral loss activation method for improved phosphopeptide sequence analysis by quadrupole ion trap mass spectrometry." Anal Chem **76**(13): 3590-3598.

Schwartz, D. and S. P. Gygi (2005). "An iterative statistical approach to the identification of protein phosphorylation motifs from large-scale data sets." Nat Biotechnol **23**(11): 1391-1398.

Selby, D. S., M. R. Larsen, *et al.* (2008). "Identification and characterization of N-glycosylated proteins using proteomics." Methods Mol Biol **484**: 263-276.

Shao, H., J. Chou, *et al.* (2006). "Spatial localization of m-calpain to the plasma membrane by phosphoinositide biphosphate binding during epidermal growth factor receptor-mediated activation." Mol Cell Biol **26**(14): 5481-5496.

Shenker, A., L. Laue, *et al.* (1993). "A constitutively activating mutation of the luteinizing hormone receptor in familial male precocious puberty." Nature **365**(6447): 652-654.

Shevchenko, A., H. Tomas, *et al.* (2006). "In-gel digestion for mass spectrometric characterization of proteins and proteomes." Nat Protoc **1**(6): 2856-2860.

Siegbahn, A., M. Johnell, *et al.* (2005). "Regulation of chemotaxis by the cytoplasmic domain of tissue factor." Thromb Haemost **93**(1): 27-34.

Skaug, B., X. Jiang, *et al.* (2009). "The role of ubiquitin in NF-kappaB regulatory pathways." Annu Rev Biochem **78**: 769-796.

Sorkin, A., K. Helin, *et al.* (1992). "Multiple autophosphorylation sites of the epidermal growth factor receptor are essential for receptor kinase activity and internalization. Contrasting significance of tyrosine 992 in the native and truncated receptors." J Biol Chem **267**(12): 8672-8678.

Sorkin, A., C. Waters, *et al.* (1991). "Multiple autophosphorylation site mutations of the epidermal growth factor receptor. Analysis of kinase activity and endocytosis." J Biol Chem **266**(13): 8355-8362.

Stocker, W. and W. Bode (1995). "Structural features of a superfamily of zinc-endopeptidases: the metzincins." Curr Opin Struct Biol **5**(3): 383-390.

Sturany, S., J. Van Lint, *et al.* (2002). "Mechanism of activation of protein kinase D2(PKD2) by the CCK(B)/gastrin receptor." J Biol Chem **277**(33): 29431-29436.

Sun, X., L. Gao, *et al.* (2006). "Down-regulation of WNK1 protein kinase in neural progenitor cells suppresses cell proliferation and migration." J Neurochem **99**(4): 1114-1121.

Sunnarborg, S. W., C. L. Hinkle, *et al.* (2002). "Tumor necrosis factor-alpha converting enzyme (TACE) regulates epidermal growth factor receptor ligand availability." J Biol Chem **277**(15): 12838-12845.

Syka, J. E., J. A. Marto, *et al.* (2004). "Novel linear quadrupole ion trap/FT mass spectrometer: performance characterization and use in the comparative analysis of histone H3 post-translational modifications." J Proteome Res **3**(3): 621-626.

Takahashi, E., J. Abe, *et al.* (1999). "p90(RSK) is a serum-stimulated Na+/H+ exchanger isoform-1 kinase. Regulatory phosphorylation of serine 703 of Na+/H+ exchanger isoform-1." J Biol Chem **274**(29): 20206-20214.

Takahata, M., M. Bohgaki, *et al.* (2008). "Ro52 functionally interacts with IgG1 and regulates its quality control via the ERAD system." Mol Immunol **45**(7): 2045-2054.

Takamune, Y., T. Ikebe, *et al.* (2007). "ADAM-17 associated with CD44 cleavage and metastasis in oral squamous cell carcinoma." Virchows Arch **450**(2): 169-177.

Tanaka, M., S. Okudaira, *et al.* (2006). "Autotaxin stabilizes blood vessels and is required for embryonic vasculature by producing lysophosphatidic acid." J Biol Chem **281**(35): 25822-25830.

Tanaka, Y., S. Miyamoto, *et al.* (2005). "Clinical significance of heparin-binding epidermal growth factor-like growth factor and a disintegrin and metalloprotease 17 expression in human ovarian cancer." Clin Cancer Res **11**(13): 4783-4792.

Thathiah, A., C. P. Blobel, *et al.* (2003). "Tumor necrosis factor-alpha converting enzyme/ADAM 17 mediates MUC1 shedding." J Biol Chem **278**(5): 3386-3394.

Tokumura, A., E. Majima, *et al.* (2002). "Identification of human plasma lysophospholipase D, a lysophosphatidic acid-producing enzyme, as autotaxin, a multifunctional phosphodiesterase." J Biol Chem **277**(42): 39436-39442.

Tzircotis, G., R. F. Thorne, *et al.* (2006). "Directional sensing of a phorbol ester gradient requires CD44 and is regulated by CD44 phosphorylation." Oncogene **25**(56): 7401-7410.

Ugi, S., T. Imamura, *et al.* (2002). "Protein phosphatase 2A forms a molecular complex with Shc and regulates Shc tyrosine phosphorylation and downstream mitogenic signaling." Mol Cell Biol **22**(7): 2375-2387.

Umezu-Goto, M., Y. Kishi, *et al.* (2002). "Autotaxin has lysophospholipase D activity leading to tumor cell growth and motility by lysophosphatidic acid production." J Cell Biol **158**(2): 227-233.

van der Geer, P. and T. Hunter (1994). "Phosphopeptide mapping and phosphoamino acid analysis by electrophoresis and chromatography on thin-layer cellulose plates." Electrophoresis **15**(3-4): 544-554.

van Meeteren, L. A., P. Ruurs, *et al.* (2006). "Autotaxin, a secreted lysophospholipase D, is essential for blood vessel formation during development." Mol Cell Biol **26**(13): 5015-5022.

Vincent, B., E. Paitel, *et al.* (2001). "The disintegrins ADAM10 and TACE contribute to the constitutive and phorbol ester-regulated normal cleavage of the cellular prion protein." J Biol Chem **276**(41): 37743-37746.

Vosseller, K., J. C. Trinidad, *et al.* (2006). "O-linked N-acetylglucosamine proteomics of postsynaptic density preparations using lectin weak affinity chromatography and mass spectrometry." Mol Cell Proteomics **5**(5): 923-934.

Wang, D., Y. C. Tan, *et al.* (2006). "G proteins G12 and G13 control the dynamic turnover of growth factor-induced dorsal ruffles." J Biol Chem **281**(43): 32660-32667.

Wang, Z., N. D. Udeshi, *et al.* (2010). "Extensive crosstalk between O-GlcNAcylation and phosphorylation regulates cytokinesis." Sci Signal **3**(104): ra2.

Washburn, M. P., D. Wolters, *et al.* (2001). "Large-scale analysis of the yeast proteome by multidimensional protein identification technology." Nat Biotechnol **19**(3): 242-247.

Wessel, D. and U. I. Flugge (1984). "A method for the quantitative recovery of protein in dilute solution in the presence of detergents and lipids." Anal Biochem **138**(1): 141-143.

Wilhelmsen, K., S. H. Litjens, *et al.* (2007). "Serine phosphorylation of the integrin beta4 subunit is necessary for epidermal growth factor receptor induced hemidesmosome disruption." Mol Biol Cell **18**(9): 3512-3522.

Winograd-Katz, S. E. and A. Levitzki (2006). "Cisplatin induces PKB/Akt activation and p38(MAPK) phosphorylation of the EGF receptor." Oncogene **25**(56): 7381-7390.

Witze, E. S., W. M. Old, *et al.* (2007). "Mapping protein post-translational modifications with mass spectrometry." Nat Methods **4**(10): 798-806.

Wu, R. C., J. Qin, *et al.* (2004). "Selective phosphorylations of the SRC-3/AIB1 coactivator integrate genomic reponses to multiple cellular signaling pathways." Mol Cell **15**(6): 937-949.

Xia, X., D. J. Mariner, *et al.* (2003). "Adhesion-associated and PKC-modulated changes in serine/threonine phosphorylation of p120-catenin." Biochemistry **42**(30): 9195-9204.

Xu, B., J. M. English, *et al.* (2000). "WNK1, a novel mammalian serine/threonine protein kinase lacking the catalytic lysine in subdomain II." J Biol Chem **275**(22): 16795-16801.

Xu, B. E., X. Min, *et al.* (2002). "Regulation of WNK1 by an autoinhibitory domain and autophosphorylation." J Biol Chem **277**(50): 48456-48462.

Xu, N., L. Bradley, *et al.* (1993). "A mutant alpha subunit of G12 potentiates the eicosanoid pathway and is highly oncogenic in NIH 3T3 cells." Proc Natl Acad Sci U S A **90**(14): 6741-6745.

Xu, P. and R. Derynck (2010). "Direct activation of TACE-mediated ectodomain shedding by p38 MAP kinase regulates EGF receptor-dependent cell proliferation." Mol Cell **37**(4): 551-566.

Young, D., G. Waitches, *et al.* (1986). "Isolation and characterization of a new cellular oncogene encoding a protein with multiple potential transmembrane domains." Cell **45**(5): 711-719.

Zagorska, A., E. Pozo-Guisado, *et al.* (2007). "Regulation of activity and localization of the WNK1 protein kinase by hyperosmotic stress." J Cell Biol **176**(1): 89-100.

Zhang, X., Q. Chen, *et al.* (2009). "Sequential phosphorylation of Nedd1 by Cdk1 and Plk1 is required for targeting of the gammaTuRC to the centrosome." J Cell Sci **122**(Pt 13): 2240-2251.

Zhang, X. A., A. L. Bontrager, *et al.* (2001). "Phosphorylation of a conserved integrin alpha 3 QPSXXE motif regulates signaling, motility, and cytoskeletal engagement." Mol Biol Cell **12**(2): 351-365.

Zhao, Y. and O. N. Jensen (2009). "Modification-specific proteomics: strategies for characterization of post-translational modifications using enrichment techniques." Proteomics **9**(20): 4632-4641.

Zhou, B. B., M. Peyton, *et al.* (2006). "Targeting ADAM-mediated ligand cleavage to inhibit HER3 and EGFR pathways in non-small cell lung cancer." Cancer Cell **10**(1): 39-50.

Zubarev, R. A., D. M. Horn, *et al.* (2000). "Electron capture dissociation for structural characterization of multiply charged protein cations." Anal Chem **72**(3): 563-573.

6. Abbreviations

Å	Ångström
ATP	Adenosintriphosphate
ADP	Adenosindiphosphate
BSA	Bovine serum albumin
°C	Degree celsius
$CaCl_2$	Calcium chloride
DMEM	Dulbecco's modified eagle medium
DTT	Dithiothreitol
ECL	Enhanced chemiluminescence
ECM	Extracellular matrix
EDTA	Ethylenediamintetraacetate
EGF	Epidermal growth factor
EGFR	Epidermal growth factor receptor
EGTA	Ethylene glycol-bis(2-aminoethyl)-N,N,N',N'-tetraacetic acid
EtOH	Ethanol
FCS	Fetal calf serum
FDR	False discovery rate
GO	Gene Ontology
GPCR	G protein-coupled receptor
h	Hour
HEPES	N-(2-Hydroxyethyl)-piperazin-N‘-2-Ethansulfonic acid
IAA	Iodoacetamide
IMAC	Immobilized metal affinity chromatography
IP	Immunoprecipitation
IPI	International Protein Index
KCl	Potassium chloride
kDa	Kilodalton
µ	Micro
l	Liter

LC	Liquid chromatography
LPA	Lysophosphatidic acid
m	Milli
M	Molar
$MgCl_2$	Magnesium chloride
min	Minute
$MnCl_2$	Manganese(II) chloride
MS	Mass spectrometry
MS^2	Tandem MS or MS/MS
NaCl	Sodium chloride
PAGE	Polyacrylamide gel elektrophoresis
PBS	Phosphate-buffered saline
PMSF	Phenylmethanesulfonyl fluoride
pSer	Phosphoserine
pThr	Phosphothreonine
pTyr	Phosphotyrosine
rpm	Rotations per minute
RT	Room temperature
RTK	Receptor tyrosine kinase
SCX	Strong cation exchange chromatography
SDS	Sodium dodecyl sulfate
SH2	Src homology domain 2
siRNA	Short interfering RNA
SILAC	Stable isotope labelling by amino acids in cell culture
STAGEtips	STopAndGoExtraction tips
TiO_2	Titanium dioxide
Tris	Tris(hydroxymethyl)aminomethan
o.n.	Overnight
V	Volt
Vol	Volume
WT	Wild type

7. Publications

Mäusbacher N, Schreiber TB, Daub H. Glycoprotein capture and quantitative phosphoproteomics indicate coordinated regulation of cell migration upon lysophosphatidic acid stimulation.
Mol Cell Proteomics. 2010 Jul 16. [Epub ahead of print]

Schreiber TB, **Mäusbacher N**, Kéri G, Cox J, Daub H. An integrated phosphoproteomics workflow reveals extensive network regulation in early lysophosphatidic acid signalling.
Mol Cell Proteomics. 2010 Jun;9(6):1047-62. Epub 2010 Jan 12.

Hadian K, Vincendeau M, **Mäusbacher N**, Nagel D, Hauck SM, Ueffing M, Loyter A, Werner T, Wolff H, Brack-Werner R. Identification of a heterogeneous nuclear ribonucleoprotein-recognition region in the HIV Rev protein.
J Biol Chem. 2009 Nov 27;284(48):33384-91.

Schreiber TB, **Mäusbacher N**, Breitkopf SB, Grundner-Culemann K, Daub H. Quantitative phosphoproteomics--an emerging key technology in signal-transduction research.
Proteomics. 2008 Nov;8(21):4416-32. Review.

8. Acknowledgement

Ich danke ganz herzlich meinem Doktorvater Herrn PD Dr. Henrik Daub für die Bereitstellung des Themas sowie die erstklassige Betreuung der Arbeit und die vielen interessanten Anregungen. Für seine Unterstützung und die Gewährleistung optimaler Arbeitsbedingungen in der Abteilung Molekularbiologie am Max-Planck-Institut für Biochemie danke ich des Weiteren Herrn Prof. Dr. Axel Ullrich.

Mein Dank gilt ebenso dem Prüfungsvorsitzenden Herrn Prof. Dr. Johannes Buchner und dem Zweitprüfer Herrn Prof. Dr. Stephan Sieber für die Begutachtung meiner Dissertation.

Ich bedanke mich ganz herzlich bei Herrn Prof. Dr. Mathias Mann und seinen Mitarbeitern für die gute Zusammenarbeit und die technische Beratung und Unterstützung beim Umgang mit dem Massenspektrometer. In diesem Zusammenhang danke ich auch Dr. Jürgen Cox für die Bereitstellung der Software MaxQuant und die geduldige Beantwortung aller damit verbundenen Fragen. Dankeschön an Matthias Schneider für die Unterstützung in der Anfangsphase dieser Arbeit. Großer Dank gilt Dr. Tiemo Schreiber für die hervorragende Zusammenarbeit. Ebenso möchte ich mich bei Renate Hornberger für die labortechnische Unterstützung bedanken.

Vielen herzlichen Dank allen Mitgliedern der Arbeitsgruppen ‚Cell Signalling` und ‚Molecular Biology‘ des Max-Planck-Institutes für Biochemie für Anregungen, Diskussionen und eine sehr gute Arbeitsatmosphäre.

Für die Förderung dieser Arbeit bedanke ich mich bei der Deutschen Forschungsgesellschaft.

Mein besonderer Dank gilt schließlich meinen Eltern, meiner Schwester und Christian für ihre großartige Unterstützung und Hilfe in jeglicher Hinsicht.